INFORMATION TO USERS

This manuscript has been reproduced from the microfilm master. UMI films the text directly from the original or copy submitted. Thus, some thesis and dissertation copies are in typewriter face, while others may be from any type of computer printer.

The quality of this reproduction is dependent upon the quality of the copy submitted. Broken or indistinct print, colored or poor quality illustrations and photographs, print bleedthrough, substandard margins, and improper alignment can adversely affect reproduction.

In the unlikely event that the author did not send UMI a complete manuscript and there are missing pages, these will be noted. Also, if unauthorized copyright material had to be removed, a note will indicate the deletion.

Oversize materials (e.g., maps, drawings, charts) are reproduced by sectioning the original, beginning at the upper left-hand corner and continuing from left to right in equal sections with small overlaps.

Photographs included in the original manuscript have been reproduced xerographically in this copy. Higher quality 6" x 9" black and white photographic prints are available for any photographs or illustrations appearing in this copy for an additional charge. Contact UMI directly to order.

Bell & Howell Information and Learning
300 North Zeeb Road, Ann Arbor, MI 48106-1346 USA
800-521-0600

A COMBINED EXPERIMENTAL AND STOCHASTIC FINITE ELEMENT ANALYSIS METHODOLOGY FOR THE PROBABILISTIC FRACTURE BEHAVIOR OF COMPOSITE LAMINATES

Md. Zakiul Haque

A Thesis

in

The Department

of

Mechanical Engineering

Presented in Partial Fulfillment of the Requirement
for the Degree of Master of Applied Science at
Concordia University
Montreal, Quebec, Canada

December 1999

Abstract

A Combined Experimental and Stochastic Finite Element Analysis Methodology for the Probabilistic Fracture Behavior of Composite Laminates

Md.Zakiul Haque

Composite laminates display significant randomness in their mechanical and fracture failure properties. This is due to the inevitable variabilities in the properties in fibers, in matrices, and at interfaces. Significant variabilities in fiber orientation, fiber volume fraction, thickness of lamina, void content, curvature of laminate, etc. are also introduced during manufacturing, and these are unavoidable. As a result, the fracture parameters and behavior become stochastic in nature. Therefore, the fracture problem has to be studied based on a stochastic formulation. In the present thesis, a combined experimental and stochastic finite element analysis methodology that can incorporate the material property variabilities and based on these, predict the stochastic characteristics of the Stress Intensity Factor (SIF) and the Strain Energy Release Rate (G) of composite laminates, is developed. Using this methodology, the probabilistic fracture analysis of laminated composites is performed. The material and geometric properties of the laminate are described in terms of homogeneous two-dimensional spatial stochastic fields and random variables that are established based on material property tests. In the finite element formulation, the elasticity matrix for the laminate is obtained based on the laminate theory. This matrix, in contrast to the deterministic finite element analysis, will be a

stochastic matrix that has different values at different Gauss point locations within the same element. The fracture behavior of the laminate is quantified through the two parameters, Stress Intensity Factor (SIF) and Energy Release Rate (ERR). The SIF is determined using Displacement Extrapolation Method (DEM) and Strain Energy Release Rate Method (SERR). A formulation for determining the reliability of composite laminates based on the probabilistic characteristics of stress intensity factor and that of the fracture toughness, is described. Different types of orthotropic laminates are analyzed, and based on the stochastic analysis, the effects of ply sequence, ply orientation, ply material properties, and thickness of lamina, as well as the effects of the correlation properties between material property variations on the fracture behavior are quantified. Based on the analysis results many useful conclusions on the design and reliability of composite laminates are deduced. These include the determination of the laminate configuration that possesses high reliability. The NCT-301 graphite-epoxy composite material system is employed in the analysis and testing for the purpose of numerical illustration.

Acknowledgments

The author wishes to express his indebtedness to his thesis supervisor Dr. Rajamohan Ganesan for his invaluable guidance, financial support and encouragement throughout the development of this thesis.

I would also like to thank Mr. P. Ouellette, Dr. M. Xie and Miss Micheline Ammar for their help in experimental work.

I thank my wife, Mrs. Marfia Begum very much for her encouragement, moral and emotional support, patience and understanding during the period of the present study. I do appreciate very much all her efforts and support.

The financial support provided by the NSERC and the Concordia University through the work study program is gratefully acknowledged. Also thanks are due to the Concordia Center for Composites (CONCOM) for the availability of computer and experimental facilities.

Table of Contents

List of Figures

List of Tables

Nomenclature

[A]	axial stiffness matrix
[a]	compliance matrix
a	the crack length
[B]	the element strain-nodal displacement matrix
C_{aa}	the covariance matrix
$\{d\}$	the global displacement vector
[E]	the elasticity matrix
f	the equivalent nodal force vector
G_I	the strain energy release rate (Mode I)
h	thickness of laminate
[J]	the Jacobian matrix
K_I	the stress intensity factor (Mode I)
[K]	the global stiffness matrix
K_{IC}	fracture toughness (Mode I)
L	lower triangular covariance matrix
m	stress intensity factor margin
[N]	the matrix of shape functions
P	distributed load
R	reliability
R_{aa}	the auto-correlation function
[T]	the transformation matrix

t	ply thickness
u, v	the two displacement components
x, y	the global co-ordinate
ξ, η	the local co-ordinate
ξ_{ij}	the separation vector
σ_0	the standard deviation of the stochastic field
σ	normal stress
ν	Poisson's ratio
τ	shear stress
γ	shear strain
r	radius; distance from the crack tip

Chapter 1

Introduction

1.1 Fracture Mechanics in Mechanical Design

The phenomenon of failure by catastrophic crack propagation in structural materials poses problems of design and analysis in many fields of engineering. The fracture behavior of a mechanical component, structure or material will depend on stress level, presence of a flaw, material properties, and the mechanism by which the fracture proceeds to completion [1]. The driving need for methods which quantify the effects of cracks on the mechanical component's performance has led to the evolution and development of fracture mechanics.

Cracks may exist in all mechanical components and structures as basic defects in materials or they may be induced during manufacturing or during service. Therefore a fundamental requirement in fracture mechanics is some means of assessing the stability of such cracks. In this respect, the most significant advance has been the introduction of

the Stress Intensity Factor (SIF) and the Strain Energy release Rate (G) as parameters for categorizing the onset of crack propagation.

Over the last decade or so, the Finite Element Method (FEM) has been firmly established as a standard computational method for the solution of practical fracture problems. However, unless extremely fine meshes are employed, problems arise in accurately modeling the singular stress field in the vicinity of the crack tip. Therefore in order to be able to apply the finite element method to the efficient solution of fracture problems, certain adaptations and further developments must be made [2]. These range from simple procedures for extrapolation of the crack tip stress intensity factors to the development of special crack elements, which model the complete crack zone stress field in anisotropic materials. In addition, the existing approaches, which are inherently deterministic, have to be modified so as to incorporate the randomness in material and geometric parameters and in loadings.

1.2 Fracture of Metals and Composites

Synthetic composites distinguish themselves from conventional materials such as metals, ceramics or polymers by the fact that they consist of two, or more, physically distinct and mechanically separable materials. They can be made by mixing the separate materials in such a way that the dispersion of one material in the other can be done in a controlled way to achieve optimum properties. Because of their complex microstructure the individual events of failure and final fracture can be complex too [3]. Fracture of the

individual phases in the composite material can take place separately, sequentially or simultaneously, depending on the type of loading, the external testing conditions, the particular microstructure of the composite and other factors.

In recent years there has been a tremendous interest in the fracture behavior of polymers and composite materials [4]. One reason for this is the increasing use of polymers and composites in structural components of aircraft, automotive, sporting and other industries.

The characteristic behavior of composite materials and their response to a tensile or compressive loading, however, are substantially different from that of metals. Whereas in metals, damage development under static loading exhibits only one primary failure mode, which is the initiation and propagation of one single crack (which can be described with simple fracture mechanics tools), composite materials exhibit a combination of different failure modes. They are the initiation and multiplication (and not propagation) of cracks, including transverse, longitudinal and angle-ply cracks in the matrix along fibers, delaminations, fiber fracture and fiber/matrix interface debonding.

If the fracture of the composite laminates is considered from the point of view of Linear Elastic Fracture Mechanics (LEFM), the engineer must be concerned with two distinct aspects of design: (1) The prediction of the stress intensity factor, which depends on the applied stress in addition to the laminate configuration and specimen geometry; (2) The experimentally determined value of the critical stress intensity factor, which defines the

onset of crack propagation as occurring when the stress intensity factor is equal or greater than the critical intensity factor.

Due to the different nature of composite materials from homogeneous isotropic materials, the stress analysis of composite structures is more complex [5-6] and inherently three dimensional [7]. Due to the inherent complexities, no exact solution for most of the problems has been found and the finite element method is usually employed to provide numerical solutions.

1.3 Randomness in Fracture Behavior

The parameters of any mechanical or structural system possess a random variation as a function of space and/or time. The randomness in fracture parameters encompasses the uncertainties involved at the design and manufacturing stages, as well as the uncertain nature of the operating conditions. At the design stage, randomness is present in the test data regarding material strength values, elastic constants, engineering constants, damage parameters, and the material properties pertinent to the service life. The randomness in material properties significantly affects the functioning of the mechanical component and is unavoidable even with the best quality control measures.

Tests on a single material specimen or structure yield a definite value for each material parameter such as the elastic constant, engineering constant and damage parameter. But when a number of specimens are tested, (i) the parameter values randomly fluctuate from

specimen to specimen, (ii) within the same structure itself, the values of any parameters display an uncertain spatial variation, (iii) due to environmental degradation the parameters have uncertain fluctuations. The sample to sample variation, spatial fluctuations within the structure, structure to structure variations and variation due to environmental effects of strength, deterioration, deformation and damage parameters of most of the present day engineering materials are random [8]. This is particularly the case with fiber reinforced composite materials. Variations in fiber size, fiber volume fraction, fiber orientation, void content, matrix properties, interfaces and thickness of lamina are always present and unavoidable. As a result, the elastic constant, engineering constant and deformation parameters of fiber reinforced composite materials possess a random variation [9].

1.4 Literature Review

Conventional fracture mechanics deals with homogeneous and isotropic materials and has been widely used because many of the practically useful materials belong to this category. The same is true, of course, for stress analysis in general, and most elasticity texts contain only a passing reference to anisotropy. The notable exceptions to this have been the works generated as a result of efforts to design load bearing structures made of wood[10]. The use of fiber reinforced composites to make laminates and also the design of plywood have produced a considerable literature and in particular the text by Lekhnitskii[11] which employed a development of the well-known Muskhelishvili[12] complex-number form of stress function analysis to produce a wide range of solutions to

problems of practical importance. In more recent times, many computer codes have been developed employing finite elements and boundary integrals, which will give solutions for anisotropic materials.

Fracture mechanics has been investigated in some details for wood[13] and found to be a very useful tool for design purposes. In spite of this, the use of fracture mechanics analysis for composites has been rather limited. In the early days, Chen[14] applied the finite-difference method to predict the stress field around an edge crack in unidirectional laminates under uniaxial tension. Lakshminarayana[6] presented a computationally efficient finite element model that can provide accurate numerical solutions to the problem of a semi-circular edge-notch in a finite size laminated composite plate under uniaxial tension. In his study cross-ply and angle-ply composite laminates were under consideration and the formulated element was based on the equivalent single layer two-dimensional theory.

The defect which may lead to premature delamination in composites may arise from microcracks and cavities formed during composite manufacturing or from in-service damage caused by impact loading. Extensive research has therefore been reported on the interlaminar fracture testing of various composite materials. The majority of the works [15-18] have been concerned with the delamination and the interlaminar fracture energy, G_c, of unidirectional laminates evaluated through the application of linear elastic fracture mechanics. Whitcomb[19] performed a parametric study of postbuckled through-width deleminations on laminated coupons. In his study, a two dimensional finite element

analysis was developed to calculate stress destributions and strain energy release rates for various delamination lengths, delamination depths, applied loads and lateral deflections.

In-service composite structures are susceptible to bolted joint failure where through-the-thickness cracks often develop in the laminate. Due to the complexity of the problem, efficient and accurate analysis techniques have not yet been fully developed. Analysis techniques have been proposed for predicting the failure of bolted connections in laminated composites [20-24]. A finite element analysis of single and two-hole bolted joints in fiber reinforced plastic was performed by Wong[25]. In his study, two dimensional plane stress four-node constant-strain quadrilateral elements are used to model pin-loaded laminated plates made of carbon fiber reinforced plastic (CFRP) and glass fiber reinforced plastic (GFRP) composites. Only one element has been used in the through-thickness direction, and further, the in-plane stresses in each ply have been obtained using laminate theory. Kurt and Paul[26] predicted bolt joint failure in generally orthotropic laminated composite plates which fail in the tension mode. The analysis is based on fracture mechanics concepts applied to a pseudo-flaw which is related to the physical cracking of the laminate at the joint.

Composite materials are extremely notch sensitive. The presence of cracks in structural components drastically reduces their load carrying capacity. For this reason, the issue of predicting composite residual strength in the presence of stress enhancers such as cracks has been an important research problem in the composites community.

A vast amount of experimental literature is available on the notched strength behavior of different composite systems. Several strength-based and fractures mechanics-based models have been proposed in the literature to predict the notched response of composite laminates under uniaxial tensile loading. The popular models, e.g., those by Whitney and Nuismer[27], Waddoups et al.,[28], Pipes et al.,[29] and Karlak[30], etc. are based on a characteristic distance concept. These models have been successfully used to predict laminate strength in the presence of notches and holes. A comprehensive review of these models has been done by Awerbuch and Madhukar[31]. An alternative approach to predicting notched strength of a class of laminates is presented by Rajesh and Sun[32]. In their study, fracture behavior of fiber-dominated center-notched AS4/3501-6 graphite/epoxy laminates is investigated and the results indicate that a constant value of fracture toughness K_Q of a laminate, is an in-situ or effective material property. Guofang[33] describes and discusses experiments on the fracture strengths and crack propagation of some aligned fiber-reinforced materials. Aronsson and Backlund[34] predicted strength of composites with through-the-thickness cracks using a model called the Damage Zone Model (DZM). Failure strength and damage mechanisms of E-glass/epoxy laminates under in-plane biaxial compressive deformation have been investigated by Wang and Darrell[35].

In the field of fracture mechanics, the Stress Intensity Factor (SIF) is an important parameter for predicting fracture strength and fatigue lives. This factor contains information on the stress field, crack size and geometry of the cracked material. Analytical solutions for stress intensity factors of cracked finite bodies are not readily

available and are often difficult to obtain. Thus numerical techniques e.g., the boundary element method, the finite element method, boundary collocation method are widely used in computing stress intensity factors. For isotropic materials, the necessary stress intensity factors for finite size sheets are often available from the literature. However, for orthotropic or composite materials, little is known about stress intensity factors for finite size laminates.

Many research efforts have focused on the calculation of stress intensity factor. One of the most important and efficient methods is based on the use of weight functions [36] to obtain the desired stress intensity factors. Lee[37] employed a finite element method with virtual crack extension technique to find the weight function of SIF for cracked composite laminates. Ruijia and Reddy[38] used the finite element alternating method to find out the stress intensity factors and weight functions for semi-elliptical cracks. The Boundary Force Method (BFM), a form of an indirect boundary element method, has been used by Tan and Bigelow[39] to analyze composite laminates that contain a hole and cracks to find out stress intensity factors. Nairn[40] used the shear-lag model to solve the crack tip stress concentrations in double-edge notch and center-notch unidirectional composites of finite width. From the stress-state solution, expressions are derived for strain energy release rate due to crack propagation through the fibers and due to crack propagation parallel to the fibers. Case *et al* [41] presented an approximate analysis to predict the stress concentrations in composites containing a single fiber fracture. Crack tip stress intensity factor in finite anisotropic plates is analyzed by Snyder and Cruse[42]. The stress intensity factor and energy release rates are determined for cracked orthotropic

sheets with riveted stiffeners by Yeh[43]. Mandell *et al* [44] calculated the stress intensity factor for single edge notched, double edge notched, and double cantilever beams. In their study, they were using a two-dimensional hybrid stress finite element analysis. Phillips[45] measured critical stress intensity factor and fracture surface energies for a series of [0/90] carbon fiber reinforced epoxy and carbon fiber reinforced glass composites. Victor and Efthimios[46] presented a simple, yet accurate, approach for the determination of the stress intensity factors in three-dimensional cracked anisotropic bodies modeled with quadratic isoparametric elements.

Finite Element Method (FEM) is one of the most effective numerical analysis tools in the engineering and physical sciences. It is a widely accepted mathematical technique for the numerical solution of partial differential equations. The fundamental idea underlying this method is to replace the continuous function by a piecewise polynomial approximation. Tian and Swanson[47] conducted a finite element analysis to investigate the fracture behavior of carbon/epoxy laminates containing internal cut fibers. Ko[48]described finite element microscopic stress analysis of cracked composite systems. The cracked composite systems are modeled with triangular and trapezoidal ring finite elements using NASTRAN finite element computer program. Heppler, Frisken and Hansen[49] employed a finite element analysis employing a high precision linear elastic fracture element to determine the stress intensity factors (Mode I) associated with a prescribed laminate and a given length-to-specimen width ratio (L/W) for rectangular specimen subjected to uniaxial tension loading with a center crack. They also investigated the mixed mode fracture of rectilinear anisotropic plates using higher order finite elements

[50]. A finite element based micromechanical failure analysis was developed by Zhu and Sankar[51]. A compact finite element formulation based on singularity transformation is presented by Yeh[52] and is used to analyze the stress singularity at the boundary-layer of an interface between adjacent layers in a laminated composite. The composite is subjected to uniform axial extension in the plane of the layers. Chen and Yang[53] developed a simple yet efficient formulation for a symmetrically laminated composite plate finite element and also adopted some highly efficient numerical algorithms using stand-alone desktop microcomputers for structural analysis and design. Nassehi *et al* [54] described a mathematical model for the analysis of the influence of interlayers on the stress distribution around cylindrical fibers. The model is based on the Galerkin finite element technique in conjunction with a penalty method. Thomas *et al* [55] presented a simple method for the analysis of fracture propagation in orthotropic materials based on finite element modeling. In their study, several theories of fracture propagation in anisotropic materials are reviewed with regard to their application to various materials. It is shown that isoparametric quarter-point elements can be used to obtain accurate stress intensity factors using orthotropic displacement correlation equations. Tasu and Plunkett[56] presented a finite element analysis of progressive failure for laminated FRP plates with in-plane loading. In their paper the proper mesh size for this analysis model has been investigated and the ultimate strength of composite laminates is predicted and compared with published experimental results in order to demonstrate the validity of this finite element computation model.

A fundamental problem in predicting the failure of a laminated composite material is the determination of the load at which an existing crack will begin to propagate as well as the direction of crack growth. A number of theories have been proposed to predict the direction of crack growth in anisotropic materials. Among them are the tensor polynomial criterion [57], the minimum strain energy density criterion [58] and the normal stress ratio criterion [59]. Kadi and Ellyin[60] investigated the problem of predicting the crack extension behavior of a center-notched unidirectional graphite/epoxy coupon. The material under investigation has been assumed to be elastic, homogeneous and anisotropic. They have also introduced a criterion based on the critical strain energy [61] to accurately predict the crack extension behavior in unidirectional composites within the elastic crack analysis.

The possibility of the application of Mode I and Mode II fracture mechanics to the characterization of the glass fiber/epoxy matrix interface has been studied by Krawczak and Pabiot[62]. Sih and Chen[63] applied the concept of fracture mechanics to analyze the brittle fracture of unidirectional composites. The analytical prediction has been based on the so-called S_c-theory. Gu[64] investigated the fracture behavior of continuous alumina fiber reinforced epoxy composites under compression at two different temperatures. Effects of fiber orientation, stacking sequence and temperature on failure mechanisms of the composite material are analyzed. William[65] introduced a failure criterion for composite materials based upon the strain invariant of finite elasticity.

Probabilistic modeling in conjunction with micromechanics fracture of composites is a promising approach for the prediction of failure and reliability characteristics of composites. It takes into account inevitable variations in properties of the constituents as well as the scatter of composite structural parameters. Ovchinskii[66], Stock, Bellini, Murthy and Chamis[67], and Fukuda[68] carried out the probabilistic analysis of composite strength and effective properties using the Monte Carlo simulation technique. The simulation procedure required extensive computational resources for any new set of structural parameters and properties of the constituents.

Composites have inherent scatter in elastic and strength properties. A probabilistic model utilizing random material characteristics to predict damage evolution in orthotropic laminated composites is presented by Dzenis *et al* [69], Joshi and Frantziskonis[70] and Larder[71]. A stochastic simulation model for the growth of multiple matrix cracks in composite laminates subjected to both static and fatigue loads is presented by Wang *et al* [72]. In their study the simulation model is based on the general concepts of the classical fracture mechanics in conjunction with an effective flaw distribution as a basic ply property. Cassenti[73] investigated the probabilistic static failure of composite materials. Probabilistic failure strength analysis of graphite/epoxy cross-ply composite laminates has been studied by Fukunaga and Chou[74]. This paper treats the failure characteristics of [0/90/0] and [90/0/90] cross ply laminates based upon the statistical strength analysis. The stress redistributions at the failure of the 90° ply are analyzed using a shear-lag model.

The well-known probabilistic theories for the tensile strength of unidirectional composites have been proposed by Rosen[75] and Zweben[76] and further developments have been reported in detail by different authors [77-81]. These models give us a satisfactory strength estimation when the composite failure is predominantly affected by the stochastic strength distribution of reinforcement fibers but are not suitable when there are other competing fracture micromechanisms.

The analysis of structures, whether subjected to random or deterministic external loads, has been developed mainly under the assumption that the structure's parameters are deterministic quantities. For a significant number of circumstances, this assumption is not valid, and the probabilistic aspects of the structure need to be taken into account. The necessity to account for random effects in determining the response of a mechanical system is due, in general, to three different sources: random external loadings, random boundary conditions, and random material parameters. In the last twenty years the powerful finite element method has undergone various new developments to incorporate these random effects, and is now termed as Stochastic Finite Element Method (SFEM). The developments in this field are reviewed by Contreras[82], Vanmarche, Shinozuka, Nakagiri, Schueller and Grigoriu[83], Benaroya and Rehak[84], Yamazaki, Shinozuka, Dasgupta[85], Ostoja-Starzewski[86], and Vanmarcke[87]. The stochastic finite element method is capable of dealing with random structural properties described by random fields very efficiently. Recent developments, such as the weighted integral technique [88-90], provide an accurate and consistent transition from continuous type random fields to discrete type stochastic finite elements.

Ramu and Ganesan[91] developed a new finite element method to analyze the structures with more than one parameter behaving in a stochastic manner using the Galerkin weighted residual method. The stochastic finite element analysis based on the local averages of random vector fields is formulated by Zhu, Ren, and Wu[92] for static, eigenvalue, and stress intensity factor problems. Jensen, and Iwan[93] presented a method for the dynamic analysis of linear systems with uncertain parameters to stochastic excitation. Liu, Belytschko, and Mani[94] studied the application of the SFEM in elastic/plastic dynamics with random material properties in details. Ghanem, and Spanos[95] proposed a new method for the solution of problems involving material variability. The material property is modeled as a stochastic process. The method makes use of a convergent orthogonal expansion of the process. Ganesan, Sankar, and Ramu[96] developed a stochastic finite element method to solve the more general non-self-adjoint eigenvalue problems. Shinozuka, Kako, and Tsurui[97] developed a method for the estimation of the structural reliability when a structure is subjected to loads that can be idealized in terms of a Gaussian random vector process. Ramu and Ganesan[98] analyzed the free vibrational characteristics of a beam-column, which is having randomly varying Young's modulus and mass density and subjected to randomly distributed axial loading. In their study, Hamilton's principle is used to formulate the problem using stochastic FEM. Ren, Elishakoff, and Shinozuka[99] proposed a new version of finite element method for the mean and covariance functions of the displacement for bending of beams with spatially random stiffness based on the variational principles. Sankar, Ramu, and Ganesan[100] derived the sensitivities of SIF and COD of cracked structural systems to fluctuations in material property values and external loadings. In their study, a Taylor

series expansion is used to express the SIF and COD in terms of averaged values. Sankar, Ramu, and Ganesan[101] described an effective method for integrating the concepts of probabilistic srtuctural mechanics with the finite element analysis for dynamic systems.

The successful application of the mechanics of composites for achieving safer and reliable designs is hindered by the inherent uncertain distribution of material and geometric properties. In recent years, composite structures involving random material properties have been studied by many researchers. Among of them Liaw and Yang[102] developed a 16-dof quadrilateral stochastic laminated thin-plate element and a solution procedure within the framework of stochastic finite element method. Ganesan and Hoa[103] presented the stress analysis of composite structures with stochastic parameters. Nakagiri, Takabatake, and Tani[104] presented a methodology of stochastic finite element method applied to the uncertain eigenvalue problem of linear vibration which arises from the fluctuation of the overall stiffness due to uncertain variation of the stacking sequence of composite laminates. Engelstad and Reddy[105] developed a probabilistic finite element analysis procedure for laminated composite shells. In their study, a total Lagrangian finite element formulation, employing a degenerated three-dimensional laminated composite shell element with the full Green-Lagrange strains and first-order shear deformable kinematics, is used. Chang and Yang[106] formulated a geometrically nonlinear stochastic thin-plate finite element to study the reliability of fiber-reinforced laminated plates with structural uncertainties under random in-plane loads. Slattery[107] developed a stochastic model of damage progression in unidirectional laminates of advanced composite materials. The modeling involves two

steps: a micromechanical simulation of the degradation of a small cell of the composite and a random-damage finite element simulation of material failure.

1.5 Scope and Objectives of the Thesis

It is clear that a better understanding of the stress concentration around the crack tip is important to the study of fracture behavior of composite laminates with cracks. The Finite Element Method (FEM) is a widely accepted technique to solve these problems.

The objectives of the present work are (1) to develop a combined experimental and stochastic finite element analysis methodology for the fracture analysis of composite laminates, (2) to develop the associated computer program using the MATLAB® software, (3) to employ the developed stochastic finite element methodology to evaluate the stochastic characteristics of the fracture parameters of composite laminates, and (4) to quantitatively evaluate through a detailed parametric study the effects of ply sequence, fiber orientation in lamina, etc. on the probabilistic fracture behavior of composite laminates that have no shear coupling. Based on the parametric study, many important aspects regarding the design and reliability of laminates are obtained. The fracture parameters considered are the stress intensity factor and the strain energy release rate under in-plane tensile loading. The experimental part involves the tensile testing of laminate specimens for material properties in tension and shear. For each property a total of 35 specimens are manufactured and tested. Based on the test data, the stochastic field

modeling of laminate material properties is performed. The isoparametric formulation using 8-node quadratic serendipity element is employed in the finite element analysis.

1.6 Organization of the Thesis

The present chapter provides a brief introduction and a literature survey regarding the probabilistic behavior of fracture of composite laminates that was studied using finite element method. Also the scope and the objectives of the thesis are provided in Chapter 1.

In Chapter 2, the basic concepts and mathematical expressions that are employed in the linear elastic finite element fracture analysis of two-dimensional problems are presented and summarized. The 8-node isoparametric element is used to model the mechanical component. A computer program using the software, MATLAB®, which can perform the fracture analysis of mechanical components made of isotropic materials is developed, described and demonstrated.

In Chapter 3, the salient aspects of linear elastic fracture mechanics of anisotropic materials are summarized. The concept and equations that are employed in the fracture analysis of anisotropic sheets are presented. The classical lamination theory of composite materials is also described in this chapter. The computer program, which is developed in

Chapter 2, is extended for composite laminates so as to evaluate the equivalent elastic constants and the stress intensity factor.

In Chapter 4, the aspects of fracture analysis with the spatial variability of material properties of composite laminates are described. The spatial variabilities are modeled as two-dimensional homogeneous stochastic fields [85]. The detailed procedure of manufacturing and tensile testing of composite laminates to determine sample random values of material properties is summarized. Also the developed computer program is modified for calculating the mean value, standard deviation and coefficient of variation of the stress intensity factor and the energy release rate of cracked composite laminates. Example applications are provided.

In Chapter 5, the parametric study, encompassing the effects of different correlation characteristics of material properties, ply angles and ply thickness on the fracture parameters of different composite laminates, is presented. Useful conclusions as to the probabilistic characteristics of the fracture of composite laminates are provided.

The thesis ends with Chapter 6, which provides the conclusions of the present thesis work and some recommendations for future work.

Chapter 2

Finite Element Analysis of Fracture of Isotropic Plates

2.1 Introduction

One of the main concerns in the design and development of mechanical components is the failure by fracture of the component. The area of Linear Elastic Fracture Mechanics (LEFM) deals with the analysis, modeling and prediction of fracture failure in mechanical components. Limited number of problems have been solved employing certain idealized models [108]. However, closed-from analytical solutions do not exist for all components used in industrial practice, which have complicated geometry and which are subjected to complex material properties, boundary conditions and loading. For these cases, the numerical solutions have to be sought and obtained.

Over the past few decades, the Finite Element Method (FEM) has been developed and established as a powerful, efficient, versatile, computational method for the numerical solution of engineering problems. Finite element formulations for fracture mechanics problems have been developed during the past two decades or so [2]. In the present thesis, the linear elastic finite element fracture analysis is employed. The present chapter deals with the case of isotropic materials.

In this Chapter, (i) the salient features and fundamental concepts of LEFM that are employed in the present thesis work are summarized, (ii) the basic theoretical expressions of linear elastic finite element fracture analysis are summarized, (iii) a computer program which can be used to perform the fracture analysis of mechanical components made of isotropic materials is developed and described, and (iv) example applications of the developed computer program are given and further, the results obtained are compared with the results provided in Reference [2]. Isoparametric formulation is employed and further, the plane 8-node serendipity isoparametric element is used to model the mechanical component. The relevant details regarding the calculation of stiffness and load matrices are given. The computer program is developed using the mathematical software MATLAB®. The subroutines, also called as "functions" in MATLAB®, which undertake and perform various operations that are required in the finite element analysis, are described in the present chapter. The complete listing of the program is presented in Appendix I.

In Section 2.2, the salient features and fundamental concepts of LEFM are summarized as mentioned in the above. In Section 2.3, the basic concepts and equations that are employed in the linear elastic finite element fracture analysis of two-dimensional problems are presented. Section 2.4 outlines the principles and formulation of isoparametric elements, with particular attention being given to the calculation of stiffness and load matrices of the 8-node serendipity element. The development of various subroutines pertaining to the linear elastic finite element fracture analysis is described in Section 2.5.

2.2 Aspects of Linear Elastic Fracture Mechanics

In a structure containing a crack and subjected to any loading, the stress field near the crack tip can be divided into three types [1], each associated with a local mode of deformation as shown in Figure 2.1. These modes are given below.

Mode I: Opening or tensile mode, in which the crack surfaces move directly apart from each other.

Mode II: Sliding or in-plane shear mode, in which the crack surfaces slide over one another in a direction perpendicular to the leading edge of the crack.

Mode III: Tearing or anti-plane shear mode, in which the crack surfaces move relative to one another and parallel to the leading edge of the crack.

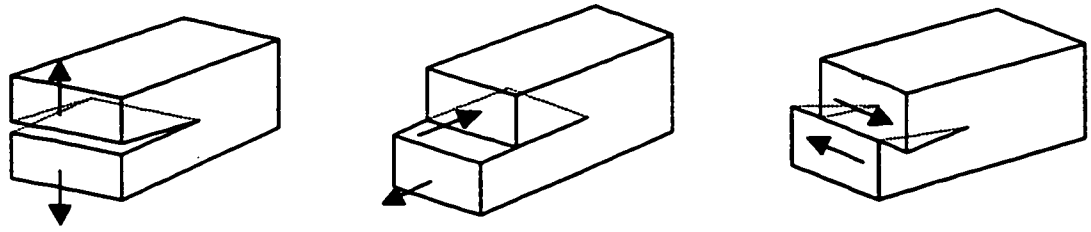

Mode I Mode II Mode III

Figure 2.1 Modes of fracture failure

Mode I loading is encountered in the overwhelming majority of actual engineering situations involving cracked components. Consequently, considerable attention has been given to both analytical and experimental methods designed to quantify Mode I stress-

crack-length relations. Mode II is found less frequently in practical situations and is of relatively little engineering importance in the case of isotropic materials. Mode III may be regarded as a pure shear problem such as that involved in a notched round bar in torsion.

2.2.1 Stress Intensity Factor

For a plate loaded in its plane and containing a crack, as shown in Figure 2.2, the stresses near the crack tip are determined according to the following equations.

$$\sigma_x = \frac{K}{\sqrt{2\pi r}} cos\frac{\theta}{2}\left(1 - sin\frac{\theta}{2} sin\frac{3\theta}{2}\right) \tag{2.1}$$

$$\sigma_y = \frac{K}{\sqrt{2\pi r}} \cos\frac{\theta}{2}\left(1 + \sin\frac{\theta}{2} \sin\frac{3\theta}{2}\right) \tag{2.2}$$

$$\tau_{xy} = \frac{K}{\sqrt{2\pi r}}\left(\sin\frac{\theta}{2}\cos\frac{\theta}{2}\cos\frac{3\theta}{2}\right) \tag{2.3}$$

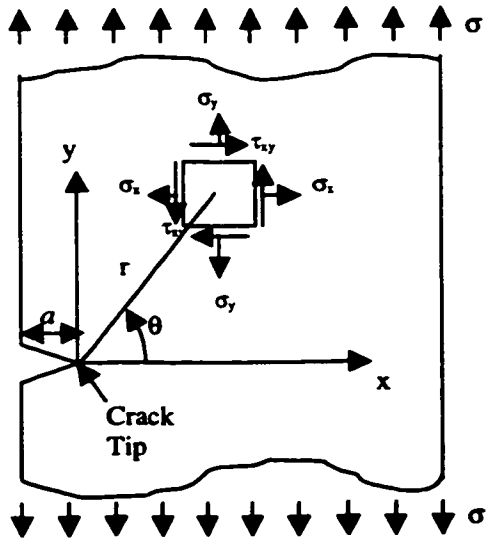

Figure 2.2 Distribution of stresses in the vicinity of crack tip

The Cartesian coordinate system, and the position coordinates r and θ are shown in Figure 2.2. An important feature of Eqs. (2.1-2.3) is the fact that the stress distributions around any crack in a component are similar and depend only on the parameters r and θ. The difference between one cracked component and another lies in the magnitude of the stress field parameter K, defined as the *Stress Intensity Factor* (SIF). In terms of the applied surface traction σ and the crack length *a*, the SIF is given by

$$K = f(\sigma, a) \tag{2.4}$$

where the functional relationship depends on the configuration of the cracked component and the manner in which the loading is applied. In other words, the *Stress intensity factor* is a function of both the applied loading and the crack length. In Eqs. (2.1-2.4), K corresponds to the particular mode of fracture of the plate, such as Mode I, Mode II or Mode III.

2.2.2 Strain Energy Release Rate

The strain energy released in forming a crack of length *a*, in an initially homogeneous and uncracked body is given by

$$U = -\frac{\sigma^2}{2E}\pi a^2 \qquad \text{for plane stress} \tag{2.5a}$$

$$U = -\frac{\sigma^2}{2E}\pi a^2\left(1-\nu^2\right) \text{ for plane strain} \tag{2.5b}$$

in which E and υ are the elastic modulus and Poisson's ratio respectively. The corresponding increase in surface energy is given by

$$W=2a\gamma \tag{2.6}$$

where γ is the surface energy density. These energy terms are plotted in Figure 2.3 for increasing crack length. It is readily seen that the crack becomes unstable at a critical length a_c when

$$\frac{\partial}{\partial a}(W+U)=0 \tag{2.7}$$

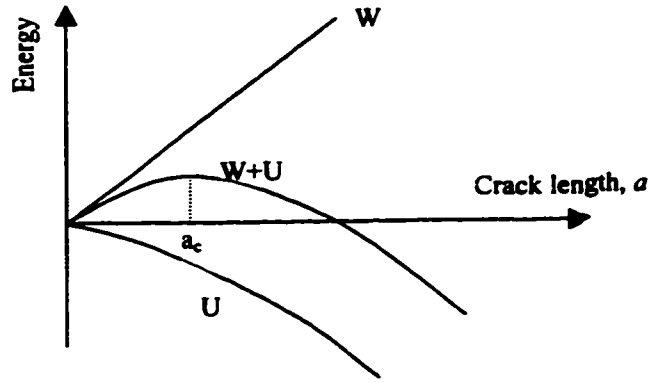

Figure 2.3 Variations of surface energy and strain energy with crack length

The energy release rate, G, is defined by

$$G=\frac{\partial U}{\partial a} \tag{2.8}$$

The stress intensity factor is related to the strain energy release rate in any structure. For example, in the crack opening mode, K_I is related to G_I as follows.

$$G_I = \frac{(k+1)}{8\mu} K_I^{\,2} \tag{2.9}$$

In the above equation, μ is the shear modulus of the material and further,

$$k = \frac{3-\nu}{1+\nu} \qquad \text{for plane stress} \tag{2.10}$$

$$k = 3-4\nu \qquad \text{for plane strain} \tag{2.11}$$

Similarly, the relations for the other two Modes, that are Mode II and Mode III, are given respectively by

$$G_{II} = \frac{(k+1)}{8\mu} K_{II}^{\,2} \tag{2.12}$$

$$G_{III} = \frac{1}{2\mu} K_{III}^{\,2} \tag{2.13}$$

If fracture occurs in a combined mode i.e. for instance in both Mode I and Mode II, then the strain energy release rate is expressed as

$$G = G_I + G_{II} = \left(K_I^{\,2} + K_{II}^{\,2}\right)\frac{(k+1)}{8\mu} \tag{2.14}$$

It is seen that the total strain energy release rate G is the sum of the energy release rates that correspond to the normal and shear loading.

2.3 Finite Element Analysis in LEFM

The displacement extrapolation method and the strain energy release rate method are the two most commonly used methods that use the Finite Element Analysis as a basis for the evaluation of SIF [2].

2.3.1 Displacement Extrapolation Method

The analytical expressions for the displacement variation along radial lines emanating from the crack tip are [2]

$$u = \frac{K_I}{4\mu}\sqrt{\frac{r}{2\pi}}\left[(2k-1)\cos\frac{\theta}{2} - \cos\frac{3\theta}{2}\right] - \frac{K_{II}}{4\mu}\sqrt{\frac{r}{2\pi}}\left[(2k+3)\sin\frac{\theta}{2} - \sin\frac{3\theta}{2}\right] \quad (2.15)$$

$$v = \frac{K_I}{4\mu}\sqrt{\frac{r}{2\pi}}\left[(2k+1)\sin\frac{\theta}{2} - \sin\frac{3\theta}{2}\right] + \frac{K_{II}}{4\mu}\sqrt{\frac{r}{2\pi}}\left[(2k-3)\cos\frac{\theta}{2} + \cos\frac{3\theta}{2}\right] \quad (2.16)$$

In the above, u and v correspond to x-direction and y-direction displacements respectively. Re-arranging the above two equations in the following form, the stress intensity factor for Mode I is written as a function of displacements u and v.

$$K_I \begin{bmatrix} (2k-1)\cos\frac{\theta}{2} - \cos\frac{3\theta}{2} \\ (2k+1)\sin\frac{\theta}{2} - \sin\frac{3\theta}{2} \end{bmatrix} = 4\mu\sqrt{\frac{2\pi}{r}}\begin{Bmatrix} u \\ v \end{Bmatrix} \tag{2.17}$$

In a similar manner, the following equation can be obtained for Mode II.

$$K_{II} \begin{bmatrix} -(2k+3)\sin\frac{\theta}{2} - \sin\frac{3\theta}{2} \\ (2k-3)\cos\frac{\theta}{2} + \cos\frac{3\theta}{2} \end{bmatrix} = 4\mu\sqrt{\frac{2\pi}{r}}\begin{Bmatrix} u \\ v \end{Bmatrix} \tag{2.18}$$

It is seen that the stress intensity factors can be evaluated from either u or v displacement components. For $\theta = 0°$ or $180°$ one or other of the trigonometric terms in Eqs. (2.17-2.18) becomes zero and therefore, the stress intensity factor must be calculated using the displacement components along radial lines that correspond to non-zero values of the trigonometric terms.

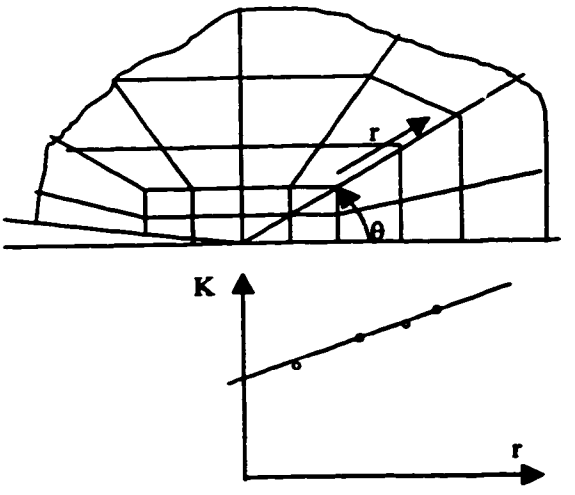

Figure 2.4 **Stress intensity factor evaluation using Displacement Extrapolation Method**

Upon substituting the values of displacements u or v and the radial distance r at nodal points along a radial line emanating from the crack tip (as shown in Figure 2.4), in Eqs. (2.17-2.18) a plot of K_I and K_{II} versus the radial distance r can be drawn. Then by discarding the results for points very close to the crack tip the plot can be extrapolated to the point at which r is equal to zero [2]. The value of K at the crack tip is thus obtained.

2.3.2 Strain Energy Release Rate Method

The strain energy that corresponds to a finite element mesh can be evaluated as

$$U = \frac{1}{2}\{d\}^T [K]\{d\} \tag{2.19}$$

or equivalently as

$$U = \frac{1}{2}\{d\}^T \{F\} \tag{2.20}$$

where $\{d\}$ and $[K]$ are respectively the global displacement vector and the global stiffness matrix, and further $\{F\}$ is the global load vector.

By performing two finite element analyses for two crack lengths a_1 and a_2 which differ by an incremental amount ∂a, and evaluating the strain energy difference (U_2-U_1), the strain energy release rate G can be calculated using Eq. 2.8 as

$$G = \frac{\partial U}{\partial a} = \frac{U_2 - U_1}{a_2 - a_1} \tag{2.21}$$

Using the value of G, the stress intensity factor is calculated using Eqs. (2.9-2.12).

$$K_I = \left(\frac{8\mu G_I}{1+k}\right)^{\frac{1}{2}}; \qquad K_{II} = \left(\frac{8\mu G_{II}}{1+k}\right)^{\frac{1}{2}} \tag{2.22}$$

In the above equation, G_I and G_{II} are the strain energy release rates that correspond to Mode I and Mode II respectively.

2.4 Formulation of the 8-Node Isoparametric Element

Since the internal nodes of the higher-order elements of Lagrange family do not contribute to the inter-element connectivity, they can be condensed out at the element level so that the size of the element matrices is reduced. The rectangular elements that have no interior nodes are known as serendipity elements. In other words, all the node points are on the boundary of the element.

The interpolation functions N_i, i = 1,2,..,8 for the 8-node (quadratic) element using the local coordinates (ξ,η) can be obtained as follows [109]. The value of the interpolation function N_1 should be zero at nodes 2,3,4,.....8, and unity at node 1. Equivalently, N_1 should vanish on sides defined by the equations 1-ξ=0, 1-η=0 and 1+ξ+η=0 as shown in Figure 2.5.

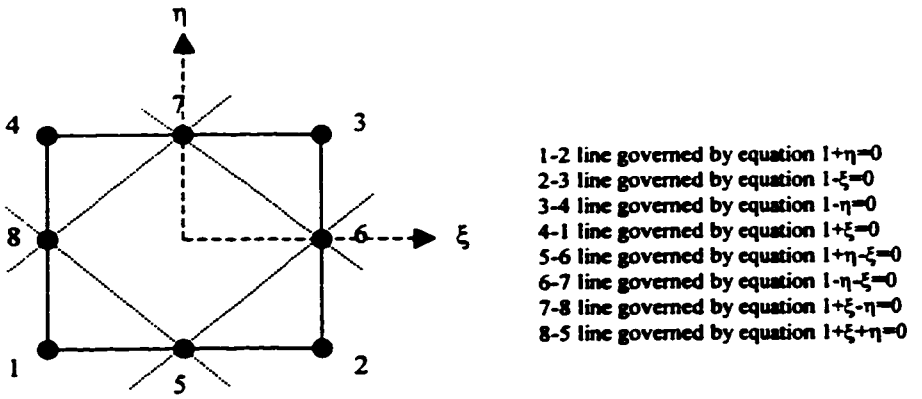

Figure 2.5 **Node numbers and the line that correspond to the equations 1-ξ=0, 1-η=0 and 1+ξ+η=0 in the 8-node serendipity element**

Therefore, N_1 is of the form

$$N_1(\xi,\eta) = C(1-\xi)(1-\eta)(1+\xi+\eta) \tag{2.23}$$

where C is a constant that should be so determined as to yield N_1(-1,-1)=1.Upon substitution one can find that C = -1/4, and therefore

$$N_1(\xi,\eta) = \frac{1}{4}(1-\xi)(1-\eta)(1+\xi+\eta) \tag{2.24}$$

Similarly, the other shape functions can be obtained:

$$N_2(\xi,\eta) = \frac{1}{4}(1+\xi)(1-\eta)(-1+\xi-\eta) \tag{2.25}$$

$$N_3(\xi,\eta)=\frac{1}{4}(1+\xi)(1-\eta)(-1+\xi-\eta) \tag{2.26}$$

$$N_4(\xi,\eta)=\frac{1}{4}(1-\xi)(1+\eta)(-1-\xi+\eta) \tag{2.27}$$

$$N_5(\xi,\eta)=\frac{1}{4}(1-\xi^2)(1-\eta) \tag{2.28}$$

$$N_6(\xi,\eta)=\frac{1}{4}(1+\xi)(1-\eta^2) \tag{2.29}$$

$$N_7(\xi,\eta)=\frac{1}{4}(1-\xi^2)(1+\eta) \tag{2.30}$$

$$N_8(\xi,\eta)=\frac{1}{4}(1-\xi)(1-\eta^2) \tag{2.31}$$

2.4.1 Plane Stress Case

If the plate thickness is very small when compared to the other dimensions of the plate, and if the loadings are applied uniformly through the thickness, the stresses are constant through the thickness of the plate and further, the thickness-direction stresses σ_z, τ_{zx} and τ_{zy} can be ignored. Thus the displacements can be expressed as

$$\{u\}=[u \quad v]^T \tag{2.32}$$

where u and v are the in-plane displacements in the x and y directions respectively.

The strain components can be written in the vector form as

$$\{\varepsilon\}=[\varepsilon_x \quad \varepsilon_y \quad \gamma_{xy}]^T \tag{2.33}$$

where for small displacements the normal strains are given by

$$\varepsilon_x = \frac{\partial u}{\partial x}, \varepsilon_y = \frac{\partial v}{\partial y} \tag{2.34}$$

and further, the shear strain is given by

$$\gamma_{xy} = \frac{\partial u}{\partial y} + \frac{\partial v}{\partial x} \tag{2.35}$$

The stress-strain relation can be written as

$$\{\sigma\} = [E]\{\varepsilon\} \tag{2.36}$$

where

$$\{\sigma\} = \begin{bmatrix} \sigma_x & \sigma_y & \tau_{xy} \end{bmatrix}^T \tag{2.37}$$

In Eq. (2.36), the matrix $[E]$ is called the elasticity matrix or the constitutive matrix or the stress-strain matrix. For linear elastic condition the stress-strain or constitutive matrix for isotropic material is given by

$$[E] = \frac{E}{1-\nu^2}\begin{bmatrix} 1 & \nu & 0 \\ \nu & 1 & 0 \\ 0 & 0 & \frac{1-\nu}{2} \end{bmatrix} \tag{2.38}$$

in which E and ν are the elastic modulus and Poisson's ratio respectively.

2.4.2 Plane Strain Case

For plane strain problems the thickness dimension normal to a certain plane (say, the *xy* plane) is large compared with the dimensions in the *xy* plane and further, the body is subjected to loads in the *xy* plane only. For plane strain problems it may be assumed that the strains in the *z* direction are negligible and that the in-plane displacements u and v are independent of *z*.

For isotropic materials the stress-strain or constitutive matrix is given by

$$[E]=\frac{E}{(1+\nu)(1-2\nu)}\begin{bmatrix}1-\nu & \nu & 0\\ \nu & 1-\nu & 0\\ 0 & 0 & \frac{1-2\nu}{2}\end{bmatrix} \tag{2.39}$$

The above equation corresponds to the linear elastic case.

2.4.3 Finite Element Formulation

The element displacements $\{u\}$ are interpolated using the shape functions as

$$\{u\}^{(e)}=[N]^{(e)}\{d\}^{(e)} \tag{2.40}$$

where

$$[N]^{(e)}=\begin{bmatrix}N_1 & 0 & N_2 & 0 & N_3 & 0 & N_4 & 0 & N_5 & 0 & N_6 & 0 & N_7 & 0 & N_8 & 0\\ 0 & N_1 & 0 & N_2 & 0 & N_3 & 0 & N_4 & 0 & N_5 & 0 & N_6 & 0 & N_7 & 0 & N_8\end{bmatrix} \tag{2.41}$$

$$\{d\}^{(e)} = \{u_1 \quad v_1 \quad u_2 \quad v_2 \quad u_3 \quad v_3 \quad u_4 \quad v_4 \quad u_5 \quad v_5 \quad u_6 \quad v_6 \quad u_7 \quad v_7 \quad u_8 \quad v_8\} \tag{2.42}$$

Also the strain matrix can be written as

$$\{\varepsilon\}^{(e)} = \begin{Bmatrix} \frac{\partial u}{\partial x} \\ \frac{\partial v}{\partial y} \\ \frac{\partial u}{\partial y} + \frac{\partial v}{\partial x} \end{Bmatrix} = [B]^{(e)}\{d\}^{(e)} \tag{2.43}$$

where $[B]^{(e)}$ is the element strain-nodal displacement matrix given by

$$[B]^{(e)} = \begin{bmatrix} \frac{\partial}{\partial x} & 0 \\ 0 & \frac{\partial}{\partial y} \\ \frac{\partial}{\partial y} & \frac{\partial}{\partial x} \end{bmatrix} [N]^{(e)} \tag{2.44}$$

In an isoparametric formulation, the following representations for the global coordinates x and y are used within an element.

$$\begin{Bmatrix} x^{(e)} \\ y^{(e)} \end{Bmatrix} = \sum_{i=1}^{8} \begin{bmatrix} N_i^{(e)} & 0 \\ 0 & N_i^{(e)} \end{bmatrix} \begin{Bmatrix} x_i^{(e)} \\ y_i^{(e)} \end{Bmatrix} \tag{2.45}$$

The derivatives $\frac{\partial N_i}{\partial x}$ and $\frac{\partial N_i}{\partial y}$ used in the strain-nodal displacement matrix given in Eq. (2.44) can be computed using the chain rule of partial differentiation.

$$\frac{\partial N_i^{(e)}}{\partial \xi} = \frac{\partial N_i^{(e)}}{\partial x}\frac{\partial x}{\partial \xi} + \frac{\partial N_i^{(e)}}{\partial y}\frac{\partial y}{\partial \xi} \tag{2.46}$$

$$\frac{\partial N_i^{(e)}}{\partial \eta} = \frac{\partial N_i^{(e)}}{\partial x}\frac{\partial x}{\partial \eta} + \frac{\partial N_i^{(e)}}{\partial y}\frac{\partial y}{\partial \eta} \tag{2.47}$$

In matrix form, the above two equations can be written as

$$\begin{Bmatrix} \frac{\partial N_i^{(e)}}{\partial \xi} \\ \frac{\partial N_i^{(e)}}{\partial \eta} \end{Bmatrix} = \begin{bmatrix} \frac{\partial x}{\partial \xi} & \frac{\partial y}{\partial \xi} \\ \frac{\partial x}{\partial \eta} & \frac{\partial y}{\partial \eta} \end{bmatrix}^{(e)} \begin{Bmatrix} \frac{\partial N_i^{(e)}}{\partial x} \\ \frac{\partial N_i^{(e)}}{\partial y} \end{Bmatrix} \tag{2.48}$$

The above matrix equation gives the relation between the derivatives of shape functions with respect to the global and local coordinates.

The matrix in Eq. (2.48) is called the Jacobian matrix of transformation, denoted by [J].

$$[J] = \begin{bmatrix} J_{11} & J_{12} \\ J_{21} & J_{22} \end{bmatrix} = \begin{bmatrix} \frac{\partial x}{\partial \xi} & \frac{\partial y}{\partial \xi} \\ \frac{\partial x}{\partial \eta} & \frac{\partial y}{\partial \eta} \end{bmatrix}^{(e)} \tag{2.49}$$

The inverse of the Jacobian matrix is denoted by [R] where

$$[R] = [J]^{-1} = \begin{bmatrix} R_{11} & R_{12} \\ R_{21} & R_{22} \end{bmatrix}^{(e)} \tag{2.50}$$

Then, Eq. (2.48) can be rewritten as

$$\begin{Bmatrix} \frac{\partial N_i^{(e)}}{\partial x} \\ \frac{\partial N_i^{(e)}}{\partial y} \end{Bmatrix} = \begin{bmatrix} R_{11} & R_{12} \\ R_{21} & R_{22} \end{bmatrix}^{(e)} \begin{Bmatrix} \frac{\partial N_i^{(e)}}{\partial \xi} \\ \frac{\partial N_i^{(e)}}{\partial \eta} \end{Bmatrix} \tag{2.51}$$

The components of the Jacobian matrix are computed as shown below

$$J_{11} = \frac{\partial x}{\partial \xi} = \sum_{i=1}^{8} \frac{\partial N_i^{(e)}}{\partial \xi} x_i \tag{2.52}$$

$$J_{12} = \frac{\partial y}{\partial \xi} = \sum_{i=1}^{8} \frac{\partial N_i^{(e)}}{\partial \xi} y_i \tag{2.53}$$

$$J_{21} = \frac{\partial x}{\partial \eta} = \sum_{i=1}^{8} \frac{\partial N_i^{(e)}}{\partial \eta} x_i \tag{2.54}$$

$$J_{22} = \frac{\partial y}{\partial \eta} = \sum_{i=1}^{8} \frac{\partial N_i^{(e)}}{\partial \eta} y_i \tag{2.55}$$

The element stiffness matrix can now be written as [2]

$$K^{(e)} = \int_{\Omega} \left[B^{(e)}\right]^T \left[E\right]^{(e)} \left[B^{(e)}\right] d\Omega \tag{2.56}$$

where the elemental volume is given as

$$d\Omega = t^{(e)} Det J^{(e)} d\xi d\eta \tag{2.57}$$

Thus the stiffness coefficient linking nodes i and j has the form

$$K_{ij}^{(e)} = \sum_{r=1}^{3} \sum_{s=1}^{3} \int_{-1}^{+1} \int_{-1}^{+1} \left[B_{ri}^{(e)}\right]^T \left[E_{rs}^{(e)}\right] \left[B_{sj}^{(e)}\right] det\, J^{(e)} d\xi d\eta \tag{2.58}$$

The elements of $K_{ij}^{(e)}$ are evaluated numerically. If the integrand in Equation (2.58) is denoted as

$$\sum_{r=1}^{3}\sum_{s=1}^{3}\left[B_{ri}^{(e)}\right]^T\left[E_{rs}^{(e)}\right]\left[B_{sj}^{(e)}\right]\det J^{(e)} = T_{ij}^{(e)} \tag{2.59}$$

then

$$K_{ij}^{(e)} = \int_{-1}^{+1}\int_{-1}^{+1} T_{ij}^{(e)} d\xi d\eta \tag{2.60}$$

The numerical integration for an isoparametric element with n x n sampling points leads to

$$K_{ij}^{(e)} = \sum_{p=1}^{n}\sum_{q=1}^{n} T\left(\xi_p, \eta_q\right)_{ij}^{(e)} W_p W_q \tag{2.61}$$

where W_p and W_q are the weighting factors and further, $\left(\xi_p, \eta_q\right)$ is a sampling position.

Any element edge can have a distributed loading per unit length in a normal and tangential direction. The equivalent nodal loads for the distributed loading can be calculated at the three nodal points that form the element edge as

$$\begin{Bmatrix} load\ at\ left\ corner\ node \\ load\ at\ middle\ node \\ load\ at\ right\ corner\ node \end{Bmatrix} = \frac{ql}{6}\begin{Bmatrix} 1 \\ 4 \\ 1 \end{Bmatrix} \tag{2.62}$$

where q is the distributed load per unit length and l is the element edge length.

2.4.3.1 Modeling of Crack Tip Singularity

Stress singularities exist at crack tips, and therefore, for the calculation of stress intensity factors, the use of finite elements that contain the required stress singularities can be effective.

The most convenient way of introducing a $1/\sqrt{r}$ strain singularity into a quadratic isoparametric element is by manipulation of the mid-side node position. Crack tip elements based on this approach were formulated independently by Barsoum [110] and Henshell and Show [111].

Consider the quadratic element shown in Figure 2.5 in which the node points are locally numbered as 1,2,3...8. The desired strain singularity can be introduced at node 1 by moving the mid-point nodes 5 and 8 to the quarter point positions as shown in Figure 2.6.

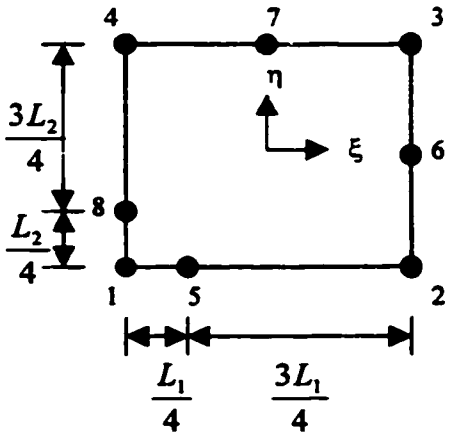

Figure 2.6 Quadratic isoparametric element with mid-side nodes at quarter points

Consider the edge 1-2, defined by $\eta = -1$. The shape functions for nodes along this edge are given by Eq.(2.24), Eq.(2.25) and Eq.(2.28) as

$$N_1 = -\frac{1}{2}\xi(1-\xi) \tag{2.63}$$

$$N_5 = (1-\xi^2) \tag{2.64}$$

$$N_2 = \frac{1}{2}\xi(1+\xi) \tag{2.65}$$

Then using Eq.(2.45), the equation for the x coordinate can be written as

$$x = \sum_{i=1,5,2} N_i x_i = -\frac{1}{2}\xi(1-\xi)x_1 + (1-\xi^2)x_5 + \frac{1}{2}\xi(1+\xi)x_2 \tag{2.66}$$

with a similar expression for the y coordinate. Locating the origin of global coordinates x and y at node 1 and denoting the length of edge of 1-2 as L_1, then $x_1 = 0$, $x_5 = \frac{L_1}{4}$, and $x_2 = L_1$. From Eq.(2.66) given above, one can write that

$$x = \frac{1}{2}\xi(1+\xi)L_1 + (1-\xi^2)\frac{L_1}{4} \tag{2.67}$$

In other words,

$$\xi = -1 + 2\sqrt{\frac{x}{L_1}} \tag{2.68}$$

The term $\frac{\partial x}{\partial \xi}$ in the Jacobian matrix given by Eq.(2.49), is now obtained from Eq.(2.67) and by making use of Eq.(2.68).

$$\frac{\partial x}{\partial \xi} = \frac{L_1}{2}(1+\xi) = \sqrt{L_1 x} \tag{2.69}$$

Therefore the Jacobian matrix is singular at node 1, where x=0. The displacement variation along edge 1-2 is given from Eq.(2.40) as

$$u = \sum_{i=1,5,2} N_i u_i = -\frac{1}{2}\xi(1-\xi)u_1 + (1-\xi^2)u_5 + \frac{1}{2}\xi(1+\xi)u_2 \tag{2.70}$$

Substituting for ξ from Eq.(2.68) gives

$$u = -\frac{1}{2}\left(-1+2\sqrt{\frac{x}{L_1}}\right)\left(2-2\sqrt{\frac{x}{L_1}}\right)u_1 + 4\left(\sqrt{\frac{x}{L_1}} - \frac{x}{L_1}\right)u_5 + \frac{1}{2}\left(-1+2\sqrt{\frac{x}{L_1}}\right)\left(2\sqrt{\frac{x}{L_1}}\right)u_2 \tag{2.71}$$

The normal strain in the x direction is then given by

$$\varepsilon_x = \frac{\partial u}{\partial x} = \frac{\partial \xi}{\partial x}\frac{\partial u}{\partial \xi}$$

$$= -\frac{1}{2}\left(\frac{3}{\sqrt{xL_1}} - \frac{4}{L_1}\right)u_1 + \left(\frac{2}{\sqrt{xL_1}} - \frac{4}{L_1}\right)u_5 + \frac{1}{2}\left(-\frac{1}{\sqrt{xL_1}} + \frac{4}{L_1}\right)u_2 \tag{2.72}$$

The strain singularity along edge 1-2 is therefore of the required order $1/\sqrt{r}$. The similar strain singularity is also obtained along edge 1-4.

2.5 Program Development for Fracture Analysis

In this section all the subroutines required for the calculation of fracture parameters using a finite element mesh are presented. The function of each subroutine is explained here. Also the corresponding MATLAB® code is provided in Appendix I.

In the programs presented, an attempt has been made to give a variable name in a logical manner. For example, the following names will be employed.

nel – Total number of elements

nnod – Number of nodes per element

ndof – Number of degrees of freedom per node

gcoord – Global coordinate values of each node

The structure of the finite element program is shown schematically in Figure 2.8 wherein the order in which various subroutines are called by the controlling or main program is indicated. The detailed description of each subroutine is provided in the following.

2.5.1 Subroutine of the Program

2.5.1.1 Subroutine *fgauss*

The function of this subroutine is to set up the sampling point positions and weighting factors for numerical integration. The Gauss quadrature process is restricted here to two,

three and four point integration rules. Arrays "pointx" and "pointy" contain the sampling point positions and further weighting factors are stored in arrays "weightx" and "weighty". The Gauss point numbering is shown in Figure 2.7.

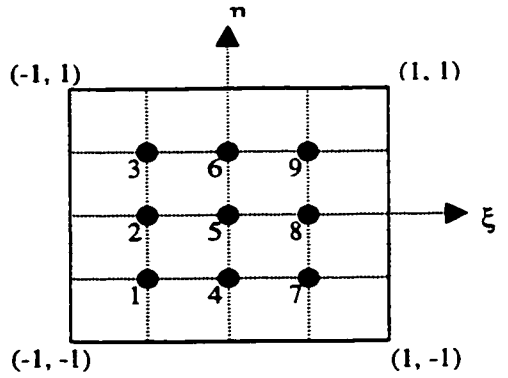

Figure 2.7 Gauss point numbering

2.5.1.2 Subroutine *fematiso*

This subroutine calculates the elasticity matrix [*E*] for either plane stress or plane strain case according to Eqs. (2.38-2.39). The [*E*] matrix is stored in the array "matmtx".

2.5.1.3 Subroutine *feisoq8*

The role of this subroutine is to evaluate the shape functions $N_i^{(e)}(\xi,\eta)$ and their derivatives $\partial N_i^{(e)}/\partial\xi$, $\partial N_i^{(e)}/\partial\eta$ at any sampling point ξ_p,η_q within each 8-node element presented in Section 2.4. The evaluated values of shape functions for each sampling position of an element are stored in the array "shape" and further, their derivatives are stored in the arrays "dhdr" and "dhds".

2.5.1.4 Subroutine *fejacob2*

This subroutine calculates the Jacobian matrix for any sampling position and stores the matrix in the array "jacob2". For two-dimensional problems the Jacobian matrix is defined by Eq. (2.49).

2.5.1.5 Subroutine *fekine2d*

The function of this subroutine is to evaluate the strain-nodal displacement matrix [B] at any position within the element. The matrix [B] is stored in the array "kinmtx2" and this matrix is given by Eq. (2.44).

2.5.1.6 Subroutine *federiv2*

The role of this subroutine is to calculate the derivatives of the isoparametric shape functions $\partial N_i^{(e)}/\partial x$, $\partial N_i^{(e)}/\partial y$ with respect to the global coordinate system and to store the values in the arrays "dhdx" and "dhdy". These quantities are defined in Eq. (2.51).

2.5.1.7 Subroutine *feeldof*

This subroutine computes the system degrees of freedom associated with each element and stores the values in the array "index".

2.5.1.8 Subroutine *feasmbl1*

The role of this subroutine is to assemble the element stiffness matrices $[K^{(e)}]$ given by Eq. (2.56) into the global stiffness matrix $[K]$ and to store the resulting matrix in the array $[KK]$.

2.5.1.9 Subroutine *feaplyc2*

The role of this subroutine is to apply the boundary condition to the matrix equation $[K]\{d\}=\{f\}$.

2.5.1.10 Subroutine *fsifisod*

The role of this subroutine is to calculate the Stress Intensity Factor (SIF) by the displacement extrapolation method for the isotropic case using Eq. (2.17). The details of the procedure are described in Section 2.3.1.

2.5.1.11 Subroutine *fsifisoe*

The purpose of this subroutine is to evaluate the SIF by the energy release rate method for the isotropic case according to Section 2.3.2 and Eq. (2.22).

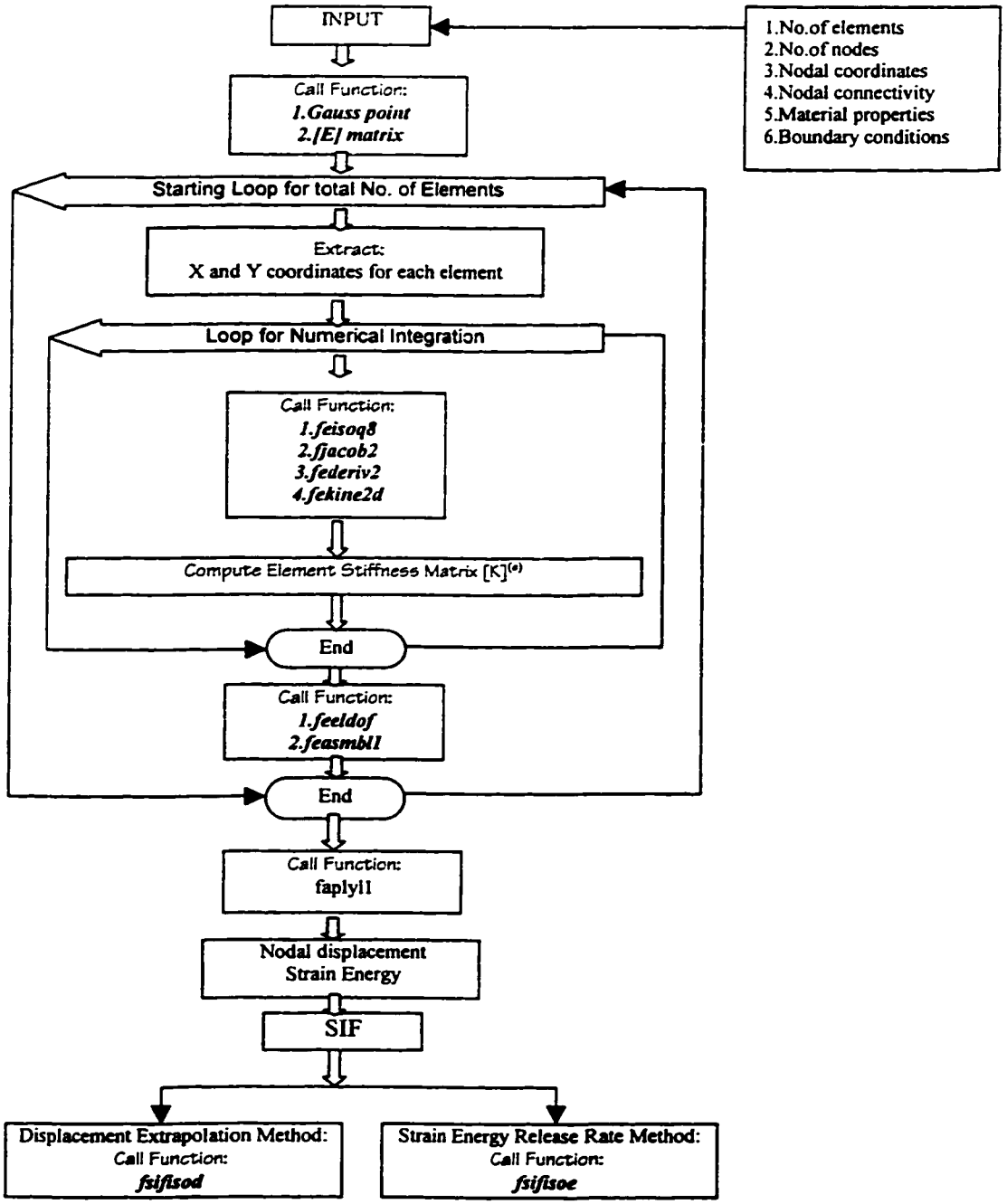

Figure 2.8 The structure of the MATLAB® program for determining nodal displacements, strain energy and fracture parameters

2.5.2 Example Applications

The computer program developed in this chapter is now demonstrated through the application to a linear elastic problem. The example considered is that of a plate under tension which contains a crack of length 2a perpendicular to the direction of loading. The initial crack length was chosen as a=0.4w, where w is the width of the plate. The finite element mesh employed in the solution is shown in Figure 2.9.

The material properties assumed in the analysis are, E=10000 units, ν=0.3, t=1 unit and applied load P=100 units. It may be noted here that these values are used with the purpose of obtaining results for displacements, stresses etc. and comparing them with that given in Ref.[2] for the same material property values.

2.5.2.1 Displacements and stresses

The nodal displacements along the crack edge and the loaded edge of the plate are listed in Table 2.1. Also, the stresses near the crack tip are computed and presented in Table 2.2. For the same example problem, the displacements and stresses were calculated and given in Ref. [2]. These values are reproduced in Table 2.3 and Table 2.4 for the purpose of comparison.

It is observed that the displacements and stresses calculated using the MATLAB program are in excellent agreement with the displacements and stresses given in Ref.[2].

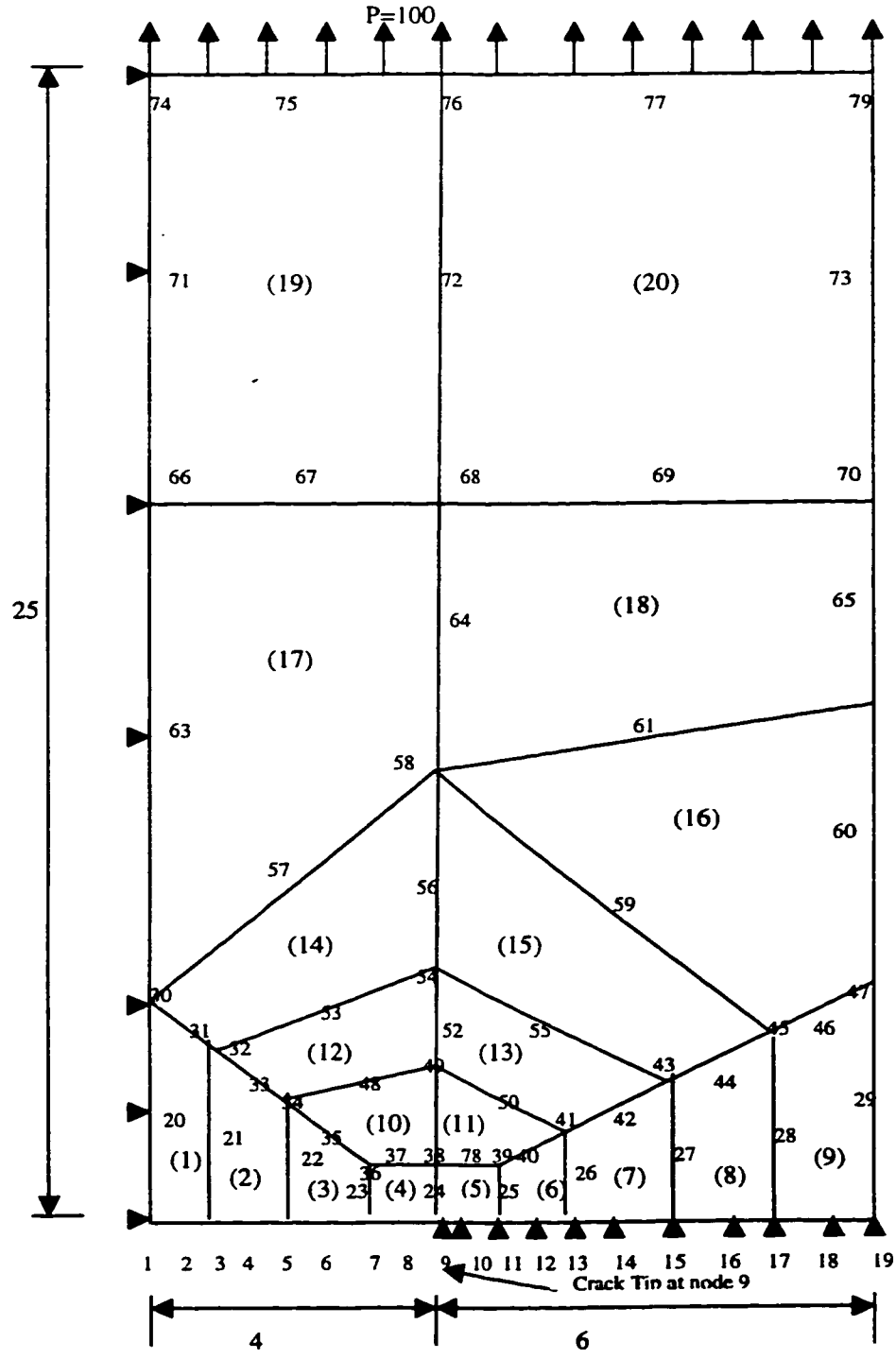

Figure 2.9 Mesh for the center-cracked plate problem

Table 2.1 **Displacements (x dir.) calculated using the MATLAB® Program described in Section 2.5 and given by Reference[2]**

Node No.		*u* (Matlab®)	*u* (Ref.[2])
Along Crack Edge	1	0.0000	0
	2	-0.0070	-0.0069
	3	-0.0144	-0.0144
	4	-0.0209	-0.0209
	5	-0.0275	-0.0275
	6	-0.0333	-0.0333
	7	-0.0385	-0.0385
	8	-0.0403	-0.0403
Along Loaded Edge	74	0.0000	0
	75	-0.0060	-0.0059
	76	-0.0118	-0.0118
	77	-0.0209	-0.0209
	79	-0.0297	-0.0297

Table 2.2 **Stresses calculated using the MATLAB® Program described in Section 2.5**

Gauss Point		σ_x	σ_y	τ_{xy}
Within element 4	1	-89.0073	-42.0030	35.8993
	2	-13.1173	4.3893	-14.9606
	3	45.0181	45.4552	-74.6298
	4	-2.1086	71.0108	-88.4156
	5	7.4544	68.8749	-80.7878
	6	-0.7374	61.4125	-81.9693
	7	155.7780	420.6510	-237.6193
	8	99.0139	369.9869	-171.5037
	9	24.4951	313.9963	-114.1975
Within element 5	1	259.2255	520.6444	145.6721
	2	85.8538	435.4262	43.0284
	3	-6.3017	374.5728	-50.3532
	4	194.0082	341.7727	70.4589
	5	64.2682	299.7456	24.7905
	6	15.7444	282.0834	-11.6158
	7	151.7659	239.4838	9.9929
	8	65.6575	240.6479	21.2998
	9	60.7654	266.1768	41.8688

Table 2.3 Displacements (y dir.) calculated using the MATLAB® Program described in Section 2.5 and given by Reference[2]

Node No.		v (Matlab®)	v (Ref. [2])
Along Crack Edge	1	0.0861	0.086136
	2	0.0851	0.085150
	3	0.0815	0.081462
	4	0.0756	0.075557
	5	0.0667	0.066708
	6	0.0560	0.055972
	7	0.0397	0.039718
	8	0.0268	0.026774
Along Loaded edge	74	0.2769	0.276943
	75	0.2765	0.276511
	76	0.2767	0.276697
	77	0.2769	0.276863
	79	0.2769	0.276875

Table 2.4 Stresses given in Reference [2]

Gauss Point		σ_x	σ_y	τ_{xy}
Within element 4	1	-89.006	-42.003	35.899
	2	-13.117	4.3893	-14.960
	3	45.018	45.455	-74.629
	4	-2.1086	71.010	-88.415
	5	7.4543	68.874	-80.787
	6	-0.73736	61.412	-81.968
	7	155.78	420.65	-237.62
	8	99.013	369.98	-171.50
	9	24.495	313.99	-114.20
Within element 5	1	259.22	520.64	145.67
	2	85.853	435.42	43.028
	3	-6.3016	374.57	-50.353
	4	194.01	341.77	70.458
	5	64.268	299.74	24.790
	6	15.744	282.08	-11.616
	7	151.76	239.48	9.9928
	8	65.657	240.65	21.300
	9	60.765	266.17	41.868

2.5.2.2 Stress Intensity Factor

(a) Displacement Extrapolation Method

In Reference [2] it is shown that for isoparametric elements the most accurate results are given by displacement extrapolation to the crack tip along the radial line $\theta = 180^{\circ}$. For the present study only the mesh given in Figure 2.9 is employed. The stress intensity factor for each nodal point along $\theta = 180^{\circ}$ is calculated and plotted in Figure 2.10. Extrapolation to the crack tip yields $K_I \approx 378$ which differs from the value of $K_I = 393.5$ that is given in Ref.[112] by 3.94%. It may be noted that elements 4 and 5 are ¼-point crack tip elements described in sub-section 2.4.3.1.

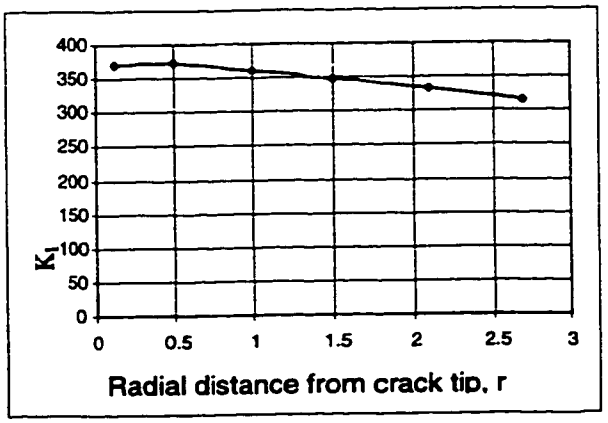

Figure 2.10 Stress intensity factor extrapolation for the mesh with singularity elements in the crack tip zone (elements 4 and 5)

(b) Strain Energy Release Rate Method

In the strain energy release rate method, the crack is advanced in the present code by releasing one node at a time. The approach of advancing the crack by two different increments, calculating K_I in each case and then extrapolating the value of K_I back to the original crack length is followed. Using the same mesh shown in Figure 2.9, the crack is advanced by releasing nodes 9 and 10 one at a time. This procedure gives an increment of crack length equal to 0.25 mm and the calculated value of K_I is equal to 402. Comparing with the value of 393.5 given in Ref. [112], the difference can be seen to be equal to 2.29%.

2.6 Conclusion and Discussion

In this chapter, the concepts of Stress Intensity Factor (denoted by K) and Strain Energy Release Rate (denoted by G) of Linear Elastic Fracture Mechanics (LEFM) as applied to isotropic materials are summarized. The formulation employing the finite element modeling and analysis for evaluating these two parameters for a plate made of isotropic material and subjected to any type of loading in Mode I and Mode II, is described. The 8-node quadratic isoparametric element is employed in the finite element analysis. Relevant details regarding the shape functions and the computation of stiffness matrix and load matrix are given. The corresponding computer program is developed in MATLAB® software environment and the program development is explained in sufficient detail. An

example problem is used to demonstrate the developed program. The program was verified by comparing the results such as the nodal displacements and stresses at Gauss points with that provided for the same problem in Ref. [2]. The values of stress intensity factor and the energy release rate determined using the developed program were also compared with that given for the same problem in Ref. [2]. The results obtained using the developed program are in excellent agreement with the results given in literature. The formulation will be extended in the next chapter for anisotropic materials and composite laminates and then, in the subsequent chapter, for the stochastic analysis.

Chapter 3

Finite Element Analysis of Fracture of Anisotropic Plates

3.1 Introduction

In recent years there has been a tremendous interest in the fracture behavior of composite materials. One reason for this is the increasing use of composites in structural components of aircraft, automotive, sporting and other industries. In such circumstances it is essential to have as complete an understanding as possible of the fracture behavior of the composite materials. Compared with the fracture mechanics of isotropic materials, the fracture mechanics of composites has not completely been understood.

In this chapter, (i) the salient aspects of linear elastic fracture mechanics of anisotropic materials are summarized, (ii) the finite element fracture analysis of anisotropic materials is developed, (iii) The MATLAB® computer program which has been developed in Chapter 2 for isotropic materials is extended for the case of anisotropic materials, and (iv)

example applications of the computer program to composite laminates are given. The program is verified using the results obtained based on ANSYS® software.

In Section 3.2, the fracture mechanics of anisotropic materials are summarized. In Section 3.3, the concept and equations that are employed in the linear elastic finite element analysis of fracture of anisotropic sheets are presented. In Section 3.4, linear elastic characteristics of fiber-reinforced material and classical lamination theory are described. The development of the computer program for the evaluation of equivalent elastic constants and stress intensity factor of composite laminates is described in Section 3.5.

3.2 Fracture Mechanics of Anisotropic Plates

The stress intensity factor for a cracked plate made of anisotropic material is obtained based on the stress analysis. For anisotropic materials, the complex analysis function theory [17] has been employed in stress analysis.

In the absence of body forces the equilibrium equations for the plane stress case are

$$\frac{\partial \sigma_x}{\partial x}+\frac{\partial \tau_{xy}}{\partial y}=0; \qquad \frac{\partial \sigma_y}{\partial y}+\frac{\partial \tau_{xy}}{\partial x}=0 \tag{3.1}$$

The equations of equilibrium are identically satisfied by the Airy stress function $\Phi(x,y)$, which is related to the stress components as follows:

$$\sigma_x = \frac{\partial^2 \Phi}{\partial y^2}, \qquad \sigma_y = \frac{\partial^2 \Phi}{\partial x^2} \quad \text{and} \quad \tau_{xy} = -\frac{\partial^2 \Phi}{\partial x \partial y} \tag{3.2}$$

The condition of compatibility for two dimensional problems is

$$\frac{\partial^2 \varepsilon_x}{\partial y^2} + \frac{\partial^2 \varepsilon_y}{\partial x^2} = \frac{\partial^2 \gamma_{xy}}{\partial x \partial y} \tag{3.3}$$

The Hooke's law for a general anisotropic material may be written in terms of the compliances as given below.

$$\varepsilon_x = a_{11}\sigma_x + a_{12}\sigma_y + a_{16}\tau_{xy} \tag{3.4}$$

$$\varepsilon_y = a_{21}\sigma_x + a_{22}\sigma_y + a_{26}\tau_{xy} \tag{3.5}$$

$$\gamma_{xy} = a_{61}\sigma_x + a_{62}\sigma_y + a_{66}\tau_{xy} \tag{3.6}$$

Symmetry condition requires that $a_{12} = a_{21}$, $a_{26} = a_{62}$ and $a_{16} = a_{61}$. In the case of orthotropic material the principal elastic directions are orthogonal to each other and further there is no coupling between deformations due to shear and normal stresses. In that case $a_{16} = a_{26} = 0$.

The orthotropic coefficients are often expressed in terms of elastic moduli and Poisson's ratios, as

$$a_{11}=\frac{1}{E_{11}},\quad a_{22}=\frac{1}{E_{22}},\quad a_{66}=\frac{1}{G_{12}}\quad \text{and}\quad a_{12}=-\frac{\nu_{12}}{E_{11}}=-\frac{\nu_{21}}{E_{22}} \tag{3.7}$$

In the subsequent analysis the following parameters are defined and used for an orthotropic material.

$$\lambda^2=\frac{a_{22}}{a_{11}}\quad ;\quad \chi=\frac{2a_{12}+a_{66}}{2a_{11}} \tag{3.8}$$

These two parameters can be calculated directly from the values of a_{11}, a_{22}, a_{12} and a_{66}.

The solution for the general case may be found by substituting Eqs.(3.4-3.6) into Eq. (3.3) and then replacing the stresses by the expressions in terms of Φ from Eqs. (3.2), giving

$$a_{11}\frac{\partial^4\Phi}{\partial y^4}-2a_{16}\frac{\partial^4\Phi}{\partial y^3\partial x}+\left(2a_{12}+a_{16}\right)\frac{\partial^4\Phi}{\partial y^2\partial x^2}-2a_{26}\frac{\partial^4\Phi}{\partial y\partial x^3}+a_{22}\frac{\partial^4\Phi}{\partial x^4}=0 \tag{3.9}$$

The solution to Eq. (3.9) can be conveniently expressed in terms of functions of a complex variable

$$z=x+\mu y \tag{3.10}$$

where $\mu=\alpha+i\beta$, α and β are real constants and $i=\sqrt{-1}$.

Now after solving the Eq.(3.9) with the help of Eq.(3.10) one can solve for the stresses near the crack tip in an anisotropic material. For Mode I failure the stress components are given as [17]

$$\sigma_x = \frac{K_I}{\sqrt{2\pi r}} \mathrm{Re}\left[\frac{\mu_1\mu_2}{\mu_1 - \mu_2}\left(\mu_2 F_2 - \mu_1 F_1\right)\right] \tag{3.11}$$

$$\sigma_y = \frac{K_I}{\sqrt{2\pi r}} \mathrm{Re}\left[\frac{1}{\mu_1 - \mu_2}\left(\mu_1 F_2 - \mu_2 F_1\right)\right] \tag{3.12}$$

$$\tau_{xy} = \frac{K_I}{\sqrt{2\pi r}} \mathrm{Re}\left[\frac{\mu_1\mu_2}{\mu_1 - \mu_2}\left(F_1 - F_2\right)\right] \tag{3.13}$$

For Mode II failure the stress components are given as [17]

$$\sigma_x = \frac{K_{II}}{\sqrt{2\pi r}} \mathrm{Re}\left[\frac{1}{\mu_1 - \mu_2}\left(\mu_2^2 F_2 - \mu_1^2 F_1\right)\right] \tag{3.14}$$

$$\sigma_y = \frac{K_I}{\sqrt{2\pi r}} \mathrm{Re}\left[\frac{1}{\mu_1 - \mu_2}\left(F_2 - F_1\right)\right] \tag{3.15}$$

$$\tau_{xy} = \frac{K_{II}}{\sqrt{2\pi r}} \mathrm{Re}\left[\frac{1}{\mu_1 - \mu_2}\left(\mu_1 F_1 - \mu_2 F_2\right)\right] \tag{3.16}$$

In Eqs.(3.11-3.16) K_I and K_{II} are respectively the Stress Intensity Factor (SIF) for Mode I failure and Mode II failure. In these equations "Re" represents the real part of the complex numbers and further, μ_1 and μ_2 are given by

$$\mu_{1,2} = \frac{i}{\sqrt{2}}\left[(\chi+\lambda)^{\frac{1}{2}} \pm (\chi-\lambda)^{\frac{1}{2}}\right] \text{ when } \chi > \lambda \tag{3.17}$$

$$\mu_{1,2} = \frac{1}{\sqrt{2}}\left[\mp(\lambda-\chi)^{\frac{1}{2}} + i(\chi+\lambda)^{\frac{1}{2}}\right] \text{ when } \chi < \lambda \tag{3.18}$$

wherein as defined before,

$$\lambda^2 = \frac{a_{22}}{a_{11}} \quad \text{and} \quad \chi = \frac{2a_{12}+a_{66}}{2a_{11}} \tag{3.19}$$

The equations for displacements in Mode I and Mode II along the crack edge of the orthotropic material are given as

$$u = \frac{K_I\sqrt{2\pi r}}{\pi}\text{Re}\left[\frac{1}{\mu_1-\mu_2}\left(\frac{\mu_1 p_2}{F_2}-\frac{\mu_2 p_1}{F_1}\right)\right] \tag{3.20}$$

$$v = \frac{K_I\sqrt{2\pi r}}{\pi}\text{Re}\left[\frac{1}{\mu_1-\mu_2}\left(\frac{\mu_1 q_2}{F_2}-\frac{\mu_2 q_1}{F_1}\right)\right] \tag{3.21}$$

$$u = \frac{K_{II}\sqrt{2\pi r}}{\pi}\text{Re}\left[\frac{1}{\mu_1-\mu_2}\left(\frac{p_2}{F_2}-\frac{p_1}{F_1}\right)\right] \tag{3.22}$$

$$v = \frac{K_{II}\sqrt{2\pi r}}{\pi}\text{Re}\left[\frac{1}{\mu_1-\mu_2}\left(\frac{q_2}{F_2}-\frac{q_1}{F_1}\right)\right] \tag{3.23}$$

where

$$p_{1,2} = \mu^2{}_{1,2}a_{11} + a_{12} - \mu_{1,2}a_{16} \tag{3.24}$$

$$q_{1,2} = \mu_{1,2}a_{12} + \frac{a_{22}}{\mu_{1,2}} - a_{26} \tag{3.25}$$

3.2.1 Stress Intensity Factor

The behavior of composite laminates with stress raisers such as cracks is of great interest in design because of the resulting strength reduction and life reduction due to damage growth around these stress raisers.

Through-thickness cracks introduce much more severe stress concentrations in composite laminates. Stress distributions near a crack tip in an orthotropic material have been obtained in terms of Mode I and Mode II Stress Intensity Factors and the laminate compliances [113]. An expression for the stress distribution ahead of the crack shown in Figure 3.1 is given by

$$\begin{aligned} \sigma_y &= \frac{\sigma_{ap}|x|}{\sqrt{x^2 - a^2}} \qquad |x| > a, \\ &= 0 \qquad\qquad\quad |x| < a. \end{aligned} \tag{3.26}$$

where

σ_y = Axial stress along transverse axis

σ_{ap} = Applied far-field stress

a = Half crack length

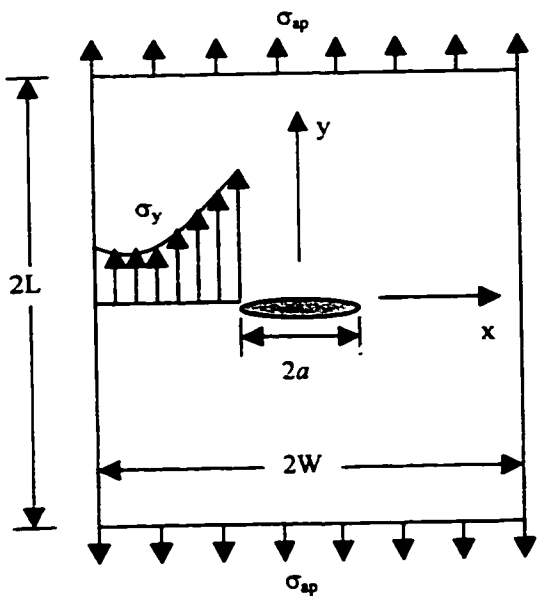

Figure 3.1 Composite laminate with a central crack under uniaxial tensile loading

By using the distance, r, from the crack tip, i.e., $r = |x - a|$, it can be seen that Eq.(3.26) has singularities of type $r^{-\frac{1}{2}}$ at the crack tips and if r is sufficiently smaller than the half crack length, the stress σ_y can be approximated by

$$\sigma_y = \frac{K_I}{\sqrt{2\pi r}} \tag{3.27}$$

where K_I is the stress intensity factor, which in the case of a center crack in an infinite plate of very large width, is given by

$$K_I = \sigma_{ap}\sqrt{\pi a} \tag{3.28}$$

In the case of a rectangular plate with a center crack, as shown in Figure 3.1, the SIF is given by

$$K_I = F\left(\frac{a}{W}, \frac{L}{W}\right)\sigma_{ap}\sqrt{\pi a} \tag{3.29}$$

where W and L are the half-width and half-length of the rectangular plate respectively. $F(a/W,L/W)$ is a non-dimensional factor which is a function of the aspect ratios a/W and L/W.

Eqs.(3.26-3.29) indicate the important points in the linear elastic fracture mechanics that the loading conditions and geometries have a direct effect on the stress intensity factor, but that the stress distributions near the crack tip are identical, independent of the finite boundary conditions. The SIF gives the intensity of the stress field near the crack tip, which is a characteristic of the material.

3.2.2 Strain Energy Release Rate

The strain energy release rate G, of collinear crack extension under general loading for Mode I and Mode II can be written as [17]

$$G_I = \frac{1}{2}\pi f_n(0)g_n(\pi)\ ;\ G_{II} = \frac{1}{2}\pi f_s(0)g_s(\pi) \tag{3.30}$$

Now using Eq.(3.30) and the relationships for f and g from Eqs.(3.11-3.16), and Eqs.(3.20-3.23) for Mode I, one can write that

$$f_n(0) = \frac{K_I}{\sqrt{2\pi}} \tag{3.31}$$

$$g_n(\pi)=-\frac{\sqrt{2\pi}}{\pi}\left[K_I\,Im\left(\frac{\mu_2 p_2-\mu_2 p_1}{\mu_1-\mu_2}\right)+K_{II}\,Im\left(\frac{q_2-q_1}{\mu_1-\mu_2}\right)\right] \tag{3.32}$$

and similarly, for Mode II,

$$f_s(0)=\frac{K_{II}}{\sqrt{2\pi}} \tag{3.33}$$

$$g_s(\pi)=-\frac{\sqrt{2\pi}}{\pi}\left[K_I\,Im\left(\frac{\mu_1 p_2-\mu_2 p_1}{\mu_1-\mu_2}\right)+K_{II}\,Im\left(\frac{p_2-p_1}{\mu_1-\mu_2}\right)\right] \tag{3.34}$$

Substituting the value of $p_{1,2}$ and $q_{1,2}$ from Eqs.(3.24-3.25) into Eqs.(3.32-3.34) it is obtained that

$$g_n(\pi)=-\frac{\sqrt{2\pi}}{\pi}a_{22}\,Im\left[\frac{K_I(\mu_1+\mu_2)+K_{II}}{\mu_1\mu_2}\right] \tag{3.35}$$

$$g_s(\pi)=\frac{\sqrt{2\pi}}{\pi}a_{11}\,Im[K_{II}(\mu_1+\mu_2)+K_I\mu_1\mu_2] \tag{3.36}$$

Now Eq.(3.30) can be rewritten using Eqs.(3.35-3.36) for Mode I as

$$G_I=-a_{22}K_I\frac{1}{2}Im\left[\frac{K_I(\mu_1+\mu_2)+K_{II}}{\mu_1\mu_2}\right] \tag{3.37}$$

and for Mode II as

$$G_{II}=a_{11}K_{II}\frac{1}{2}Im[K_{II}(_1+\mu_2)+K_I\mu_{12}] \tag{3.38}$$

For orthotropic case, from Eqs.(3.17-3.18) it can be written that

$$\mu_1+\mu_2=i\sqrt{2}(\chi+\lambda)^{\frac{1}{2}}\ ;\ \mu_1\mu_2=-\lambda \tag{3.39}$$

By substituting Eq.(3.39) into Eqs.(3.37-3.38) the strain energy release rate for orthotropic material can be written for Mode I and Mode II as

$$G_I = K_I^2 a_{22}\left[\frac{(\chi+\lambda)^{\frac{1}{2}}}{\sqrt{2\lambda}}\right] \quad ; \quad G_{II} = K_{II}^2 a_{11}\left[\frac{(\chi+\lambda)^{\frac{1}{2}}}{\sqrt{2}}\right] \tag{3.40}$$

3.3 Finite Element Analysis for Fracture

The displacement extrapolation method and the strain energy release rate method are the most commonly used methods that use the Finite Element Analysis as a basis for the calculation of Stress Intensity Factor for orthotropic materials.

3.3.1 Displacement Extrapolation Method

The equation for displacements for Mode I and Mode II along the crack edge in the orthotropic material are given by Eqs.(3.20-3.23). Re-arranging these four equations for Mode I and Mode II, the stress intensity factor can be expressed in terms of displacements u and v as

$$K_I\begin{bmatrix}\mathrm{Re}\left[\frac{1}{\mu_1-\mu_2}\left(\frac{\mu_1 p_2}{F_2}-\frac{\mu_2 p_1}{F_1}\right)\right]\\ \mathrm{Re}\left[\frac{1}{\mu_1-\mu_2}\left(\frac{\mu_1 q_2}{F_2}-\frac{\mu_2 q_1}{F_1}\right)\right]\end{bmatrix} = \frac{\pi}{\sqrt{2\pi r}}\begin{Bmatrix}u\\ v\end{Bmatrix} \tag{3.41}$$

$$K_{II}\begin{bmatrix} \mathrm{Re}\left[\frac{1}{\mu_1-\mu_2}\left(\frac{p_2}{F_2}-\frac{p_1}{F_1}\right)\right] \\ \mathrm{Re}\left[\frac{1}{\mu_1-\mu_2}\left(\frac{q_2}{F_2}-\frac{q_1}{F_1}\right)\right] \end{bmatrix} = \frac{\pi}{\sqrt{2\pi r}}\begin{Bmatrix} u \\ v \end{Bmatrix} \tag{3.42}$$

For radial angle θ equal to $\pm\pi$, F_1 and F_2 are both equal to $-i$ and so the first component in the Equations (3.41 - 3.42) becomes zero. In that case the SIF for Mode I and Mode II can be calculated only from the second component of each of the Eqs. (3.41-3.42) respectively.

Thus the SIF can be calculated according to the procedure described in the Chapter 2 (Section 2.3.1) and by using Eqs.(3.41-3.42).

3.3.2 Strain Energy Release Rate Method

The Strain Energy Release Rate G for orthotropic materials is given by [17]

$$G_I = K_I^2 a_{22}\left[\frac{(\chi+\lambda)^{\frac{1}{2}}}{\sqrt{2\lambda}}\right] \tag{3.43}$$

$$G_{II} = K_{II}^2 a_{11}\left[\frac{(\chi+\lambda)^{\frac{1}{2}}}{\sqrt{2}}\right] \tag{3.44}$$

From G, the stress intensity factor is calculated using Eqs.(3.43-3.44) as

$$K_I = \left(\frac{\sqrt{2\lambda} G_I}{a_{11}(\chi+\lambda)^{\frac{1}{2}}} \right)^{\frac{1}{2}}; \qquad K_{II} = \left(\frac{\sqrt{2} G_I}{a_{11}(\chi+\lambda)^{\frac{1}{2}}} \right)^{\frac{1}{2}} \tag{3.45}$$

in which K_I and K_{II} are the SIF under Mode I and Mode II respectively.

Thus the SIF for orthotropic materials can be evaluated by the procedure similar to that described in Chapter 2 (Section 2.3.2) and using Eq.(3.45.)

3.4 Elasticity Matrix for Composite Laminates

In the following sections, the aspects of laminate theory that are relevant to the present thesis are summarized. The presentation follows that of Ref.[114] and Ref.[115]. For clarity, continuity and brevity, the information is given in sufficient detail.

3.4.1 Aspects of Laminate Theory

For fiber-reinforced composite materials, if all the three stresses σ_1, σ_2 and σ_3 are applied simultaneously as shown in Figure 3.2, the matrix of normal strains as a result of the combined effects can be written as [114]

$$\begin{Bmatrix} \varepsilon_1 \\ \varepsilon_2 \\ \varepsilon_3 \end{Bmatrix} = \begin{bmatrix} \frac{1}{E_1} & \frac{-\nu_{21}}{E_2} & \frac{-\nu_{31}}{E_3} \\ \frac{-\nu_{12}}{E_1} & \frac{1}{E_2} & \frac{-\nu_{32}}{E_3} \\ \frac{-\nu_{13}}{E_1} & \frac{-\nu_{23}}{E_2} & \frac{1}{E_3} \end{bmatrix} \begin{Bmatrix} \sigma_1 \\ \sigma_2 \\ \sigma_3 \end{Bmatrix} \tag{3.46}$$

where E_1, E_2, and E_3 are the elastic modulus in the 1, 2 and 3 directions respectively, and ν_{12}, ν_{21}, ν_{31}, etc. are the Poisson's ratios. The first subscript of Poisson's ratios refers to the direction of applied tensile stress and the resulting extensional strain. The second subscript refers to the direction of contraction.

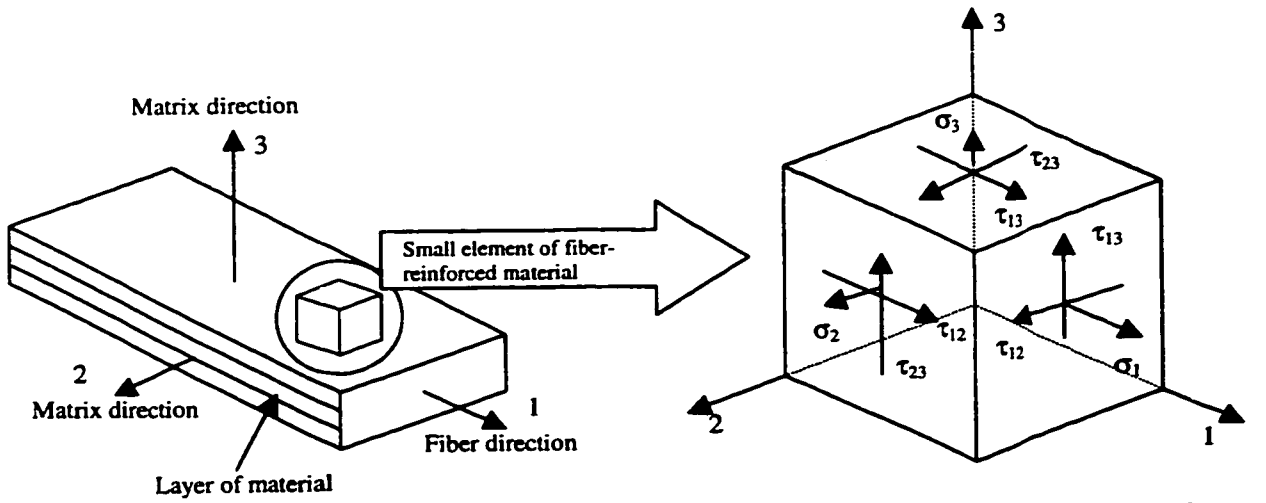

Figure 3.2 Stresses acting on a small element of fiber-reinforced composite material

The engineering shear strains are given by

$$\begin{Bmatrix} \gamma_{23} \\ \gamma_{13} \\ \gamma_{12} \end{Bmatrix} = \begin{bmatrix} \frac{1}{G_{23}} & 0 & 0 \\ 0 & \frac{1}{G_{13}} & 0 \\ 0 & 0 & \frac{1}{G_{12}} \end{bmatrix} \begin{Bmatrix} \tau_{23} \\ \tau_{13} \\ \tau_{12} \end{Bmatrix} \tag{3.47}$$

where τ_{23}, τ_{13}, and τ_{12} are the applied shearing stresses and further, G_{23}, G_{13}, and G_{12} are the shear modulus in the 2-3 plane, 1-3 plane and 1-2 plane respectively.

All the relationships between the stresses and strains take the collective form

$$\begin{Bmatrix} \varepsilon_1 \\ \varepsilon_2 \\ \varepsilon_3 \\ \gamma_{23} \\ \gamma_{13} \\ \gamma_{12} \end{Bmatrix} = \begin{bmatrix} \frac{1}{E_1} & \frac{-\nu_{21}}{E_2} & \frac{-\nu_{31}}{E_3} & 0 & 0 & 0 \\ \frac{-\nu_{12}}{E_1} & \frac{1}{E_2} & \frac{-\nu_{32}}{E_3} & 0 & 0 & 0 \\ \frac{-\nu_{13}}{E_1} & \frac{-\nu_{23}}{E_2} & \frac{1}{E_3} & 0 & 0 & 0 \\ 0 & 0 & 0 & \frac{1}{G_{23}} & 0 & 0 \\ 0 & 0 & 0 & 0 & \frac{1}{G_{13}} & 0 \\ 0 & 0 & 0 & 0 & 0 & \frac{1}{G_{12}} \end{bmatrix} \begin{Bmatrix} \sigma_1 \\ \sigma_2 \\ \sigma_3 \\ \tau_{23} \\ \tau_{13} \\ \tau_{12} \end{Bmatrix} \tag{3.48}$$

The square six-by-six matrix of material properties is called the compliance matrix, commonly denoted by S. In terms of S, the stress-strain relations are written as

$$\begin{Bmatrix} \varepsilon_1 \\ \varepsilon_2 \\ \varepsilon_3 \\ \gamma_{23} \\ \gamma_{13} \\ \gamma_{12} \end{Bmatrix} = \begin{bmatrix} S_{11} & S_{12} & S_{13} & 0 & 0 & 0 \\ S_{21} & S_{22} & S_{23} & 0 & 0 & 0 \\ S_{31} & S_{32} & S_{33} & 0 & 0 & 0 \\ 0 & 0 & 0 & S_{44} & 0 & 0 \\ 0 & 0 & 0 & 0 & S_{55} & 0 \\ 0 & 0 & 0 & 0 & 0 & S_{66} \end{bmatrix} \begin{Bmatrix} \sigma_1 \\ \sigma_2 \\ \sigma_3 \\ \tau_{23} \\ \tau_{13} \\ \tau_{12} \end{Bmatrix} \tag{3.49}$$

The inverse of the compliance matrix given by Eq.(3.49) is called the stiffness matrix, sometimes known as the modulus matrix or elasticity matrix, and is commonly denoted by C. The inverse matrix always exists due to the symmetry property of the compliance matrix. With the inverse defined, the stress-strain relations become

$$\begin{Bmatrix}\sigma_1\\ \sigma_2\\ \sigma_3\\ \tau_{23}\\ \tau_{13}\\ \tau_{12}\end{Bmatrix}=\begin{bmatrix}C_{11} & C_{12} & C_{13} & 0 & 0 & 0\\ C_{21} & C_{22} & C_{23} & 0 & 0 & 0\\ C_{31} & C_{32} & C_{33} & 0 & 0 & 0\\ 0 & 0 & 0 & C_{44} & 0 & 0\\ 0 & 0 & 0 & 0 & C_{55} & 0\\ 0 & 0 & 0 & 0 & 0 & C_{66}\end{bmatrix}\begin{Bmatrix}\varepsilon_1\\ \varepsilon_2\\ \varepsilon_3\\ \gamma_{23}\\ \gamma_{13}\\ \gamma_{12}\end{Bmatrix} \tag{3.50}$$

For shorthand notation, the relations between stresses and strains will be written as

$$\{\varepsilon\}_1=[S]\{\sigma\}_1, \text{ and } \{\sigma\}_1=[C]\{\varepsilon\}_1 \tag{3.51}$$

The subscript 1 outside the bracket means that the stresses and strains are referred to the 1-2-3 coordinate system.

According to the Maxwell-Betti Reciprocal Theorem[114]

$$\frac{\nu_{12}}{E_1}=\frac{\nu_{21}}{E_2} \tag{3.52}$$

In a similar manner

$$\frac{\nu_{13}}{E_1}=\frac{\nu_{31}}{E_3}, \qquad \frac{\nu_{23}}{E_2}=\frac{\nu_{32}}{E_3} \tag{3.53}$$

As a result, the compliance matrix given by Eq.(3.49), and the stiffness matrix given by Eq.(3.40) are symmetric i.e., $S_{ij} = S_{ji}$ and $C_{ij} = C_{ji}$. The symmetry of these two matrices is an important property.

After incorporating the reciprocity relation, the [S] and [C] matrices of Eqs.(3.49-3.50) become as

$$\begin{Bmatrix} \varepsilon_1 \\ \varepsilon_2 \\ \varepsilon_3 \\ \gamma_{23} \\ \gamma_{13} \\ \gamma_{12} \end{Bmatrix} = \begin{bmatrix} S_{11} & S_{12} & S_{13} & 0 & 0 & 0 \\ S_{12} & S_{22} & S_{23} & 0 & 0 & 0 \\ S_{13} & S_{23} & S_{33} & 0 & 0 & 0 \\ 0 & 0 & 0 & S_{44} & 0 & 0 \\ 0 & 0 & 0 & 0 & S_{55} & 0 \\ 0 & 0 & 0 & 0 & 0 & S_{66} \end{bmatrix} \begin{Bmatrix} \sigma_1 \\ \sigma_2 \\ \sigma_3 \\ \tau_{23} \\ \tau_{13} \\ \tau_{12} \end{Bmatrix} \tag{3.54}$$

In the above equation

$$\begin{aligned} S_{11} &= \frac{1}{E_1}, \quad S_{12} = -\frac{\nu_{12}}{E_1}, \quad S_{13} = -\frac{\nu_{13}}{E_1} \\ S_{22} &= \frac{1}{E_2}, \quad S_{23} = -\frac{\nu_{23}}{E_2}, \quad S_{33} = \frac{1}{E_3} \\ S_{44} &= \frac{1}{G_{23}}, \quad S_{55} = \frac{1}{G_{13}}, \quad S_{66} = \frac{1}{G_{12}} \end{aligned} \tag{3.55}$$

and

$$\begin{Bmatrix} \sigma_1 \\ \sigma_2 \\ \sigma_3 \\ \tau_{23} \\ \tau_{13} \\ \tau_{12} \end{Bmatrix} = \begin{bmatrix} C_{11} & C_{12} & C_{13} & 0 & 0 & 0 \\ C_{12} & C_{22} & C_{23} & 0 & 0 & 0 \\ C_{13} & C_{23} & C_{33} & 0 & 0 & 0 \\ 0 & 0 & 0 & C_{44} & 0 & 0 \\ 0 & 0 & 0 & 0 & C_{55} & 0 \\ 0 & 0 & 0 & 0 & 0 & C_{66} \end{bmatrix} \begin{Bmatrix} \varepsilon_1 \\ \varepsilon_2 \\ \varepsilon_3 \\ \gamma_{23} \\ \gamma_{13} \\ \gamma_{12} \end{Bmatrix} \tag{3.56}$$

In terms of the compliances, the components of the [C] matrix are given by

$$
\begin{aligned}
C_{11} &= \frac{S_{22}S_{33} - S_{23}S_{23}}{S} & C_{12} &= \frac{S_{13}S_{23} - S_{12}S_{33}}{S} & C_{44} &= \frac{1}{S_{44}} \\
C_{22} &= \frac{S_{33}S_{11} - S_{13}S_{13}}{S} & C_{13} &= \frac{S_{12}S_{23} - S_{13}S_{22}}{S} & C_{55} &= \frac{1}{S_{55}} \\
C_{33} &= \frac{S_{11}S_{22} - S_{12}S_{12}}{S} & C_{23} &= \frac{S_{12}S_{13} - S_{23}S_{11}}{S} & C_{66} &= \frac{1}{S_{66}}
\end{aligned}
\tag{3.57}
$$

where

$$
S = S_{11}S_{22}S_{33} - S_{11}S_{23}S_{23} - S_{22}S_{13}S_{13} - S_{33}S_{12}S_{12} + 2S_{12}S_{23}S_{13} \tag{3.58}
$$

3.4.2 Plane Stress Case

An important assumption in the development of the mechanics of fiber-reinforced materials is the Plane Stress assumption, which is based on the manner in which fiber-reinforced composite materials are used in many structures. Specifically beams, plates, cylinders, and other structural shapes that have at least one characteristic geometric dimension, which is an order of magnitude less than the other two dimensions belong to this case. With a plate, for example, the stresses in the plane of the plate are much larger than the stresses perpendicular to that plane.

A thin, unidirectional lamina is assumed to be under a state of plane stress; therefore, the stresses σ_3, τ_{23}, and τ_{13} are set to zero in Eqs.(3.54-3.56). First considering the Eq.(3.54),

$$\begin{Bmatrix} \varepsilon_1 \\ \varepsilon_2 \\ \varepsilon_3 \\ \gamma_{23} \\ \gamma_{13} \\ \gamma_{12} \end{Bmatrix} = \begin{bmatrix} S_{11} & S_{12} & S_{13} & 0 & 0 & 0 \\ S_{12} & S_{22} & S_{23} & 0 & 0 & 0 \\ S_{13} & S_{23} & S_{33} & 0 & 0 & 0 \\ 0 & 0 & 0 & S_{44} & 0 & 0 \\ 0 & 0 & 0 & 0 & S_{55} & 0 \\ 0 & 0 & 0 & 0 & 0 & S_{66} \end{bmatrix} \begin{Bmatrix} \sigma_1 \\ \sigma_2 \\ 0 \\ 0 \\ 0 \\ \tau_{12} \end{Bmatrix} \tag{3.59}$$

From this it is obvious that

$$\gamma_{23} = 0 \quad \text{and} \quad \gamma_{13} = 0 \tag{3.60}$$

and the Poisson's effect is given by

$$\varepsilon_3 = S_{13}\sigma_1 + S_{23}\sigma_2 \tag{3.61}$$

Due to the fact that ε_3 is not zero, the plane stress assumption leads to a relation involving only $\varepsilon_1, \varepsilon_2, \gamma_{12}$ and $\sigma_1, \sigma_2, \tau_{12}$. By eliminating the third, fourth and fifth rows and columns of Eq.(3.59), one gets

$$\begin{Bmatrix} \varepsilon_1 \\ \varepsilon_2 \\ \gamma_{12} \end{Bmatrix} = \begin{bmatrix} S_{11} & S_{12} & 0 \\ S_{12} & S_{22} & 0 \\ 0 & 0 & S_{66} \end{bmatrix} \begin{Bmatrix} \sigma_1 \\ \sigma_2 \\ \tau_{12} \end{Bmatrix} \tag{3.62}$$

where the components of the [S] matrix are

$$S_{11} = \frac{1}{E_1}, \quad S_{12} = -\frac{\nu_{12}}{E_1} = -\frac{\nu_{21}}{E_2}, \quad S_{22} = \frac{1}{E_2}, \quad S_{66} = \frac{1}{G_{12}} \tag{3.63}$$

The 3×3 matrix of compliance is called the Reduced Compliance Matrix. Now considering the Eq.(3.56),

$$\begin{Bmatrix} \sigma_1 \\ \sigma_2 \\ 0 \\ 0 \\ 0 \\ \tau_{12} \end{Bmatrix} = \begin{bmatrix} C_{11} & C_{12} & C_{13} & 0 & 0 & 0 \\ C_{12} & C_{22} & C_{23} & 0 & 0 & 0 \\ C_{13} & C_{23} & C_{33} & 0 & 0 & 0 \\ 0 & 0 & 0 & C_{44} & 0 & 0 \\ 0 & 0 & 0 & 0 & C_{55} & 0 \\ 0 & 0 & 0 & 0 & 0 & C_{66} \end{bmatrix} \begin{Bmatrix} \varepsilon_1 \\ \varepsilon_2 \\ \varepsilon_3 \\ \gamma_{23} \\ \gamma_{13} \\ \gamma_{12} \end{Bmatrix} \tag{3.64}$$

and the plane stress condition described above , one can conclude that

$$\gamma_{23} = 0 \qquad \gamma_{13} = 0 \tag{3.65}$$

and

$$0 = C_{13}\varepsilon_1 + C_{23}\varepsilon_2 + C_{33}\varepsilon_3 \tag{3.66}$$

After rearranging, Eq.(3.66) becomes

$$\varepsilon_3 = -\frac{C_{13}}{C_{33}}\varepsilon_1 - \frac{C_{23}}{C_{33}}\varepsilon_2 \tag{3.67}$$

This relationship also indicates that in the state of plane stress ε_3 exists and it can be computed by knowing ε_1 and ε_2. It may be noted here that $C_{33} \neq 0$.

The Eq.(3.64) cannot be reduced directly to obtain a relation involving only $\sigma_1, \sigma_2, \tau_{12}$ and $\varepsilon_1\ \varepsilon_2, \gamma_{12}$ by simply eliminating rows and columns.

However Eq.(3.67) can be used as follows: From Eq.(3.64), the expressions for σ_1 and σ_2 are

$$\sigma_1 = C_{11}\varepsilon_1 + C_{12}\varepsilon_2 + C_{13}\varepsilon_3 \tag{3.68}$$

$$\sigma_2 = C_{12}\varepsilon_1 + C_{22}\varepsilon_2 + C_{23}\varepsilon_3 \tag{3.69}$$

Substituting the value of ε_3 and using Eq.(3.67) into the Eqs.(3.68-3.69) gives

$$\sigma_1 = C_{11}\varepsilon_1 + C_{12}\varepsilon_2 + C_{13}\left(-\frac{C_{13}}{C_{33}}\varepsilon_1 - \frac{C_{23}}{C_{33}}\varepsilon_2\right)$$

$$= \left(C_{11} - \frac{C_{13}^2}{C_{33}}\right)\varepsilon_1 + \left(C_{22} - \frac{C_{13}C_{23}}{C_{33}}\right)\varepsilon_2 \tag{3.70}$$

and

$$\sigma_2 = C_{12}\varepsilon_1 + C_{22}\varepsilon_2 + C_{23}\left(-\frac{C_{13}}{C_{33}}\varepsilon_1 - \frac{C_{23}}{C_{33}}\varepsilon_2\right)$$

$$= \left(C_{12} - \frac{C_{13}C_{23}}{C_{33}}\right)\varepsilon_1 + \left(C_{22} - \frac{C_{23}^2}{C_{33}}\right)\varepsilon_2 \tag{3.71}$$

Including the shear stress-shear strain relation, the relation between stresses and strains for the state of plane stress is written as

$$\begin{Bmatrix}\sigma_1\\ \sigma_2\\ \tau_{12}\end{Bmatrix} = \begin{bmatrix}Q_{11} & Q_{12} & 0\\ Q_{12} & Q_{22} & 0\\ 0 & 0 & Q_{66}\end{bmatrix}\begin{Bmatrix}\varepsilon_1\\ \varepsilon_2\\ \gamma_{12}\end{Bmatrix} \tag{3.72}$$

Here the [Q] matrix is called the Reduced Stiffness Matrix and the components of [Q] matrix can be calculated by using Eqs.(3.70-3.71) and Eq.(3.64), as

$$
\begin{aligned}
Q_{11} &= C_{11} - \frac{C_{13}^2}{C_{33}} \\
Q_{12} &= C_{12} - \frac{C_{13}C_{23}}{C_{33}} \\
Q_{22} &= C_{22} - \frac{C_{23}^2}{C_{33}} \\
Q_{66} &= C_{66}
\end{aligned}
\tag{3.73}
$$

By inverting Eq.(3.62) and comparing it with Eq.(3.72) leads to

$$
\begin{aligned}
Q_{11} &= \frac{S_{22}}{S_{11}S_{22} - S_{12}^2} \\
Q_{12} &= -\frac{S_{12}}{S_{11}S_{22} - S_{12}^2} \\
Q_{22} &= \frac{S_{11}}{S_{11}S_{22} - S_{12}^2} \\
Q_{66} &= \frac{1}{S_{66}}
\end{aligned}
\tag{3.74}
$$

Now substituting the values of S_{ij} from Eq.(3.63) into the Eq.(3.74) leads to

$$
\begin{aligned}
Q_{11} &= \frac{E_1}{1 - \nu_{12}\nu_{21}} \\
Q_{12} &= \frac{\nu_{12}E_2}{1 - \nu_{12}\nu_{21}} = \frac{\nu_{21}E_1}{1 - \nu_{12}\nu_{21}} \\
Q_{22} &= \frac{E_2}{1 - \nu_{12}\nu_{21}} \\
Q_{66} &= G_{12}
\end{aligned}
\tag{3.75}
$$

3.4.3 Transformation of Stress and Strain

In many cases, the lamina principal axes (1,2) do not coincide with the loading or global axes (x,y) which is shown in Figure 3.3.

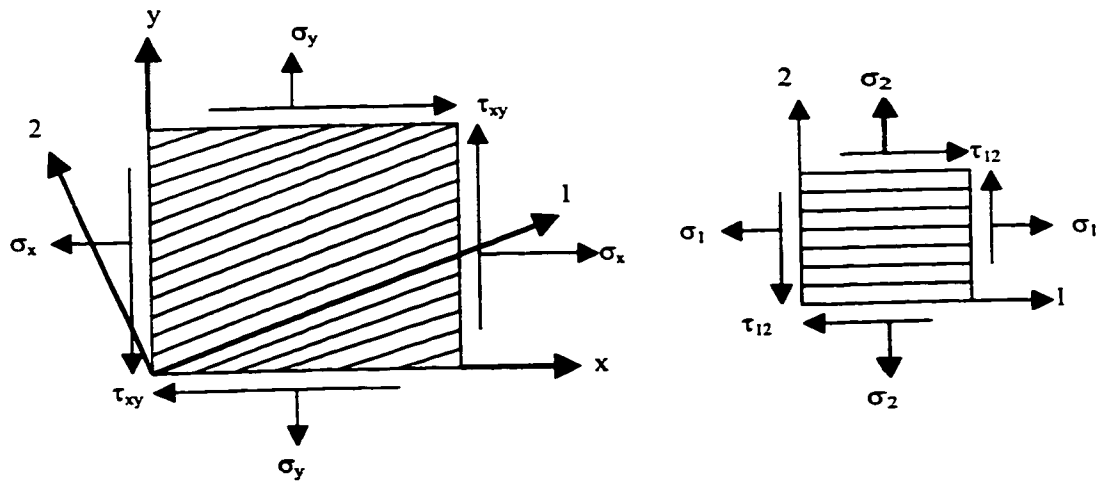

Figure 3.3 Stress components in unidirectional ply referred to global and material axes

The stress and strain components referred to the principal material axes (1,2) can be expressed in terms of those referred to the global axes (x,y) by the following transformation relation

$$\begin{Bmatrix} \sigma_1 \\ \sigma_2 \\ \tau_{12} \end{Bmatrix} = [T] \begin{Bmatrix} \sigma_x \\ \sigma_y \\ \tau_{xy} \end{Bmatrix} \tag{3.76}$$

and

$$\begin{Bmatrix} \varepsilon_1 \\ \varepsilon_2 \\ \frac{1}{2}\gamma_{12} \end{Bmatrix} = [T] \begin{Bmatrix} \varepsilon_x \\ \varepsilon_y \\ \frac{1}{2}\gamma_{xy} \end{Bmatrix} \tag{3.77}$$

Note that the tensor shear strain, ε_{xy}, not the engineering shear strain is used in the above equation and further, the relations between them are $\varepsilon_{12} = \frac{1}{2}\gamma_{12}$ and $\varepsilon_{xy} = \frac{1}{2}\gamma_{xy}$.

The transformation matrix [T] is given by

$$[T]=\begin{bmatrix} m^2 & n^2 & 2mn \\ n^2 & m^2 & -2mn \\ -mn & mn & m^2-n^2 \end{bmatrix} \tag{3.78}$$

where, $m=\cos\theta$ and $n=\sin\theta$. The angle θ is measured positive counterclockwise from the x-axis to the 1-axis.

By inversion of Eqs.(3.76 –3.77) the following equation is obtained.

$$\begin{Bmatrix} \sigma_x \\ \sigma_y \\ \tau_{xy} \end{Bmatrix}=[T]^{-1}\begin{Bmatrix} \sigma_1 \\ \sigma_2 \\ \tau_{12} \end{Bmatrix} \tag{3.79}$$

Further,

$$\begin{Bmatrix} \varepsilon_x \\ \varepsilon_y \\ \frac{1}{2}\gamma_{xy} \end{Bmatrix}=[T]^{-1}\begin{Bmatrix} \varepsilon_1 \\ \varepsilon_2 \\ \frac{1}{2}\gamma_{12} \end{Bmatrix} \tag{3.80}$$

where

$$[T]^{-1}=\begin{bmatrix} m^2 & n^2 & -2mn \\ n^2 & m^2 & 2mn \\ mn & -mn & m^2-n^2 \end{bmatrix} \tag{3.81}$$

Now considering Eq.(3.62) in a slightly modified form to account for the use of the tensor shear strain rather than the engineering shear strain as

$$\begin{Bmatrix} \varepsilon_1 \\ \varepsilon_2 \\ \frac{1}{2}\gamma_{12} \end{Bmatrix} = \begin{bmatrix} S_{11} & S_{12} & 0 \\ S_{12} & S_{22} & 0 \\ 0 & 0 & \frac{1}{2}S_{66} \end{bmatrix} \begin{Bmatrix} \sigma_1 \\ \sigma_2 \\ \tau_{12} \end{Bmatrix} \tag{3.82}$$

Using the transformations given by Eqs.(3.79 –3.80) in Eq.(3.82) leads to

$$[T]\begin{Bmatrix} \varepsilon_x \\ \varepsilon_{2y} \\ \frac{1}{2}\gamma_{xy} \end{Bmatrix} = \begin{bmatrix} S_{11} & S_{12} & 0 \\ S_{12} & S_{22} & 0 \\ 0 & 0 & \frac{1}{2}S_{66} \end{bmatrix} [T] \begin{Bmatrix} \sigma_x \\ \sigma_y \\ \tau_{xy} \end{Bmatrix} \tag{3.83}$$

and multiplying both sides of Eq.(3.83) by $[T]^{-1}$ gives

$$\begin{Bmatrix} \varepsilon_x \\ \varepsilon_{2y} \\ \frac{1}{2}\gamma_{xy} \end{Bmatrix} = [T]^{-1} \begin{bmatrix} S_{11} & S_{12} & 0 \\ S_{12} & S_{22} & 0 \\ 0 & 0 & \frac{1}{2}S_{66} \end{bmatrix} [T] \begin{Bmatrix} \sigma_x \\ \sigma_y \\ \tau_{xy} \end{Bmatrix} \tag{3.84}$$

Substituting for [T] and $[T]^{-1}$ from Eqs.(3.78–3.81) and from Eq.(3.73) it is found that by multiplying these three matrices together and multiplying the third row throughout by a factor of 2, one can get the following equation.

$$\begin{Bmatrix} \varepsilon_x \\ \varepsilon_y \\ \gamma_{xy} \end{Bmatrix} = \begin{bmatrix} \bar{S}_{11} & \bar{S}_{12} & \bar{S}_{16} \\ \bar{S}_{12} & \bar{S}_{22} & \bar{S}_{26} \\ \bar{S}_{16} & \bar{S}_{26} & \bar{S}_{66} \end{bmatrix} \begin{Bmatrix} \sigma_x \\ \sigma_y \\ \tau_{xy} \end{Bmatrix} \tag{3.85}$$

The $\bar{S}_{ij}$ are called the transformed reduced compliances and are defined by

$$
\begin{aligned}
\bar{S}_{11} &= S_{11}m^4 + (2S_{12} + S_{66})n^2m^2 + S_{22}n^4 \\
\bar{S}_{12} &= (S_{11} + S_{22} - S_{66})n^2m^2 + S_{12}(n^4 + m^4) \\
\bar{S}_{16} &= (2S_{11} - 2S_{12} - S_{66})nm^3 - (2S_{22} - 2S_{12} - S_{66})n^3m \\
\bar{S}_{22} &= S_{11}n^4 + (2S_{12} + S_{66})n^2m^2 + S_{22}m^4 \\
\bar{S}_{26} &= (2S_{11} - 2S_{12} - S_{66})n^3m - (2S_{22}2S_{12} - S_{66})nm^3 \\
\bar{S}_{66} &= 2(2S_{11} + 2S_{22} - 4S_{12} - S_{66})n^2m^2 + S_{66}(n^4 + m^4)
\end{aligned}
\tag{3.86}
$$

Now by the similar procedure the inverse of the Eq.(3.85) can be derived as

$$
\begin{Bmatrix} \sigma_x \\ \sigma_y \\ \tau_{xy} \end{Bmatrix} = \begin{bmatrix} \bar{Q}_{11} & \bar{Q}_{12} & \bar{Q}_{16} \\ \bar{Q}_{12} & \bar{Q}_{22} & \bar{Q}_{26} \\ \bar{Q}_{16} & \bar{Q}_{26} & \bar{Q}_{66} \end{bmatrix} \begin{Bmatrix} \varepsilon_x \\ \varepsilon_y \\ \gamma_{xy} \end{Bmatrix} \tag{3.87}
$$

The $\bar{Q}_{ij}$ are called the transformed reduced stiffnesses, and are defined by

$$
\begin{aligned}
\bar{Q}_{11} &= Q_{11}m^4 + 2(Q_{12} + 2Q_{66})n^2m^2 + Q_{22}n^4 \\
\bar{Q}_{12} &= (Q_{11} + Q_{22} - 4Q_{66})n^2m^2 + Q_{12}(n^4 + m^4) \\
\bar{Q}_{16} &= (Q_{11} - Q_{12} - 2Q_{66})nm^3 + (Q_{12} - Q_{22} + 2Q_{66})n^3m \\
\bar{Q}_{22} &= Q_{11}n^4 + 2(Q_{12} + 2Q_{66})n^2m^2 + Q_{22}m^4 \\
\bar{Q}_{26} &= (Q_{11} - Q_{12} - 2Q_{66})n^3m + (Q_{12} - Q_{22} + 2Q_{66})nm^3 \\
\bar{Q}_{66} &= (Q_{11} + Q_{22} - 2Q_{12} - 2Q_{66})n^2m^2 + Q_{66}(n^4 + m^4)
\end{aligned}
\tag{3.88}
$$

3.4.4 Laminate Stiffness Matrix

The overall behavior of a multidirectional laminate is a function of the properties and stacking sequence of the individual layers. The classical laminate theory predicts the behavior of the laminate within the framework of the following assumptions:

1. Each layer (lamina) of the laminate is quasi-homogeneous and orthotropic.
2. The laminate and its layers are in a state of plane stress
3. All displacements are small compared with the thickness of the laminate.
4. Displacements are continuous throughout the laminate.
5. In-plane displacements vary linearly through the thickness of the laminate.
6. Straight lines normal to middle surface remain straight and normal to that surface after deformation.
7. Strain-displacement and strain-stress relations are linear.
8. Normal distances from the middle surface remain constant, i.e., the transverse normal strain is negligible.

From Figure 3.4 the in-plane displacement components of a point P of coordinate z are

$$u = u_0 - \alpha z \tag{3.89}$$

$$v = v_0 - \alpha z \tag{3.90}$$

where u_0 and v_0 are the mid-plane displacements. α is the slope and z is the coordinate variable of a general point of the cross section.

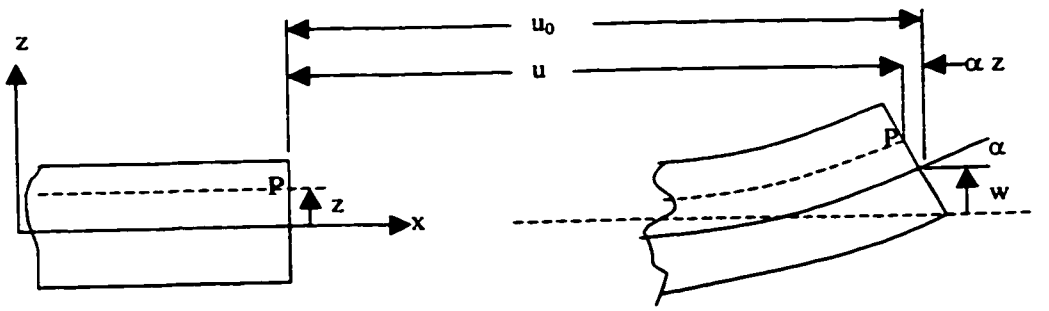

Figure 3.4 Laminate before and after deformation

So in general

$$\begin{aligned} u &= u_0 - z\frac{\partial w}{\partial x} \\ v &= v_0 - z\frac{\partial w}{\partial y} \\ w &= w_0 \end{aligned} \tag{3.91}$$

And the strains are

$$\varepsilon_x = \frac{\partial u}{\partial x} = \frac{\partial u_0}{\partial x} - z\frac{\partial^2 w}{\partial x^2} \tag{3.92}$$

$$\varepsilon_y = \frac{\partial v}{\partial y} = \frac{\partial v_0}{\partial y} - z\frac{\partial^2 w}{\partial y^2} \tag{3.93}$$

$$\gamma_{xy} = \frac{\partial u}{\partial y} + \frac{\partial v}{\partial x} = \frac{\partial u_0}{\partial y} + \frac{\partial v_0}{\partial x} - 2z\frac{\partial^2 w}{\partial x \partial y} \tag{3.94}$$

In the above equation mid-plane strains are defined as

$$\varepsilon_x^0 = \frac{\partial u_0}{\partial x}, \quad \varepsilon_y^0 = \frac{\partial v_0}{\partial y}, \quad \gamma_{xy}^0 = \frac{\partial u_0}{\partial y} + \frac{\partial v_0}{\partial x} \tag{3.95}$$

and the curvatures of the laminate as

$$k_x = -\frac{\partial^2 w}{\partial x^2}, \quad k_y = -\frac{\partial^2 w}{\partial y^2}, \quad k_{xy} = -2\frac{\partial^2 w}{\partial x \partial y} \tag{3.96}$$

Now in matrix form these strains can be written as

$$\begin{bmatrix} \varepsilon_x \\ \varepsilon_y \\ \gamma_{xy} \end{bmatrix} = \begin{bmatrix} \varepsilon_x^0 \\ \varepsilon_y^0 \\ \gamma_{xy}^0 \end{bmatrix} + z \begin{bmatrix} k_x \\ k_y \\ k_{xy} \end{bmatrix} \tag{3.97}$$

Now consider an individual ply say k in a laminate whose mid-plane is at a distance z from the laminate mid-plane. The stresses in that ply for plane stress case can be written from Eq.(3.87) and Eq.(3.97) as

$$\begin{Bmatrix} \sigma_x \\ \sigma_y \\ \tau_{xy} \end{Bmatrix}_k = \begin{bmatrix} \bar{Q}_{11} & \bar{Q}_{12} & \bar{Q}_{16} \\ \bar{Q}_{12} & \bar{Q}_{22} & \bar{Q}_{26} \\ \bar{Q}_{16} & \bar{Q}_{26} & \bar{Q}_{66} \end{bmatrix}_k \begin{Bmatrix} \varepsilon_x^0 + zk_x \\ \varepsilon_y^0 + zk_y \\ \gamma_{xy}^0 + zk_{xy} \end{Bmatrix} \tag{3.98}$$

Now the force and moment resultants for the ply k can be written as (referring to Figure (3.5)).

$$N_x^k = \int_{-\frac{t}{2}}^{\frac{t}{2}} \sigma_x dz, \qquad N_y^k = \int_{-\frac{t}{2}}^{\frac{t}{2}} \sigma_y dz, \text{ and} \qquad N_{xy}^k = \int_{-\frac{t}{2}}^{\frac{t}{2}} \tau_{xy} dz \tag{3.99}$$

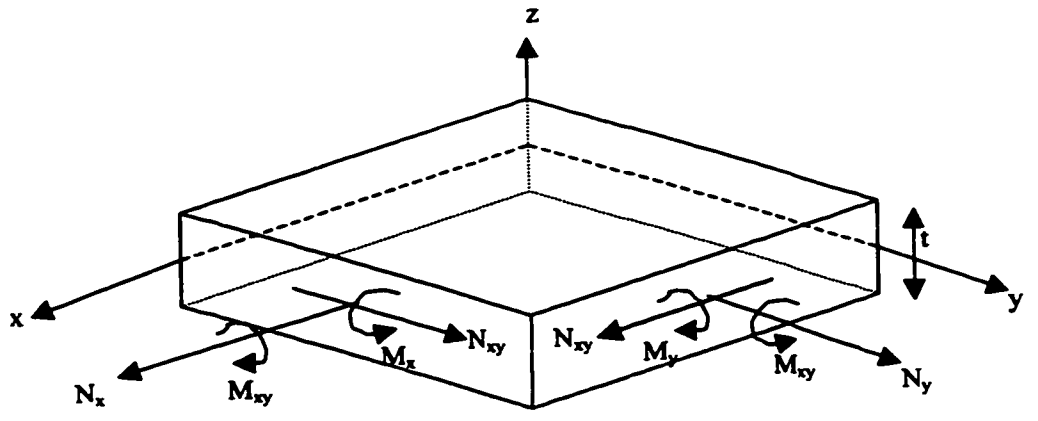

Figure 3.5 Single ply with force and moment resultants

and

$$M_x^k = \int_{-\frac{t}{2}}^{\frac{t}{2}} \sigma_x z dz, \qquad M_y^k = \int_{-\frac{t}{2}}^{\frac{t}{2}} \sigma_y z dz, \text{ and} \qquad M_{xy}^k = \int_{-\frac{t}{2}}^{\frac{t}{2}} \tau_{xy} z dz \tag{3.100}$$

where

z = the coordinate variable of a point in the cross section

t = ply thickness

In the case of a multilayer laminate the total force and moment resultants are obtained by summing the contributions from all layers. Thus for the laminate with n plies as shown in Figure (3.6), the force and moment resultants can be written as

$$\begin{Bmatrix} N_x \\ N_y \\ N_{xy} \end{Bmatrix} = \sum_{k=1}^{n} \int_{h_{k-1}}^{h_k} \begin{Bmatrix} \sigma_x \\ \sigma_y \\ \tau_{xy} \end{Bmatrix}_k dz \tag{3.101}$$

and

$$\begin{Bmatrix} M_x \\ M_y \\ M_{xy} \end{Bmatrix} = \sum_{k=1}^{n} \int_{h_{k-1}}^{h_k} \begin{Bmatrix} \sigma_x \\ \sigma_y \\ \tau_{xy} \end{Bmatrix}_k z dz \tag{3.92}$$

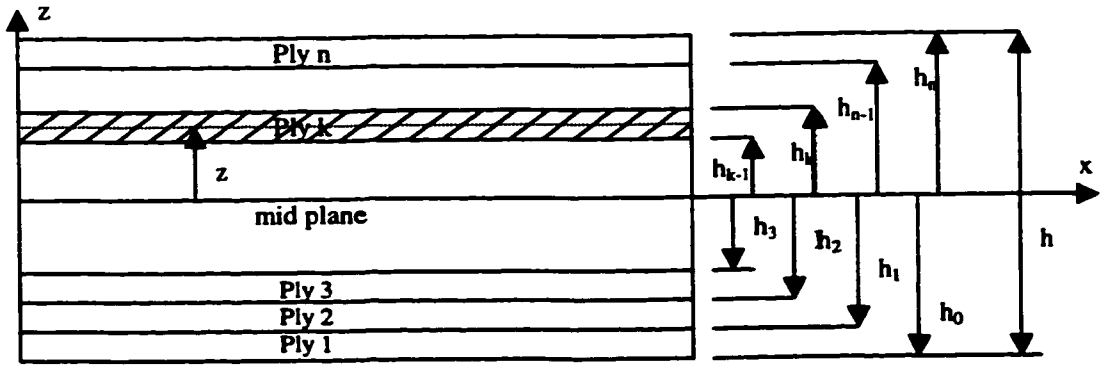

Figure 3.6 Multilayer laminate with coordinate notations for individual plies

Substituting Eq.(3.98) in Eqs.(3.101-3.102) it can be shown that

$$\begin{Bmatrix} N_x \\ N_y \\ N_{xy} \end{Bmatrix} = \sum_{k=1}^{n} \left\{ \begin{bmatrix} \bar{Q}_{11} & \bar{Q}_{12} & \bar{Q}_{16} \\ \bar{Q}_{12} & \bar{Q}_{22} & \bar{Q}_{26} \\ \bar{Q}_{16} & \bar{Q}_{26} & \bar{Q}_{66} \end{bmatrix}_k \begin{Bmatrix} \varepsilon_x^0 \\ \varepsilon_y^2 \\ \gamma_{xy}^0 \end{Bmatrix} \int_{h_{k-1}}^{h_k} dz + \begin{bmatrix} \bar{Q}_{11} & \bar{Q}_{12} & \bar{Q}_{16} \\ \bar{Q}_{12} & \bar{Q}_{22} & \bar{Q}_{26} \\ \bar{Q}_{16} & \bar{Q}_{26} & \bar{Q}_{66} \end{bmatrix}_k \begin{Bmatrix} k_x \\ k_y \\ k_{xy} \end{Bmatrix} \int_{h_{k-1}}^{h_k} z dz \right\} \quad (3.103)$$

and

$$\begin{Bmatrix} M_x \\ M_y \\ M_{xy} \end{Bmatrix} = \sum_{k=1}^{n} \left\{ \begin{bmatrix} \bar{Q}_{11} & \bar{Q}_{12} & \bar{Q}_{16} \\ \bar{Q}_{12} & \bar{Q}_{22} & \bar{Q}_{26} \\ \bar{Q}_{16} & \bar{Q}_{26} & \bar{Q}_{66} \end{bmatrix}_k \begin{Bmatrix} \varepsilon_x^0 \\ \varepsilon_y^2 \\ \gamma_{xy}^0 \end{Bmatrix} \int_{h_{k-1}}^{h_k} z dz + \begin{bmatrix} \bar{Q}_{11} & \bar{Q}_{12} & \bar{Q}_{16} \\ \bar{Q}_{12} & \bar{Q}_{22} & \bar{Q}_{26} \\ \bar{Q}_{16} & \bar{Q}_{26} & \bar{Q}_{66} \end{bmatrix}_k \begin{Bmatrix} k_x \\ k_y \\ k_{xy} \end{Bmatrix} \int_{h_{k-1}}^{h_k} z^2 dz \right\} \quad (3.104)$$

In the Eqs.(3.103-3.104) given above, the in-plane strains and curvatures refer to the entire laminate and are the same for all plies. Thus the strains and curvatures can be factored outside the summation sign as follows.

$$\{N\} = \left[\sum_{k=1}^{n} \left[\bar{Q}\right]_k \int_{h_{k-1}}^{h_k} dz \right] \{\varepsilon^0\} + \left[\sum_{k=1}^{n} \left[\bar{Q}\right]_k \int_{h_{k-1}}^{h_k} z dz \right] \{k\} \quad (3.105)$$

$$\{N\} = \left[\sum_{k=1}^{n} \left[\bar{Q}\right]_k \left(h_k - h_{k-1}\right) \right] \{\varepsilon^0\} + \left[\sum_{k=1}^{n} \left[\bar{Q}\right]_k \left(h_k^2 - h_{k-1}^2\right) \right] \{k\} \quad (3.106)$$

$$\{N\} = [A]\{\varepsilon^0\} + [B]\{k\} \quad (3.107)$$

and

$$\{M\} = \left[\sum_{k=1}^{n} \left[\bar{Q}\right]_k \int_{h_{k-1}}^{h_k} z dz \right] \{\varepsilon^0\} + \left[\sum_{k=1}^{n} \left[\bar{Q}\right]_k \int_{h_{k-1}}^{h_k} z^2 dz \right] \{k\} \quad (3.108)$$

$$\{M\} = \left[\sum_{k=1}^{n} \left[\bar{Q}\right]_k \left(h_k^2 - h_{k-1}^2\right) \right] \{\varepsilon^0\} + \left[\sum_{k=1}^{n} \left[\bar{Q}\right]_k \left(h_{k-1}^3 - h_k^3\right) \right] \{k\} \quad (3.109)$$

$$\{M\} = [B]\{\varepsilon^0\} + [D]\{k\} \quad (3.110)$$

where

$$A_{ij} = \sum_{k=1}^{n} \bar{Q}_{ij}^{k} \left(h_k - h_{k-1} \right) \text{ (Axial stiffness)} \tag{3.111}$$

$$B_{ij} = \frac{1}{2} \sum_{k=1}^{n} \bar{Q}_{ij}^{k} \left(h_k^2 - h_{k-1}^2 \right) \text{ (Axial-bending coupling stiffness)} \tag{3.112}$$

$$D_{ij} = \frac{1}{3} \sum_{k=1}^{n} \bar{Q}_{ij}^{k} \left(h_k^3 - h_{k-1}^3 \right) \text{ (Bending stiffness)} \tag{3.113}$$

with $i,j = 1, 2, 6$.

Thus the full form of the force-deformation relation of Eq.(3.103) is

$$\begin{Bmatrix} N_x \\ N_y \\ N_{xy} \end{Bmatrix} = \begin{bmatrix} A_{11} & A_{12} & A_{16} \\ & A_{22} & A_{26} \\ symm & & A_{66} \end{bmatrix} \begin{Bmatrix} \varepsilon_x^0 \\ \varepsilon_y^2 \\ \gamma_{xy}^0 \end{Bmatrix} + \begin{bmatrix} B_{11} & B_{12} & B_{16} \\ & B_{22} & B_{26} \\ symm & & B_{66} \end{bmatrix} \begin{Bmatrix} k_x \\ k_y \\ k_{xy} \end{Bmatrix} \tag{3.114}$$

and the moment-deformation relation of Eq.(3.104) is

$$\begin{Bmatrix} M_x \\ M_y \\ M_{xy} \end{Bmatrix} = \begin{bmatrix} B_{11} & B_{12} & B_{16} \\ & B_{22} & B_{26} \\ symm & & B_{66} \end{bmatrix} \begin{Bmatrix} \varepsilon_x^0 \\ \varepsilon_y^2 \\ \gamma_{xy}^0 \end{Bmatrix} + \begin{bmatrix} D_{11} & D_{12} & D_{16} \\ & D_{22} & D_{26} \\ symm & & D_{66} \end{bmatrix} \begin{Bmatrix} k_x \\ k_y \\ k_{xy} \end{Bmatrix} \tag{3.115}$$

The combined form of the Eqs.(3.114-3.115) is called the laminate constitutive equation and can be written as

$$\left\{\begin{array}{c} N_x \\ N_Y \\ N_{XY} \\ \hline M_X \\ M_Y \\ M_{XY} \end{array}\right\} = \left[\begin{array}{ccc:ccc} A_{11} & A_{12} & A_{16} & B_{11} & B_{12} & B_{16} \\ & A_{22} & A_{26} & & B_{22} & B_{26} \\ symm & & A_{66} & symm & & B_{66} \\ \hdashline B_{11} & B_{12} & B_{16} & D_{11} & D_{12} & D_{16} \\ & B_{22} & B_{26} & & D_{22} & D_{26} \\ symm & & B_{66} & symm & & D_{66} \end{array}\right] \left\{\begin{array}{c} \varepsilon_x^0 \\ \varepsilon_y^0 \\ \gamma_{xy}^0 \\ \hline k_x \\ k_y \\ k_{xy} \end{array}\right\} \tag{3.116}$$

3.4.5 Equivalent Elastic Constants

In-plane forces for symmetric laminates, for which the axial bending siffnesses B_{ij} are zero, can be written from Eq.(3.114) as

$$\begin{Bmatrix} N_x \\ N_y \\ N_{xy} \end{Bmatrix} = \begin{bmatrix} A_{11} & A_{12} & A_{16} \\ A_{12} & A_{22} & A_{26} \\ A_{16} & A_{26} & A_{66} \end{bmatrix} \begin{Bmatrix} \varepsilon_x^0 \\ \varepsilon_y^2 \\ \gamma_{xy}^0 \end{Bmatrix} \tag{3.117}$$

Inversion of the Eq.(3.117) gives

$$\begin{Bmatrix} \varepsilon_x^0 \\ \varepsilon_y^2 \\ \gamma_{xy}^0 \end{Bmatrix} = \begin{bmatrix} a_{11} & a_{12} & a_{16} \\ a_{12} & a_{22} & a_{26} \\ a_{16} & a_{26} & a_{66} \end{bmatrix} \begin{Bmatrix} N_x \\ N_y \\ N_{xy} \end{Bmatrix} \tag{3.118}$$

where $[a]$ is the extensional laminate compliance matrix, which is the inverse of the corresponding stiffness matrix, as given below

$$[a]=[A]^{-1} \tag{3.119}$$

The average laminate stresses can be defined as

$$\bar{\sigma}_x = \frac{N_x}{h}, \qquad \bar{\sigma}_y = \frac{N_y}{h}, \text{ and } \quad \bar{\tau}_{xy} = \frac{N_{xy}}{h} \tag{3.120}$$

where h is the laminate thickness.

So Eq.(3.118) can be rewritten in terms of average laminate stresses as

$$\begin{Bmatrix} \varepsilon_x^0 \\ \varepsilon_y^2 \\ \gamma_{xy}^0 \end{Bmatrix} = \begin{bmatrix} ha_{11} & ha_{12} & ha_{16} \\ ha_{12} & ha_{22} & ha_{26} \\ ha_{16} & ha_{26} & ha_{66} \end{bmatrix} \begin{Bmatrix} \frac{N_x}{h} = \bar{\sigma}_x \\ \frac{N_y}{h} = \bar{\sigma}_y \\ \frac{N_{xy}}{h} = \bar{\tau}_{xy} \end{Bmatrix} \tag{3.121}$$

A uniaxial stress σ_x produces the following strains

$$\varepsilon_x = \frac{1}{E_x}\sigma_x, \quad \varepsilon_y = -\frac{\nu_{xy}}{E_x}\sigma_x, \text{ and } \gamma_{xy} = -\frac{m_x}{E_x}\sigma_x \tag{3.122}$$

where E_x, ν_{xy}, and $m_x = -\frac{\gamma_{xy}}{\varepsilon_x}$ are the x-directional modulus, Poisson's ratio and shear coupling coefficient respectively.

In a similar manner, a uniaxial stress σ_y produces the following strains.

$$\varepsilon_x = -\frac{\nu_{yx}}{E_y}\sigma_y, \quad \varepsilon_y = \frac{1}{E_y}\sigma_y, \text{ and } \gamma_{xy} = -\frac{m_y}{E_y}\sigma_y \tag{3.123}$$

A pure shear stress τ_{xy} produces the following strains.

$$\varepsilon_x = -\frac{\tau_{xy}}{G_{xy}m_x}, \quad \varepsilon_y = -\frac{\tau_{xy}}{G_{xy}m_y}, \text{ and } \gamma_{xy} = \frac{\tau_{xy}}{G_{xy}} \tag{3.124}$$

By superposition of the three loadings σ_x, σ_y, and τ_{xy} the following strain-stress relation can be obtained in terms of engineering constants.

$$\begin{Bmatrix} \varepsilon_x \\ \varepsilon_y \\ \gamma_{xy} \end{Bmatrix} = \begin{bmatrix} \frac{1}{E_x} & -\frac{\nu_{yx}}{E_y} & -\frac{1}{G_{xy}m_x} \\ -\frac{\nu_{xy}}{E_x} & \frac{1}{E_y} & -\frac{1}{G_{xy}m_y} \\ -\frac{m_x}{E_x} & -\frac{m_y}{E_y} & \frac{1}{G_{xy}} \end{bmatrix} \begin{Bmatrix} \sigma_x \\ \sigma_y \\ \tau_{xy} \end{Bmatrix} \tag{3.125}$$

From symmetry considerations of the compliance matrix, the following equations are obtained.

$$\frac{\nu_{xy}}{E_x} = \frac{\nu_{yx}}{E_y}, \qquad \frac{m_x}{E_x} = \frac{1}{G_{xy}m_x}, \text{ and } \frac{m_y}{E_y} = \frac{1}{G_{xy}m_y} \tag{3.126}$$

Comparison of equivalent strain-stress relations in Eq.(3.121) and Eq.(3.125) yields the following relations for equivalent engineering constants.

$$\begin{gathered} E_x = \frac{1}{ha_{11}}, \qquad E_y = \frac{1}{ha_{22}}, \qquad G_{xy} = \frac{1}{ha_{33}}, \\ \nu_{xy} = -\frac{a_{12}}{a_{11}}, \ \nu_{yx} = -\frac{a_{12}}{a_{33}}, \ m_x = -\frac{a_{13}}{a_{11}}, \ m_y = -\frac{a_{23}}{a_{22}} \end{gathered} \tag{3.127}$$

The equivalent elasticity matrix [E] for a composite laminate can be calculated by inverting Eq.(3.121) as

$$\begin{Bmatrix} \bar{\sigma}_x \\ \bar{\sigma}_y \\ \bar{\tau}_{xy} \end{Bmatrix} = \begin{bmatrix} ha_{11} & ha_{12} & ha_{16} \\ ha_{12} & ha_{22} & ha_{26} \\ ha_{16} & ha_{26} & ha_{66} \end{bmatrix}^{-1} \begin{Bmatrix} \varepsilon_x^0 \\ \varepsilon_y^2 \\ \gamma_{xy}^0 \end{Bmatrix} \tag{3.128}$$

Now comparing Eq.(3.128) with Eq.(2.36) in Chapter 2 (Section 2.4.1) for calculating the elasticity matrix [E], gives

$$[E]=\begin{bmatrix} ha_{11} & ha_{12} & ha_{16} \\ ha_{12} & ha_{22} & ha_{26} \\ ha_{16} & ha_{26} & ha_{66} \end{bmatrix}^{-1} \tag{3.129}$$

3.5 Program Development

The finite element program which has been already developed in Chapter 2 for isotropic material, is now modified for anisotropic material. The modification is necessary only for the Elasticity matrix [E] and in the SIF calculation. The details of the computer coding for these modifications are presented in Appendix II.

3.5.1 Subroutine *fsifcomd*

The main function of this subroutine is to calculate the Stress Intensity Factor of the orthotropic laminate by the displacement extrapolation method described in the Section 3.3.1.

3.5.2 Subroutine *fsifcome*

This subroutine is used to calculate the SIF for an orthotropic laminate by the energy release rate method according to Section 3.3.2.

3.5.3 Subroutine *fcompo*

The function of this subroutine is to calculate the equivalent elasticity matrix [E] for anisotropic material only for the plane stress case and for a symmetric laminate using Eq.(3.129).

The flow chart of this subroutine is shown in Figure 3.7. The [E] matrix is stored in the array " matmtx".

3.6 Example Applications

The MATLAB® computer program, developed in this chapter, is now demonstrated through the application to two composite laminates made from NCT-301 graphite/epoxy composite material. The structure considered is that of a $[0/90]_{5S}$ laminate under tension which contains a crack of length $2a$ perpendicular to the direction of loading. The initial crack length was chosen as $a = 0.334W$, where $W = 120$ mm, is the width of the plate and L=240 mm, is the length of the plate. The finite element mesh employed in the solution is shown in Figure 3.8.

The mean values of the elastic constants for NCT-301 graphite/epoxy composite material are listed in Table 4.2 in Chapter 4, which are determined experimentally. The details of the experimental procedures are described in Chapter 4. The value of the distributed load

is taken to be equal to 60% of the laminate strength, which is calculated to be equal to 1.5 KN/mm.

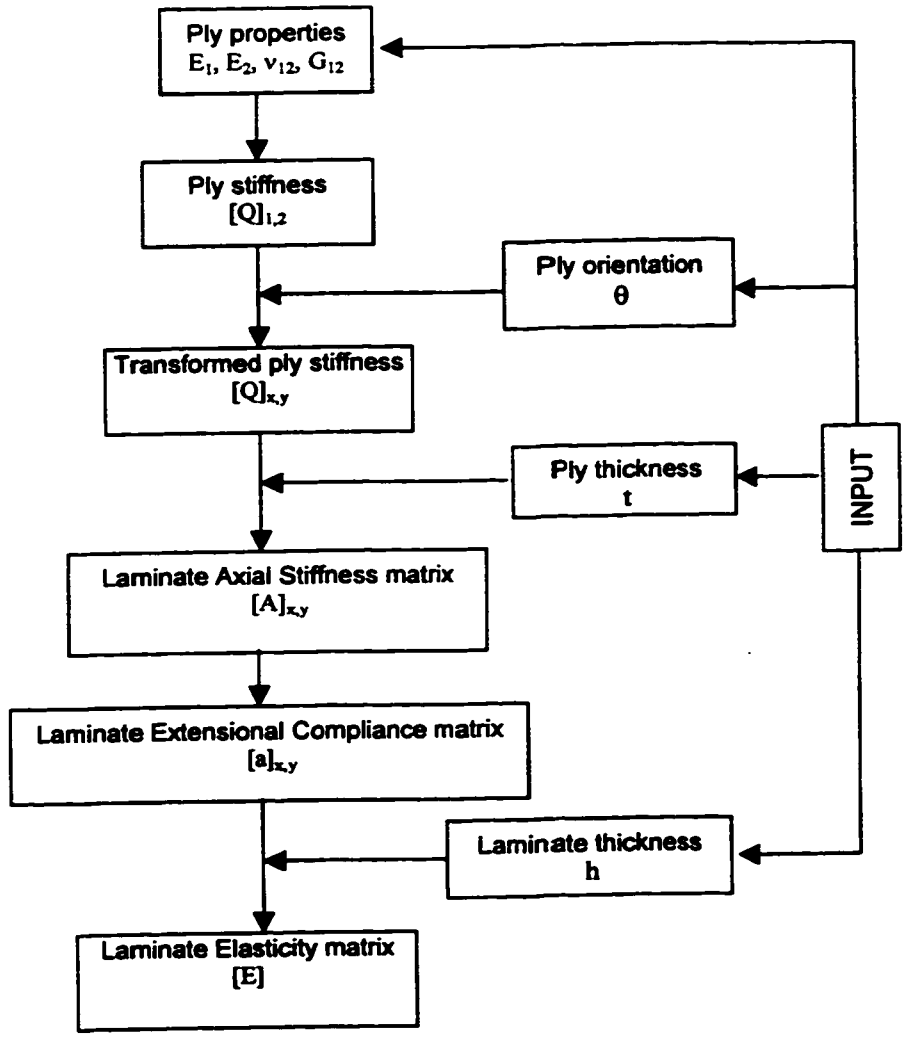

Figure 3.7 Computation of the elasticity matrix of multidirectional laminates

❑ **Displacements**

The nodal displacements along the crack edge and the loaded edge of the cross-ply laminate $[0/90]_{5S}$ are computed using the developed program. The same problem is also analyzed using ANSYS® software to find the nodal displacements for the purpose of verification, which are listed in the Table 3.1.

It is observed that the displacements calculated using the MATLAB® program are in excellent agreement with the displacements calculated using the ANSYS® software.

Table 3.1 Nodal displacements using MATLAB® Program and ANSYS® software

Node Number		MATLAB® Program		ANSYS® Software	
		u (mm)	*v* (mm)	*u* (mm)	*v* (mm)
Crack edge	1	0	1.5656	0	1.535
	2	-0.1027	1.5236	-0.10186	1.5712
	3	-0.1973	1.3199	-0.1967	1.2656
	4	-0.2629	1.0099	-0.28033	1.1040
	5	-0.2868	0	-0.32436	0
Loaded edge	110	0	2.8339	0	2.847
	111	0.0436	2.7691	0.047992	2.783
	112	0.0778	2.6152	0.087217	2.6279
	113	0.0829	2.4449	0.088825	2.4588
	114	0.0783	2.3149	0.080224	2.3235
	115	0.0660	2.2415	0.067566	2.2475
	116	0.0533	2.1988	0.05404	2.197

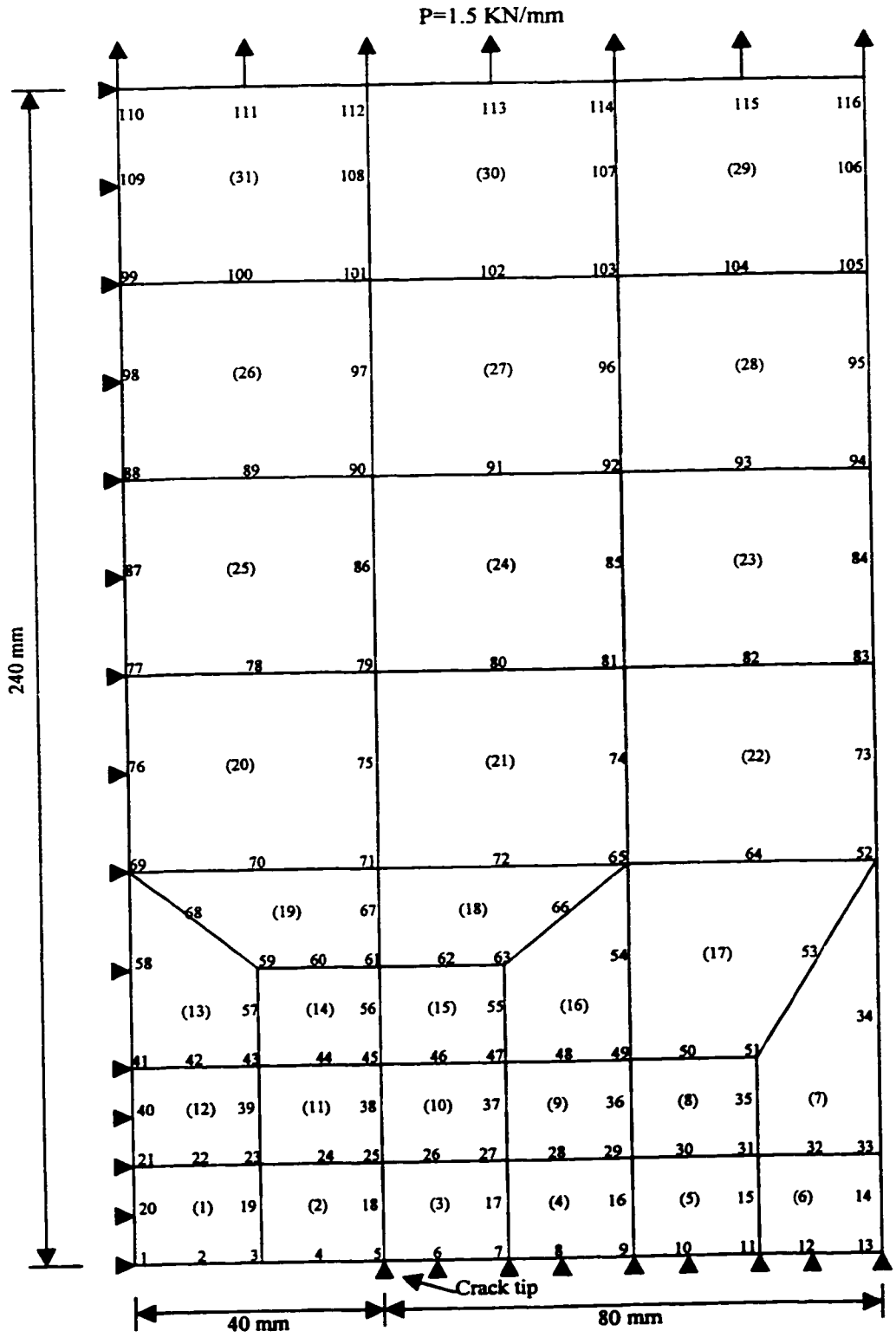

Figure 3.8 Finite element mesh for the center-cracked plate problem

❑ Stress Intensity Factor

The SIF is evaluated for a symmetric orthotropic laminate where there is no shear coupling between in-plane axial loading and in-plane shear deformation. The Eqs.(3.41-3.45) hold good for this condition. Laminate configurations of $[0/90]_{5S}$, and $[90]_{10S}$ are considered in the present analysis.

(a) Displacement Extrapolation Method

For the present study the mesh given in Figure 3.8 is employed. The stress intensity factors for node 3 and node 4 along $\theta = 180^{\circ}$ are calculated and plotted in Figure 3.9. and Figure 3.10. Extrapolation to the crack tip yields the value for SIF. The SIF for the $[0/90]_{5S}$ laminate is 71 MPa$\sqrt{m}$ and for the $[90]_{10S}$ laminate the SIF is 60 MPa$\sqrt{m}$

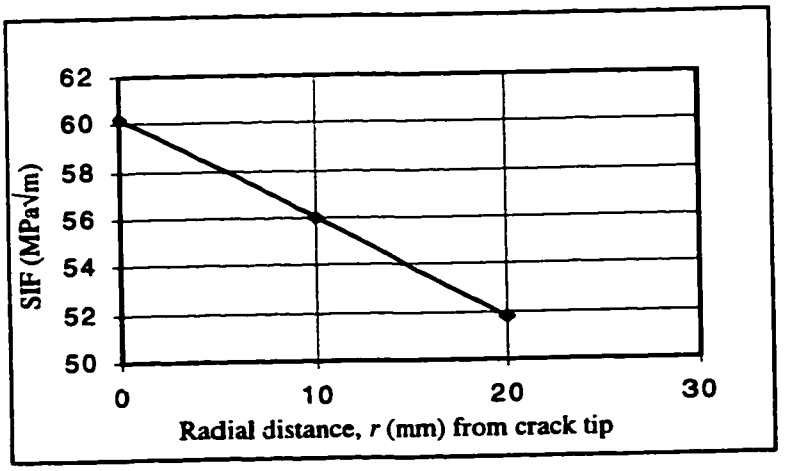

Figure 3.9 Extrapolation of SIF for $[90]_{10S}$ laminate

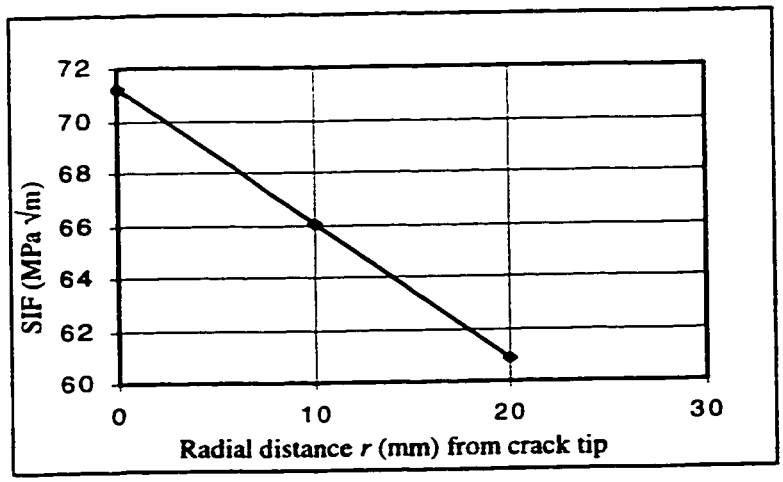

Figure 3.10 Extrapolation of SIF for $[0/90]_{5S}$ laminate

(b) Strain Energy Release Rate Method

In the strain energy release rate method, the crack is advanced in the present code by releasing one node at a time. The approach of advancing the crack by two different increments, calculating K_I in each case and then extrapolating the value of K_I back to the original crack length is followed. Using the same mesh shown in Figure 3.8, the crack is advanced by releasing nodes 5 and 6 one at a time. This procedure gives final crack length equal to 50 mm and 60 mm respectively. The energy release rate(G) is determined at each increment of crack length. G_I= 1.65 KJ/m for the $[0/90]_{5S}$ laminate and G_I=1.57 KJ/m for the $[90]_{10S}$ laminate, when the crack advances by 10 mm. And when the crack advances by 20 mm, G_I= 2.78 KJ/m for the $[0/90]_{5S}$ laminate and G_I=2.71 KJ/m for $[90]_{10S}$ laminate. After extrapolation to the original crack length of 40 mm from Figure 3.11 and Figure 3.12 the value of K_I for the $[0/90]_{5S}$ laminate is calculated to be equal to

65 MPa$\sqrt{m}$ and for the $[90]_{10S}$ laminate it is equal to 62 MPa$\sqrt{m}$. By comparing the value of SIF, for the $[0/90]_{5S}$ laminate, obtained by the two methods (a) and (b) it can be seen that the strain energy release rate method predicts a lower value for SIF. However, the same is not true for the $[90]_{10S}$ laminate, in this case, the strain energy release rate method predicts a higher value for SIF.

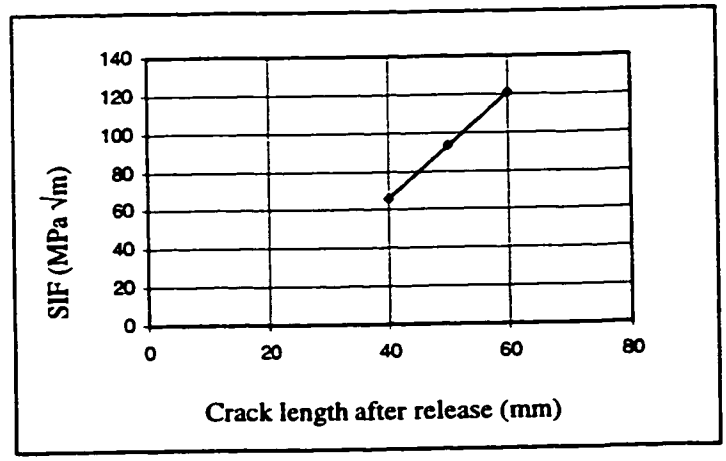

Figure 3.11 Variation of SIF with crack length for $[0/90]_{5S}$ laminate

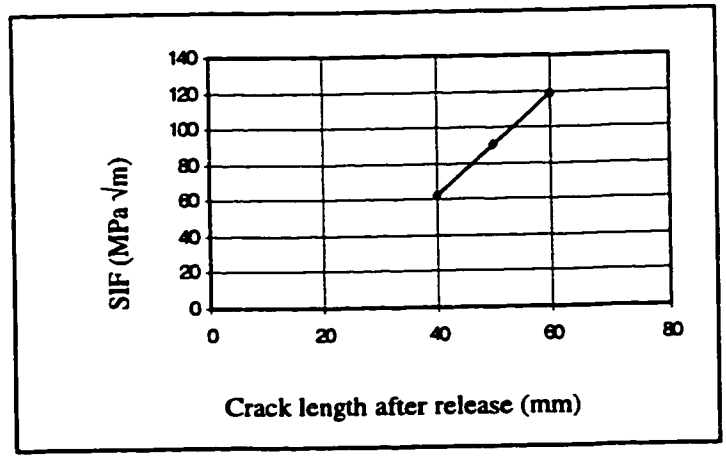

Figure 3.12 Variation of SIF with crack length for $[90]_{10S}$ laminate

3.5 Conclusion and Discussion

In this chapter, the concepts of Stress Intensity Factor (denoted by K) and Strain Energy Release Rate (denoted by G) of Linear Elastic Fracture Mechanics (LEFM) as applied to anisotropic materials under plane stress condition are summarized. The formulation employing the finite element modeling and analysis for evaluating these two parameters for a plate made of anisotropic material and subjected to any type of loading in Mode I and Mode II, is described. Also the description of elastic behavior of unidirectional and multidirectional anisotropic laminates is presented in this chapter. The computer program, which was developed using MATLAB® software in Chapter 2, is modified for composite laminates based on equivalent elastic constants of the laminate. Two example problems are used to demonstrate the modified program. The program was verified by comparing the results such as the nodal displacements with that provided for the same problem by the ANSYS® software. The values of stress intensity factor determined based on the displacement extrapolation and the energy release rate method using the modified program were compared for the same laminate configuration. Two different types of laminates were analyzed this way. The formulation will be extended in the next chapter for the stochastic analysis of fracture behavior of composite laminates.

Chapter 4

Stochastic Finite Element Fracture Analysis of Composite Laminates

4.1 Introduction

Most modern structural systems possess a high degree of structural complexity. Therefore, when their behavior is to be predicted under various loading and environmental conditions, advanced analytical and numerical techniques are required. However, most of these applications are limited to dealing with deterministic loading and environmental conditions despite the fact that they intrinsically involve randomness and uncertainty to a considerable degree.

In the case of composite laminates, significant randomness is present. This is due to the stochastic spatial variations of properties in fibers, in materials and at interfaces. In addition, the fiber volume fraction, void content, fiber orientation angle at various plies, thickness of lamina, etc. display significant variabilities due to manufacturing conditions. As a result, tests on a single material specimen provide a specific value for each material

parameter and mechanical property. However, when a number of specimens are tested, different randomly distributed values are obtained for the same mechanical property or the material parameter. Therefore, the analysis of laminates has to be performed based on a probabilistic approach. When Finite Element Analysis (FEA) is performed based on a stochastic approach, such that a stochastic description can be provided for the response of the laminate, the resulting FEA is known as Stochastic Finite Element Analysis (SFEA).

The present chapter deals with the probabilistic fracture analysis of laminates. The fracture parameters as well as their variability resulting from the spatial variability of the material properties of the composite laminates when they are subjected to static loads of a deterministic nature, are determined using stochastic finite element analysis.

In this chapter, (i) the manufacturing and testing of the composite laminate for evaluating the material properties are summarized, (ii) the analytical modeling of material properties as stochastic processes is described, (iii) the MATLAB program which has been developed in Chapter 3 for anisotropic materials is extended so as to incorporate the stochastic description of material properties and the stochastic finite element analysis, and (iv) an example application of the computer program to composite laminates that have variable elastic constants, ply angles and ply thicknesses is given.

In Section 4.2, the manufacturing and the tensile testing of unidirectional composite laminate are summarized. In Section 4.3, the concept and the equations that are employed in the stochastic modeling of material properties are presented. In Section 4.4, the

stochastic finite element analysis methodology is described. The development of the MATLAB® program for the evaluation of the Stress Intensity Factor (SIF) and the Strain Energy Release Rate after incorporating the stochastic description of material properties of composite laminates is described in Section 4.5.

4.2 Manufacturing and Experimental Investigation

The analysis and design of composite structures require the input of reliable experimental data. One of the major objectives for testing of composite materials is the determination of basic mechanical properties of the unidirectional lamina for use as an input in structural design and analysis.

In the present thesis preimpregnated NCT-301 graphite/epoxy material is considered and the uniaxial properties of this composite material are determined.

4.2.1 Tensile Testing Procedure

Uniaxial tensile tests are conducted on unidirectional laminate to determine the longitudinal and transverse Young's modulus, E_1 and E_2, respectively. The major and minor Poisson's ratio, ν_{12} and ν_{21} respectively, are also determined.

Tensile specimens are straight-sided coupons of constant cross-section with adhesively bonded non-woven E-glass tabs (3 mm thick) as shown in Figure 4.1. More details are given in ASTM specification D 3039-76 (1989) [116].

The longitudinal (0°) laminate is 1.27 cm wide, 0.75 mm thick (six plies), while the transverse (90°) laminate is 2.54 cm wide, 1 mm thick (eight plies). Both specimens have an overall length of 22.9 cm and a gage length of 15.2 cm.

The specimens are mounted in the grips of the universal MTS testing machine and are loaded to failure under uniaxial tensile loading. A continuous record of loading and deformation is obtained by an appropriate digital data acquisition system.

Axial strains are obtained by means of a strain gage (model CEA-06-125UW-350 of MTS) mounted on one side of the longitudinal specimen for determining fiber direction Young's modulus. Axial and transverse strains are obtained by a double strain gage (model CEA-06-125UT-350 of MTS) mounted on the transverse specimen for the determination of matrix direction Young's modulus and Poisson's ratio.

After recording all the data, for each value of load, the fiber direction stress σ_1 is calculated using the following equation

$$\sigma_1 = \frac{P_x}{bt} \tag{4.1}$$

where P_x is the applied tensile load in units of N, and b and t are the width and thickness of the specimen respectively, in units of mm.

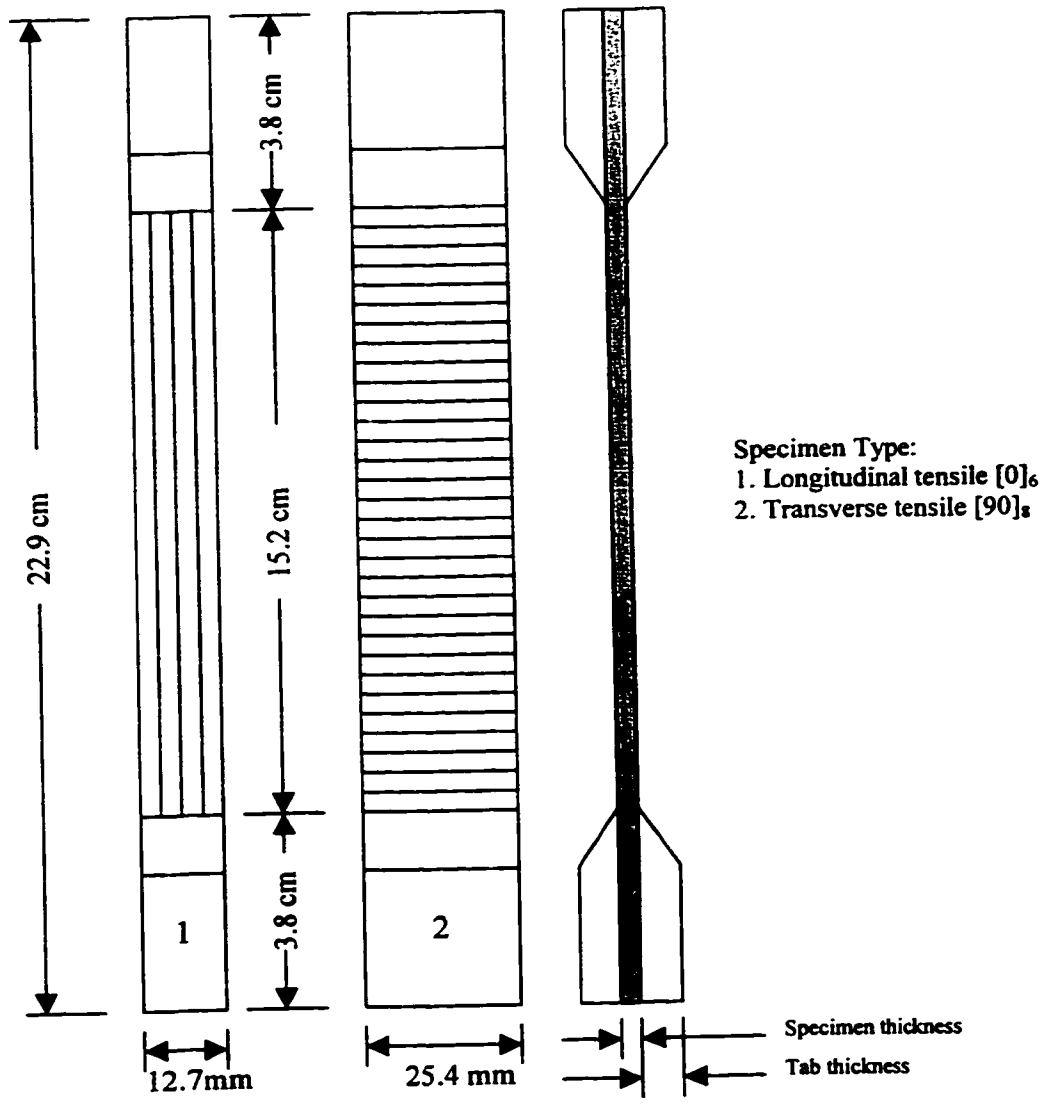

Figure 4.1 Longitudinal and transverse tensile test specimens

The fiber direction stress σ_1 is plotted against the fiber direction strain ε_1 as shown in Figure 4.2. The slope $\Delta\sigma_1/\Delta\varepsilon_1$ of this graph in the linear region is the fiber direction Young's modulus E_1. Similarly Figure 4.3 is drawn as a graph of σ_2 versus ε_2 and the

slope $\Delta\sigma_2/\Delta\varepsilon_2$ gives the matrix direction Young's modulus E_2. The minor Poisson's ratio ν_{21} is obtained by plotting ε_1 versus ε_2 which is shown in Figure 4.4.

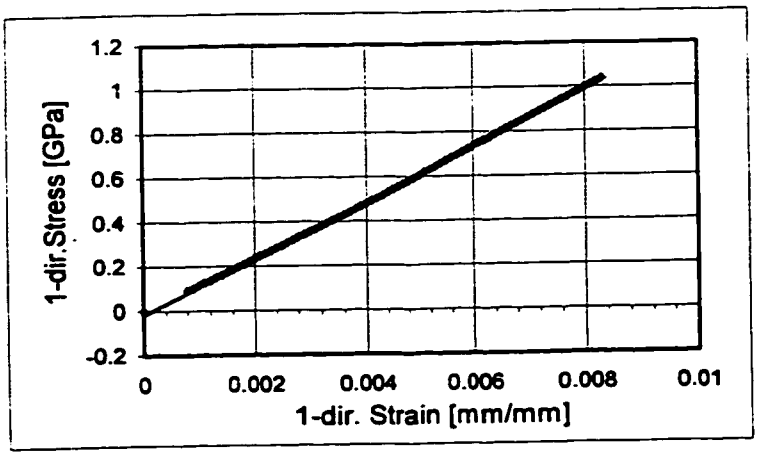

Figure 4.2 **Stress-strain curve for $[0]_6$ graphite/epoxy specimen under uniaxial tensile loading**

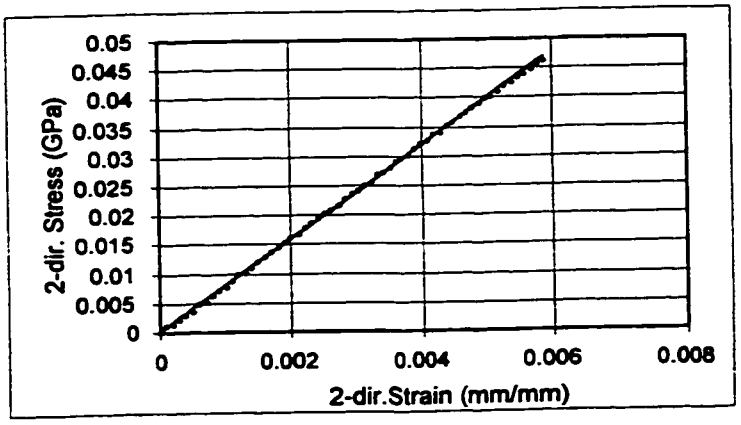

Figure 4.3 **Stress-strain curve for $[90]_8$ graphite/epoxy specimen under uniaxial tensile loading**

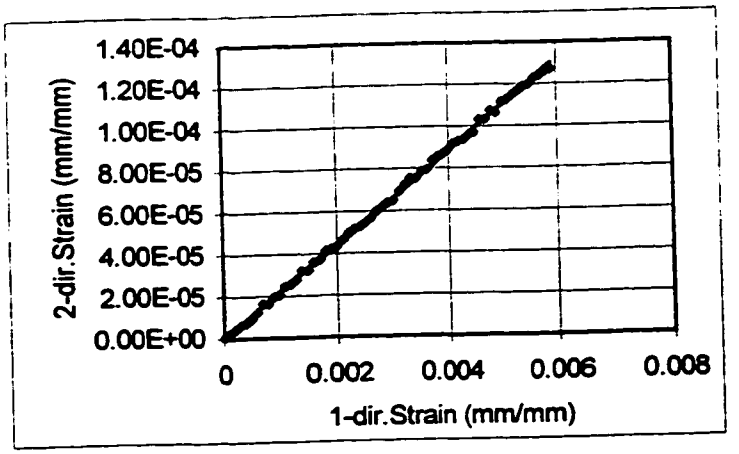

Figure 4.4 **Strain-strain curve for $[90]_8$ graphite/epoxy specimen under uniaxial tensile loading**

4.2.2 In-Plane Shear Testing Procedure

Uniaxial tensile tests are conducted on a balanced, symmetric laminate which is composed of only +45° and -45° plies i.e., $[\pm 45]_{2S}$ laminate to determine the shear modulus G_{12} of the material.

Tensile specimens are straight-sided coupons of constant cross-section with adhesively bonded beveled glass/epoxy tabs as shown in Figure 4.5. More details are given in ASTM specification D 3518 - 91 [117].

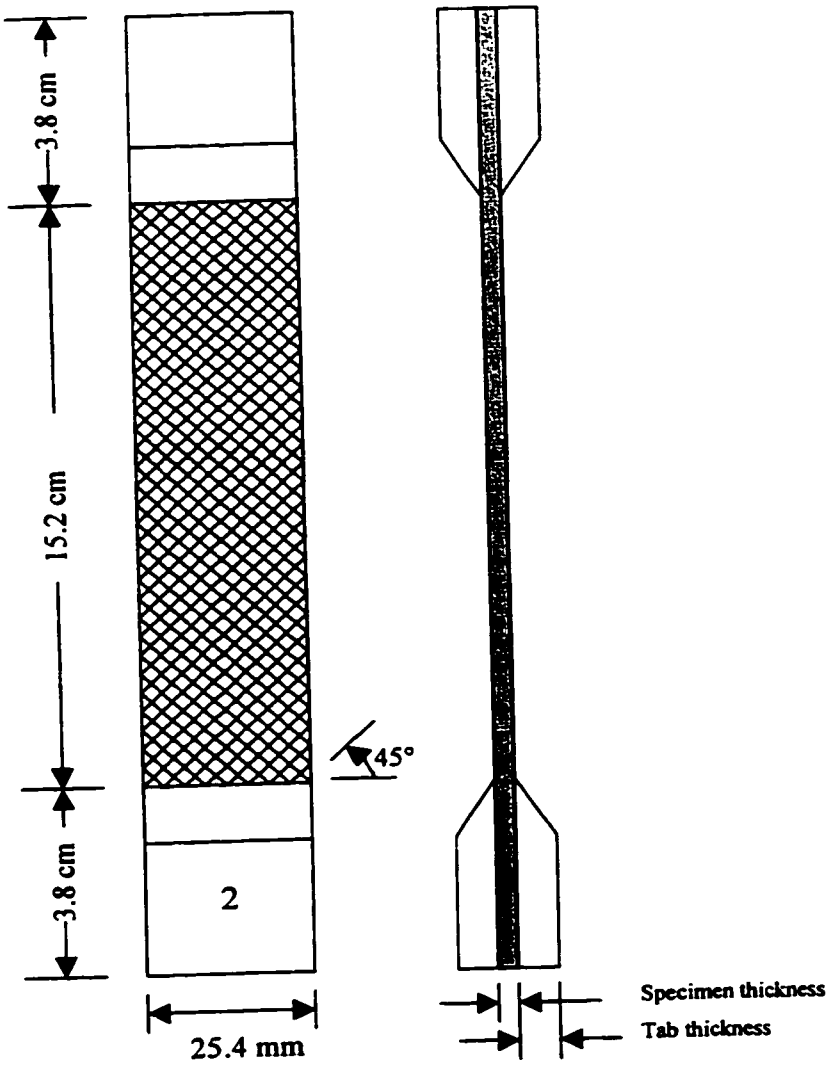

Figure 4.5 The $[45/-45]_{2S}$ tensile test specimen

The specimen $(\pm 45°$ laminate$)$ is 2.54 cm wide, 1 mm thick (eight plies), of overall length of 22.9 cm and of a gage length of 15.2 cm. Axial and transverse strains are obtained using a double strain gage (model CEA-06-125UT-350 of MTS) bonded to the

specimen. A tensile test is performed on the $\pm 45°$ laminate in accordance with the procedure described in the previous section.

After recording all the data, the shear stresses and shear strains in the $\pm 45°$ laminate tensile coupon, are calculated using the following equations

$$\tau_{12} = \frac{P_x}{2bt} \tag{4.2}$$

$$\gamma_{12} = \varepsilon_x - \varepsilon_y \tag{4.3}$$

where

τ_{12} = In-plane shear stress in 1-2 plane

γ_{12} = In-plane shear strain in 1-2 plane

P_x = Applied tensile load in N

ε_x = Longitudinal strain

ε_y = Transverse strain

b = Width of tensile test coupon in mm

t = Thickness of tensile test coupon in mm

Now using the shear stress τ_{12} and shear strain γ_{12} which are shown in Figure 4.6, the shear modulus G_{12} is calculated as

$$G_{12} = \frac{\Delta\tau_{12}}{\Delta\gamma_{12}} \tag{4.4}$$

where $\Delta\tau_{12}/\Delta\gamma_{12}$ is the slope of the plot of the shear stress-shear strain curve (Figure 4.6) within the linear portion of the curve.

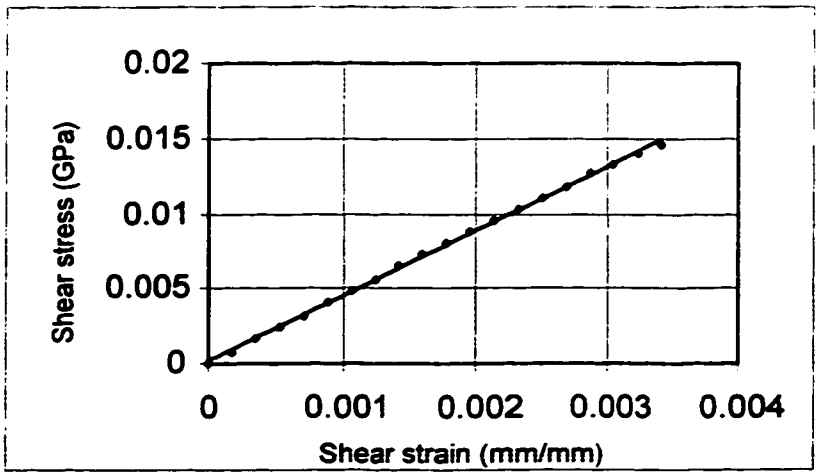

Figure 4.6 **Shear stress-shear strain curve for $[\pm 45]_{2S}$ NCT-301 graphite/epoxy composite material**

4.2.3 Manufacturing of Test Specimens

The manufacturing of composite laminates can be categorized into two phases: (1) fabrication and (2) processing. In the fabrication phase the fiber reinforcement and accompanying matrix material are placed or shaped into a structural form such as a flat or curved plate, a cylinder or other body of revolution, and the like. In the present study, a flat plate is manufactured from layers, or plies, of preimpregnated NCT-301 graphite/epoxy material. During the processing phase, an autoclave is used which provides the proper levels of heat and pressure to solidify and consolidate the structure.

4.2.3.1 Fabrication

Tooling:

All fabrication methods require tools to provide the shape of the composite structure during the processing. A flat aluminum tool is used to manufacture flat composite plate.

Specialty Materials:

Many secondary or specialty materials are used in composites manufacturing such as release coating, peel plies, release films, bleeder plies, breather plies, vacuum bags and sealant tape. Each of these materials serves a specific function [114]. A cross section of typical lay-up of a composite structure prepared for autoclave processing is shown in Figure 4.7

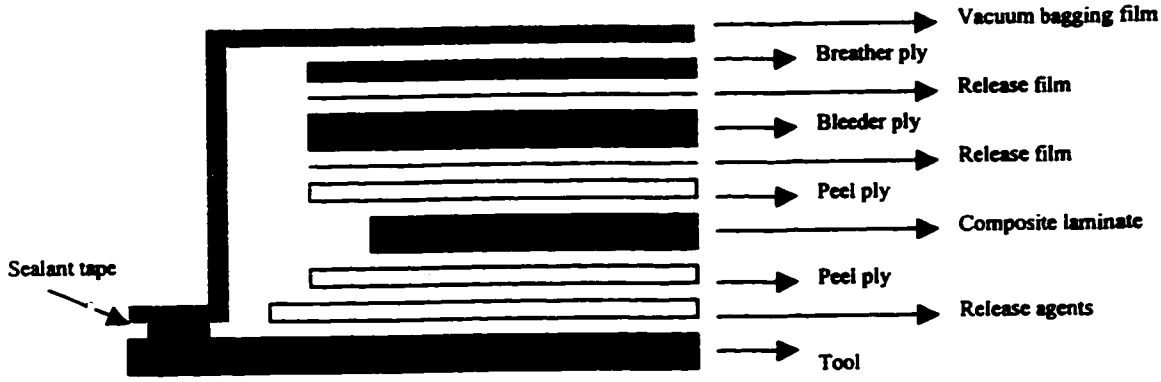

Figure 4.7 Typical cross section of autoclave lay-up

Hand Lay-up:

The lay-up of preimpregnated material by hand is the oldest and most common fabrication method for advanced composite structures. Each step in the hand lay-up of a flat composite laminate must follow in successive fashion in order to obtain a high-quality composite laminate after final processing. A description of these steps is given in Ref.[114].

At first the surface of the tool is cleaned and a release agent is applied and a peel ply is placed on the top of the tool. The preimpregnated plies are cut according to design specifications, i.e. 12 inch by 12 inch. The first prepreg ply is oriented and placed upon the tool. Subsequent plies are placed one upon another according to laminate configuration; a roller is used to compact the plies and remove entrapped air that could later lead to voids or layer separations. After that a peel ply, a sheet of porous release film, the bleeder plies, another release film and the breather plies are placed on top of the laminate one by one according to Figure 4.7.

When the laminate fabrication is completed the sealant tape is placed around the entire periphery of the tool and the vacuum bag is placed over the entire tool.

It is important to ensure that the bag is adequately sealed before proceeding to the processing cycle. The vacuum port is installed through the bag and the contents are evacuated by vacuum pump.

4.2.3.2 Processing

Once the composite plies are combined with desired shape and orientation, it is necessary to apply the proper temperature and pressure for specific periods of time to produce the fiber-reinforced laminate. The temperature cycle is usually referred to as the cure cycle, as it is the heating of the resin that initiates the cure reaction. The overall cycle, which indicates pressurization and the temperature cycle, is referred to as the process cycle.

The best quality laminates are cured using an autoclave. An autoclave consists of a large cylindrical metal pressure vessel with end enclosures that is thermally insulated and heated. A typical autoclave is shown in a schematic form in Figure 4.8.

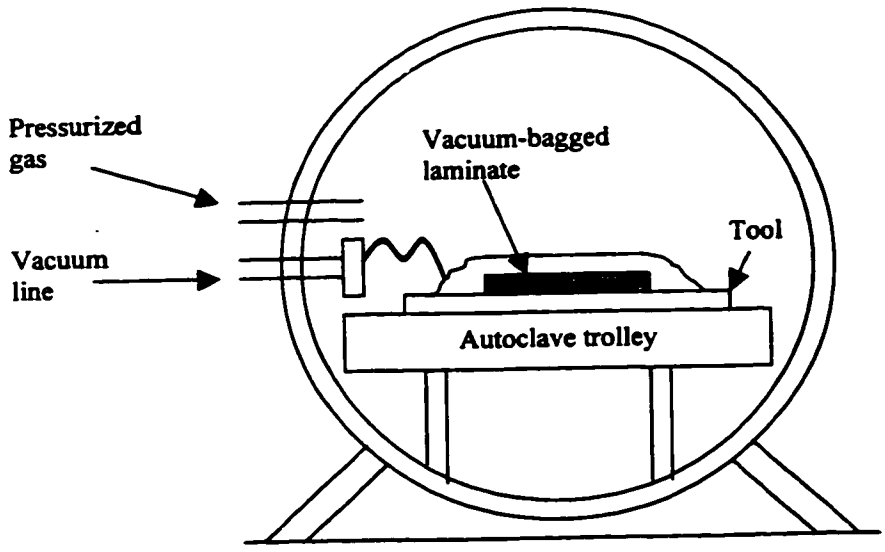

Figure 4.8 Schematic of an autoclave

A typical cure cycle for NCT-301 graphite/epoxy composites is a two step cycle shown in Figure 4.9. In such a cycle the temperature of the material is increased from room temperature to 104° C, and this temperature is held constant for half an hour (first dwell). Afterwards, the temperature is again increased to 140° C, and held constant for one hour (second dwell). After that the part is cooled to room temperature at constant rate.

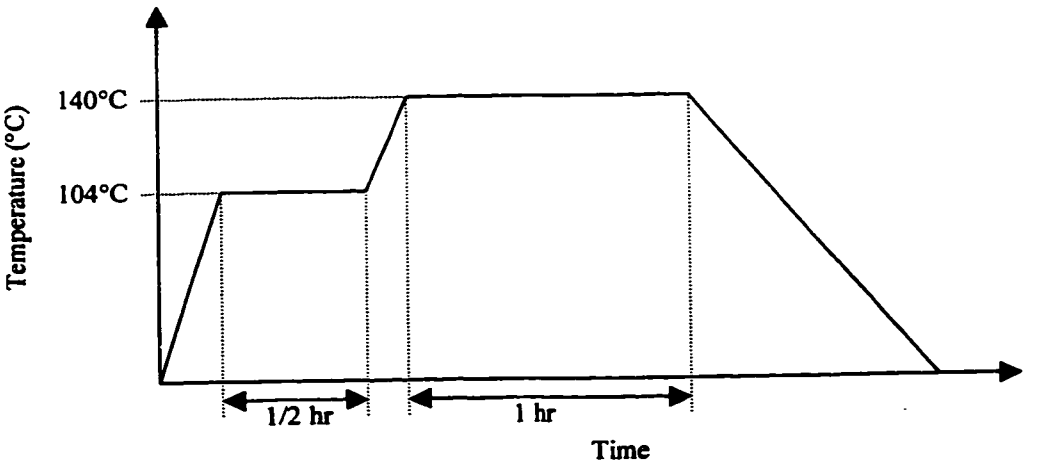

Figure 4.9 Cure cycle for NCT-301 graphite/epoxy composite material

The purpose of the first dwell is to allow gases (entrapped air, water vapor, or volatiles) to escape from the matrix material and to allow the matrix to flow, facilitating compaction of the part. The purpose of the second dwell is to allow cross-linking of the resin to take place. The strength and related mechanical properties of the composite are developed during the second dwell. A constant 60 psi pressure is maintained inside the autoclave throughout the processing time. After cooling to room temperature the composite plate is ready for use.

4.2.3.3 Statistical Parameters

Each specimen is cut with a diamond blade (with coolant) to a width described in Figure 4.1 and Figure 4.5 from the corresponding configured plate (12" by 12") after bonding the tab material. For each series of tests a total of 35 specimens are prepared. The average value, standard deviation and coefficient of variation for each material property are calculated as

$$\bar{X} = \frac{1}{n}\sum_{i=1}^{n} X_i \tag{4.5}$$

$$s = \sqrt{\frac{\left(\sum_{i=1}^{n} X^2 - n\bar{X}^2\right)}{(n-1)}} \tag{4.6}$$

$$v = 100\frac{s}{\bar{X}} \tag{4.7}$$

where $\bar{X}$ = Average value

s = Estimated standard deviation

X_i = Test value obtained for the i^{th} specimen

n = number of specimens

v = Coefficient of variation

4.2.4 Test Data

According to the test procedures described in Section 4.2.1 and Section 4.2.2, the material properties for 35 specimens are determined and listed in Table 4.1.

Table 4.1 Material properties for NCT-301 graphite/epoxy

Specimen No.	E_1 (GPa)	E_2 (GPa)	ν_{21}	ν_{12}*	G_{12} (GPa)	Fiber dir. Failure load (N)	Matrix dir. Failure load (N)
01	129.88	8.6165	0.02280	0.343674	4.4469	11454	1225
02	131.31	7.5825	0.02020	0.349814	4.1669	12735	1386
03	134.29	8.5739	0.02270	0.355542	3.8683	12200	1237
04	124.40	8.3849	0.02230	0.330847	3.8760	21800	1289
05	131.90	8.4109	0.02410	0.377937	3.7718	17197	1200
06	129.59	7.7485	0.01710	0.285989	3.8533	20686	1455
07	124.40	7.9039	0.02206	0.347204	4.4950	13055	1461
08	133.17	8.0944	0.01710	0.281331	4.4910	20668	1440
09	130.46	7.4498	0.01727	0.302430	4.3718	17253	1453
10	129.30	7.9864	0.01876	0.303725	4.1871	17987	1399
11	134.39	7.8917	0.01970	0.335477	4.0002	20073	1453
12	130.81	7.7695	0.02048	0.344808	4.3794	14503	1098
13	130.09	7.4797	0.02137	0.371676	4.4606	19175	1383
14	127.45	7.6708	0.01937	0.321832	4.4559	20650	1448
15	129.70	7.5836	0.01986	0.339660	4.3429	20502	1448
16	126.59	7.9150	0.01910	0.305479	4.6786	14654	1228
17	131.32	8.3703	0.02098	0.329151	4.4408	17887	1165
18	129.54	8.0736	0.02620	0.420376	4.3060	19990	1242
19	127.89	7.6533	0.01850	0.309143	4.3140	20302	1314
20	129.89	8.1246	0.01905	0.304557	4.4366	20170	1317
21	127.13	7.5460	0.01868	0.314708	4.3812	20573	958
22	128.34	7.8101	0.02087	0.342948	4.2994	18705	1534
23	123.95	7.6938	0.01926	0.310286	4.3581	20569	1351
24	126.54	7.8727	0.01995	0.320662	4.0095	20187	1154
25	124.30	8.0745	0.01990	0.306451	4.3940	19913	1186
26	128.41	8.5289	0.02210	0.332735	4.5672	19124	983
27	133.19	7.9467	0.02120	0.355321	3.7026	19303	1202
28	133.03	8.0652	0.02059	0.339618	4.2741	18592	1163
29	134.88	8.2131	0.02555	0.419596	4.2627	20685	1226
30	130.17	8.1838	0.02040	0.324479	4.4004	20192	874
31	129.18	8.2487	0.01824	0.285650	4.4959	19613	1051
32	128.06	8.5962	0.02280	0.339658	4.3851	21372	947
33	128.04	7.7382	0.02020	0.334239	4.2991	19809	1124
34	128.15	7.9830	0.01916	0.307573	4.4293	19982	1422
35	130.45	8.0221	0.02023	0.328967	4.3092	20037	1210

* $\nu_{12} = \frac{E_1 \nu_{21}}{E_2}$ (Calculated from symmetry)

The average value, standard deviation and coefficient of variation of the material properties are calculated from Table 4.1 using Eqs.(4.5-4.7) which are listed in Table 4.2.

Table 4.2 The Mean value, standard deviation and coefficient of variation of elastic constants for NCT-301 graphite/epoxy composite material

	E_1 (GPa)	E_2 (GPa)	ν_{21}	ν_{12}*	G_{12} (GPa)	Fiber dir. Failure load (N)	Matrix dir. Failure load (N)
$\bar{X}$	129.43	7.99	0.0205	0.3322	4.28	18617.06	1257.886
s	2.8719	0.3298	0.0021	0.0317	0.2366	2789.088	169.3392
v	2.22	4.12	10.43	9.55	5.52	14.98	13.46

$\bar{X}$ = Mean value, s = Standard deviation, v = Coefficient of variation

From Table 4.2 it can be seen that the value of coefficient of variation of E_1 (2.22) is lowest when compared to other material properties. The variability is high for the case of Poisson's ratio being is almost five times than that of E_1. It is also observed that the coefficients of variation of E_2 and G_{12} are two times than that of E_1 e.g., the fluctuations of fiber direction elastic constant for NCT-301 graphite/epoxy composite material is less. The important observation is shown for the case of failure strengths that the variability in failure strength is more for the composite materials than material properties and it is almost seven times that of E_1.

4.3 Stochastic Field Modeling of Material Properties

The spatial variations of material properties, such as the Young modulus, Poisson's ratio and Shear modulus, are considered to constitute, in each case, a two dimensional

homogeneous stochastic process. The fluctuating component $a(\mathbf{X})$ of a material property then has a zero mean. For illustrative purposes, first the case of E_1 is described. A similar procedure is applicable to E_2, G_{12}, ν_{12}, ply orientation angle and ply thickness.

$$E_1 = \bar{E}_1\left[1 + a(\mathbf{X})\right];\ E[a(\mathbf{X})] = 0 \tag{4.8}$$

The auto-correlation function is given by [85]

$$R_{aa}(\xi) = E\left[a(\mathbf{X})a(\mathbf{X}+\xi)\right] \tag{4.9}$$

In the above, $\mathbf{X} = [x, y]^T$ indicates the position vector; and $\xi = \left[\xi_x, \xi_y\right]^T$, the separation vector between two points $\mathbf{X}$ and $\mathbf{X}+\xi$.

In the present thesis work, each material property is considered to vary at each Gauss point of all the finite elements. Thus, if there are n finite elements in total, then there are N (= $n \times$ *Number of Gauss points* in each element) material property values associated with these n elements.

Consider only the fluctuating component of the homogeneous stochastic field, which models the material property variations around its expected value. Then these N values, $a_i = a(\mathbf{X}_i)$ (i = 1,2,3,.....,N), are random variables with mean zero but correlated, where $\mathbf{X}_i$ corresponds to the location of each Gauss point. Their correlational characteristics can be specified in terms of the covariance matrix C_{aa}, whose ij^{th} - component is given by

$$c_{ij} = \text{Cov}\,[a_i a_j] = E[a_i a_j] = R_{aa}(\xi_{ij}) \tag{4.10}$$

where $\xi_{ij} = \mathbf{X}_j - \mathbf{X}_i$ = the separation distance between the Gauss points i and j.

A vector $\mathbf{a} = [a_1 \;\; a_2 \ldots . a_N]^T$ can then be generated by

$$\mathbf{a} = \mathbf{LZ} \tag{4.11}$$

in which $\mathbf{Z} = [Z_1 \;\; Z_2 \ldots . . Z_N]^T$ is a vector consisting of N independent Gaussian random variables with mean zero and unit standard deviation; and $\mathbf{L}$ is a lower triangular matrix obtained by the Cholesky decomposition of the covariance matrix C_{aa}. Thus

$$\mathbf{L}\mathbf{L}^T = C_{aa} \tag{4.12}$$

Once the Cholesky decomposition is accomplished, different sample vectors of $\mathbf{a}$ are easily obtained by generating different samples for the independent Gaussian random vectors $\mathbf{Z}$.

The correlation properties of the stochastic field representing the fluctuating components of material properties are expressed using four different correlation models. The choice of these models in this work is due to their wide use in the literature (Vanmarcke[118]). These correlation models are:

1. Gaussian correlation model
2. Markov model (or First-Order autoregressive model)
3. Second-Order autoregressive model
4. Triangular correlation model

4.3.1 Gaussian Correlation Model

The squared exponential correlation model which is commonly known as the Gaussian correlation model is given by

$$R_{aa}(\xi) = \sigma_0^2 \exp\left[-\left(\frac{|\xi|}{d}\right)^2\right] \tag{4.13}$$

where d is a positive parameter such that when it is large the correlation disappears more slowly and σ_0 is the standard deviation of the stochastic field. This model is illustrated in Figure 4.10 for three values of d, viz. 10, 30 and 50.

In Figure 4.10, it is shown that at the separation distance of 20, the correlation values are 0.02, 0.65 and 0.85 for d=10, 30, and 50 respectively, e.g., the correlation is more in the case of a high value of d.

4.3.2 Markov Model

The First-Order autoregressive correlation model is given by

$$R_{aa}(\xi) = \sigma_0^2 \exp\left[-\left(\frac{|\xi|}{d}\right)\right] \tag{4.14}$$

where d and σ_0 are as described above. Figure 4.11 shows a sketch of the Markov model as a function of the separation distance for three values of d= 10,30 and 50.

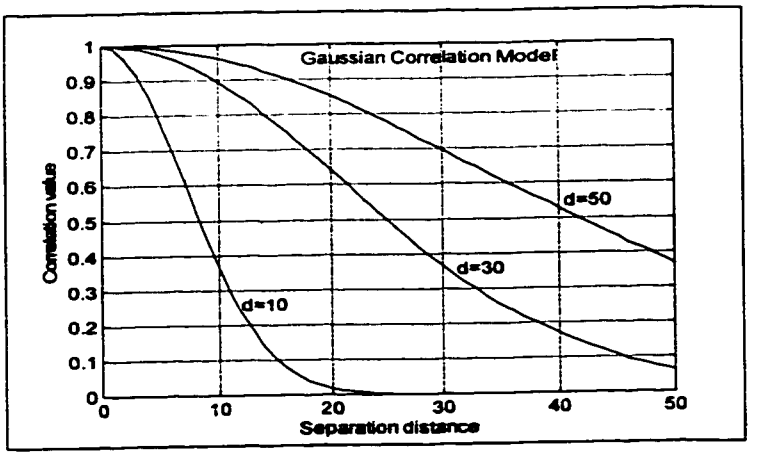

Figure 4.10 The Gaussian correlation function for d = 10, 30 and 50

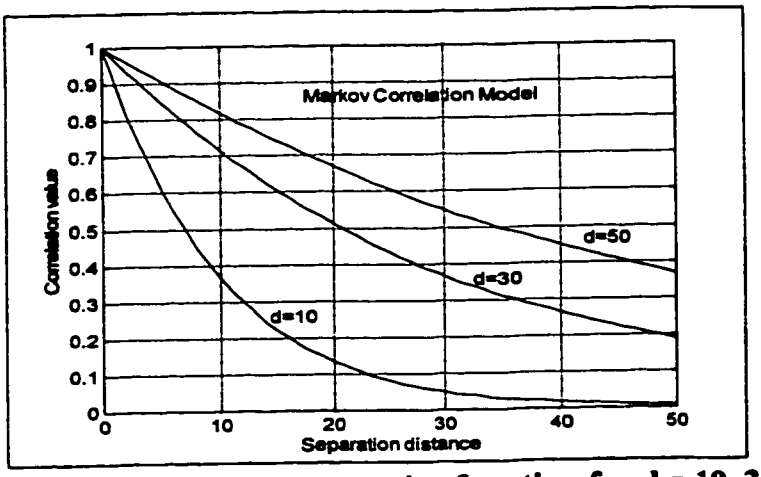

Figure 4.11 The First-Order autoregressive function for d = 10, 30 and 50

From Figure 4.11, it is observed that the nature of all graphs is similar e.g., all are of concave shape and the correlation values are 0.14, 0.51 and 0.69 at a separation distance of 20 for $d = 10$, 30, and 50 respectively.

4.3.3 Second-Order Autoregressive Model

The correlation function in the case of Second-order Autoregressive corelation model is given by

$$R_{aa}(\xi) = \sigma_0^2\left(1+\frac{|\xi|}{d}\right)\exp\left[-\left(\frac{|\xi|}{d}\right)\right] \tag{4.15}$$

The correlation values of this model are shown in Figure 4.12 as a function of separation distance ξ. The influence of the constant d on these correlation values is presented for d = 10, 30 and 50.

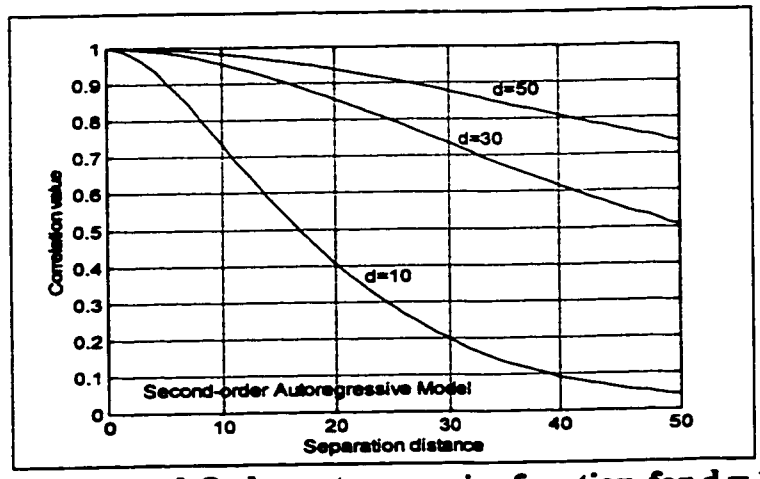

Figure 4.12 The Second-Order autoregressive function for d = 10, 30 and 50

It is observed from Figure 4.12 that at d = 10 the nature of the graph is concave but at d =30 and 50, the nature of the graphs is convex. The correlation values are 0.41, 0.86 and 0.95 at a separation distance of 20 for d = 10, 30 and 50.

4.3.4 Triangular Correlation Model

The Triangular correlation function is given by

$$R_{aa}(\xi) = 1 - \frac{|\xi|}{d} \qquad \text{for} \quad |\xi| < d \tag{4.16a}$$

$$R_{aa}(\xi) = 0 \qquad \text{for} \quad |\xi| \geq d \tag{4.16b}$$

The correlation values of the triangular model are plotted in Figure 4.13 as a function of separation distance ξ. The effect of constant d on the correlation properties are brought out for $d = 10$, 30 and 50.

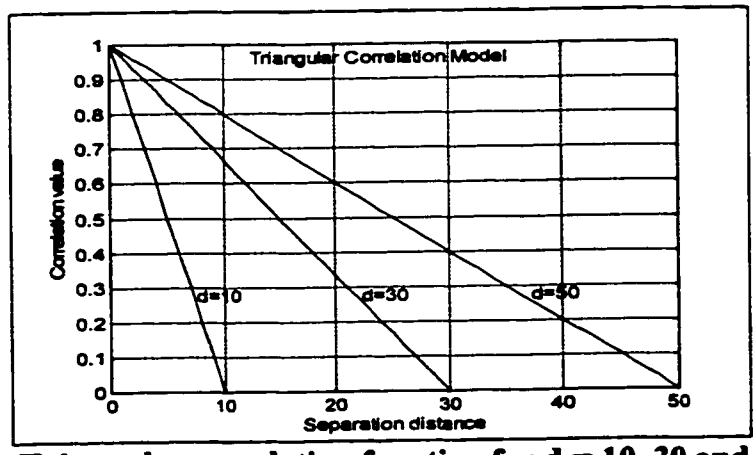

Figure 4.13 The Triangular correlation function for d = 10, 30 and 50

By comparison of all the correlation models at a separation distance of 20 it is shown that the Second Order autoregressive model gives the highest correlation value which are 0.41, 0.86 and 0.95 for d = 20, 30 and 50 respectively. In Gaussian Correlation Model the

correlation value (0.02) is less for d =10 but for d = 50 the correlation value (0.85) is higher than that of Markov correlation model and Triangular correlation model.

The stochastic field $a(\mathbf{X})$ represents the deviatoric components of the material property with autocorrelation function as given in Eqs.(4.13-4.16). The stochastic field $a(\mathbf{X})$ for each Gauss point is represented by the value of a_g of $a(\mathbf{X})$ at the Gauss point $\mathbf{X}_g$ of the structure, i.e. $a_g = a(\mathbf{X}_g)$.

The basic material properties such as the elastic modulus and Poisson's ratio are assumed to have a Gaussian distribution as indicated in the following.

$$E_{1g} = E_{1m}(1+a_g) \qquad \text{1-directional Young modulus} \qquad (4.17)$$

$$E_{2g} = E_{2m}(1+b_g) \qquad \text{2-directional Young modulus} \qquad (4.18)$$

$$\nu_{12g} = \nu_{12m}(1+c_g) \qquad \text{1-2 directional Poisson's ratio} \qquad (4.19)$$

$$G_{12g} = G_{12m}(1+d_g) \qquad \text{Shear modulus} \qquad (4.20)$$

where E_{1m} and E_{2m} are the mean values of Young's modulus in fiber and matrix direction respectively. Further, ν_{12m}, and G_{12m} are the mean values of Poisson's ratio and shear modulus respectively.

It is noted here that the standard deviations of a_g,b_g,c_g, and d_g represent the coefficients of variation of the material properties E_{1g}, E_{2g}, ν_{12g} and G_{12g}. The assumption of Gaussian distribution implies the possibility of generating negative values of materials properties.

In order to avoid this difficulty, the values of random variable a_g in the case of Monte Carlo simulation are confined to the range

$$-1+\varepsilon \le a_g \le 1-\varepsilon \tag{4.21}$$

in which ε is a positive constant considered to avoid the mathematical complications that would arise if a_g indeed becomes zero. For numerical calculations, a value of ε=0.05 is used in the present work.

It is noted that the variation of orientation angle θ_g and thickness of plies t_g are evaluated in a similar manner as

$$\theta_g = \theta_m (1+e_g) \tag{4.22}$$

$$t_g = t_m (1+f_g) \tag{4.23}$$

where θ_m and t_m are the mean values of the ply angle and ply thickness respectively.

4.4 Stochastic Finite Element Analysis

4.4.1 Stochastic Elasticity Matrix

Using the test data on elastic constants of the composite material from Table 4.2, the stochastic processes that correspond to the Young's modulus, Poisson's ratio, and shear modulus are determined according to Eqs.(4.17-4.20), and further, sample realizations at each Gauss point in a finite element mesh are obtained. For instance, if a three-point integration is used for the elements, then there are nine Gauss points in each element, and

at these nine Gauss points nine different sample realizations of the stochastic process that corresponds to each elastic constant are generated and used. A set of sample realizations of these parameters for one simulation are shown in Figure 4.14.

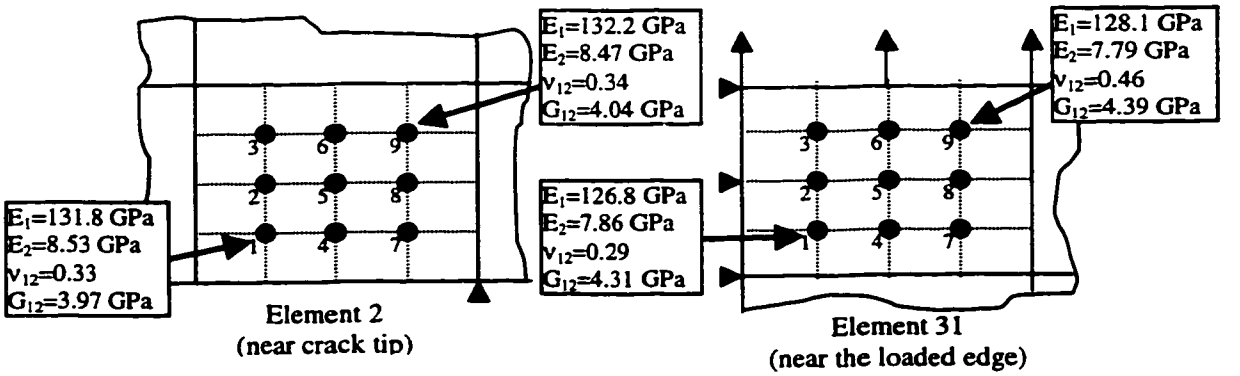

Figure 4.14 A set of sample realizations of elastic constants at different Gauss points

Using the generated sample realizations of elastic constants at each Gauss point, the stochastic laminate elasticity matrix [E] at the corresponding Gauss point is calculated according to Eq.(3.129) in Chapter 3. A sample realization of the stochastic elasticity matrix [E] for a $[0/90]_{6S}$ laminate for the simulation that is the same as the one shown in Figure 4.14, is now shown in Figure 4.15.

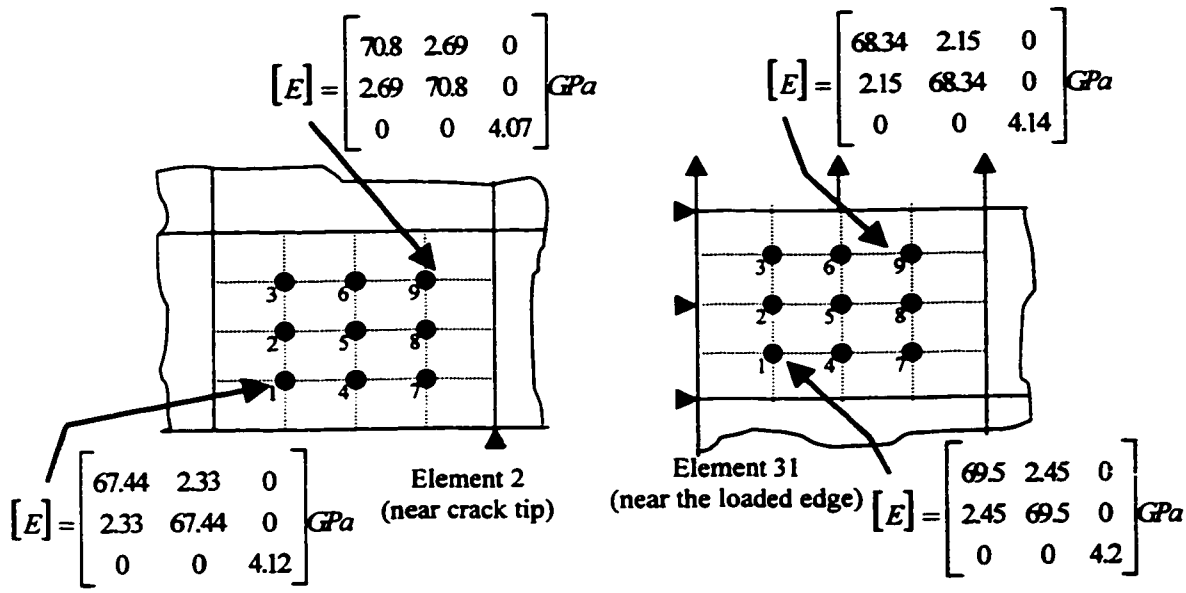

Figure 4.15 A set of sample realizations of stochastic elasticity matrix at different Gauss points

4.4.2 Finite Element Solution Process

Now for one particular simulation, the nine elasticity matrices that correspond to the nine Gauss points of an element are used to calculate the stiffness matrix $[K]^{(e)}$ of that particular element based on the numerical integration that involves these nine Gauss points and the corresponding weighting factors as [2]

$$[K]^{(e)} = \sum_{i=1}^{9} [B]^T [E]_i [B] t (\det J) W_i \tag{4.24}$$

where $[E]_i$ is the sample realization of the laminate elasticity matrix and other terms are defined in Chapter 2.

Similarly, all the element stiffness matrices are calculated using the generated sample realizations of the stochastic elasticity matrix at the corresponding Gauss points.

These stochastic element stiffness matrices are assembled in the same way as in the standard finite element formulation. For instance, for a mesh of 31 elements (refer to Figure 3.8 in Chapter 3) one can write

$$[K] = \sum_{e=1}^{31} [K]^{(e)} \tag{4.25}$$

After the boundary conditions are imposed, the stochastic values of nodal displacements and strain energy(SE) are calculated respectively as

$$[K]\{U\} = \{f\}; \qquad SE = \frac{1}{2}\{U\}\{f\} \tag{4.26}$$

where $\{U\}$ and $\{f\}$ are the displacement and force vectors respectively.

A sample set of stochastic nodal displacement values for a $[0/90]_{6s}$ NCT-301 laminate for one particular simulation, is presented in Table 4.3.

Table 4.3 A set of sample realizations of nodal displacements for a $[0/90]_{6s}$ NCT-301 laminate

Disp. (mm)	Crack edge				Loaded edge						
	Node 1	Node 2	Node 3	Node 4	Node 110	Node 111	Node 112	Node 113	Node 114	Node 115	Node 116
u	0	-0.081	-0.016	-0.207	0	0.036	0.063	0.066	0.063	0.055	0.047
v	1.305	1.269	1.099	0.848	2.36	2.30	2.17	2.037	1.935	1.868	1.828

The corresponding sample realization of the strain energy is 186.18 J.

4.4.3 Calculation of K_I based on Displacement Extrapolation Method

After calculating the sample realizations of the nodal displacements, the sample realizations of K_I that correspond to two different nodal points along the crack edge θ = 180° are determined using Eq.(3.30) in Chapter 3, for one simulation. Finally the K_I at the original crack tip is calculated by extrapolation to the crack tip using the equation of straight line as

$$K = ma + C \tag{4.27}$$

where a is the radial distance from the crack tip along the line θ = 180° and further, m and C are the slope of the straight line and a constant respectively, which can be determined for two different radial distances as

$$m = \frac{K_2 - K_1}{a_2 - a_1}; \qquad C = K_1 - ma_1 \tag{4.28}$$

These values of C and m are are the sample realization of the stochastic variables C and m. Now by performing a total of 250 simulations according to the above procedure, the corresponding 250 sample realizations of K_{Ii}, where i=1,2,...,250, are generated. Using these sample values, the mean value, the standard deviation and the coefficient of variation of K_I are calculated using Eqs.(4.3-4.7).

4.4.4 Calculation of K_I based on Energy Release Rate Method

According to the Section 4.4.1 and Section 4.4.2, the strain energy is calculated for a particular crack length for one simulation. The crack length is advanced (say, by da) which is achieved in the Finite Element Analysis by releasing one node at a time. The strain energy before and after releasing the node are calculated. Using these values the Energy Release Rate (G_I) is calculated as

$$G_I = \frac{U_2 - U_1}{a_2 - a_1} \tag{4.29}$$

where U_2 and U_1 are the values of strain energy corresponding to two crack lengths a_2 and a_1 respectively.

The approach [2] of advancing the crack by two different increments, calculating the K_I in each case using Eq.(3.43) in Chapter 3 and finally determining the value of K_I at original crack length by extrapolation of K_I values to original crack length (using Eqs.(4.27-4.28)), is followed

In a similar manner, 250 sample realizations of G_I and K_I are calculated by performing a total of 250 simulations. Using these sample realizations the mean value, the standard deviation and the coefficient of variation of G_I and that of the K_I are calculated.

4.5 Program Development

A computer subprogram is developed which could estimate the response variability due to material property variability and geometry variation at each Gauss point. The details of the routine are described in Appendix II.

Once the random values of the material properties at each Gauss point are evaluated then it is necessary to calculate the elasticity matrix [E] at each Gauss point because the elasticity matrix depends on the material properties. So the FEM program, which has been developed in Chapter 3 has been modified for the case of the random values of the material properties. The modified program is shown schematically in Figure 4.14 and Figure 4.15.

4.5.1 Subroutine *fmdlrand*

The main purpose of this subroutine is to evaluate the random values of the material properties at each Gauss point according to the autocorrelation functions described in Section 4.3. First of all this subroutine calculates the separation distance between all the Gauss points of a mesh, and then it calculates the covariance matrix using Eqs.(4.13-4.16). The subroutine then evaluates the different sample vectors of stochastic field *a, b, c* and *d* by the Cholesky decomposition of the covariance matrix and lastly, the random sample values of Young's modulus, Poisson's ratio and shear modulus are evaluated using Eqs.(4.17-4.20) and stored in the arrays E11, E22, P12 and G. The program flow chart is shown in Figure 4.14. The sample stochastic fields of E_1 are shown in Figure 4.16 for two simulations.

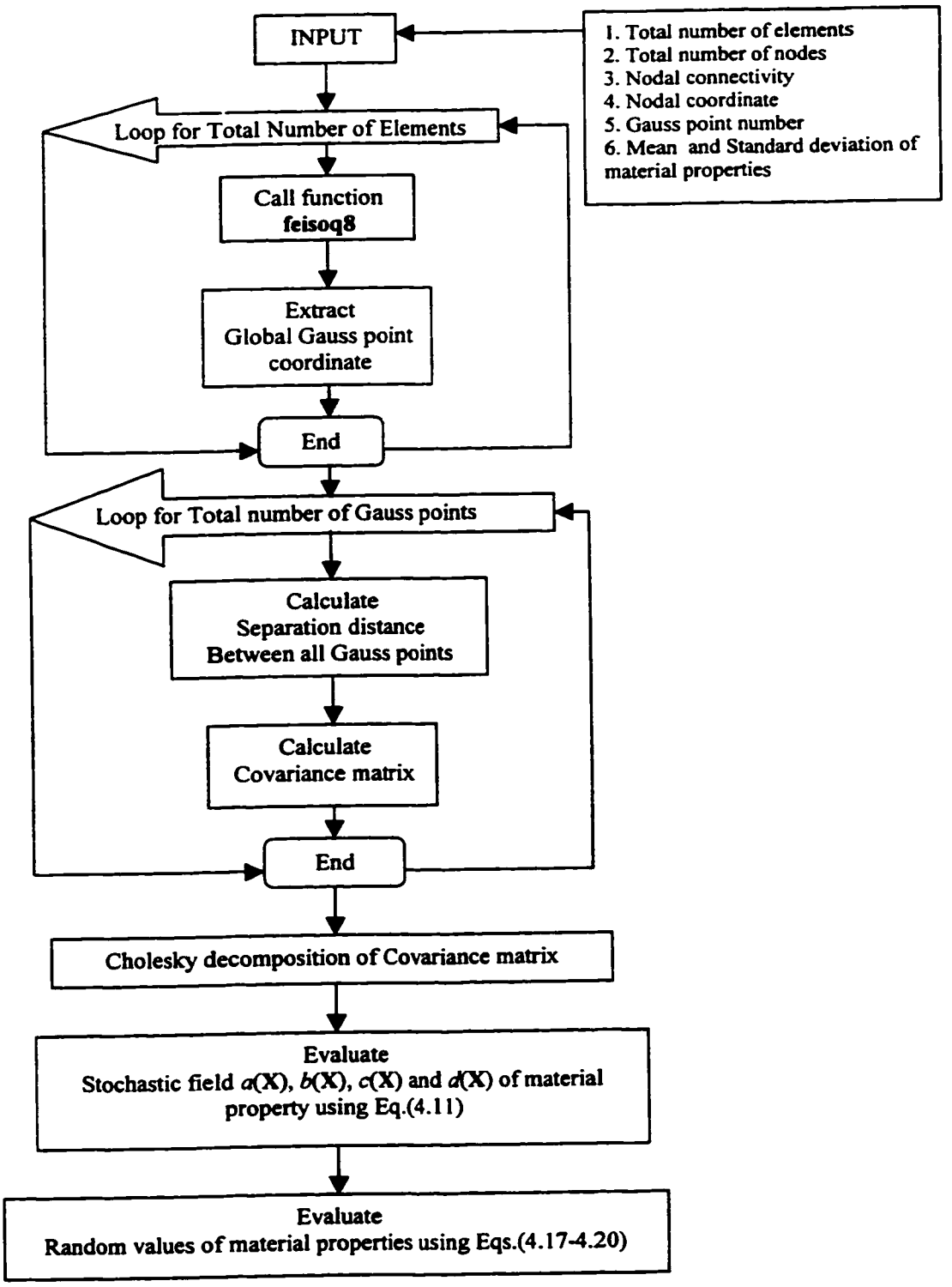

Figure 4.16 Program flow chart for the calculation of stochastic fields for elastic constants

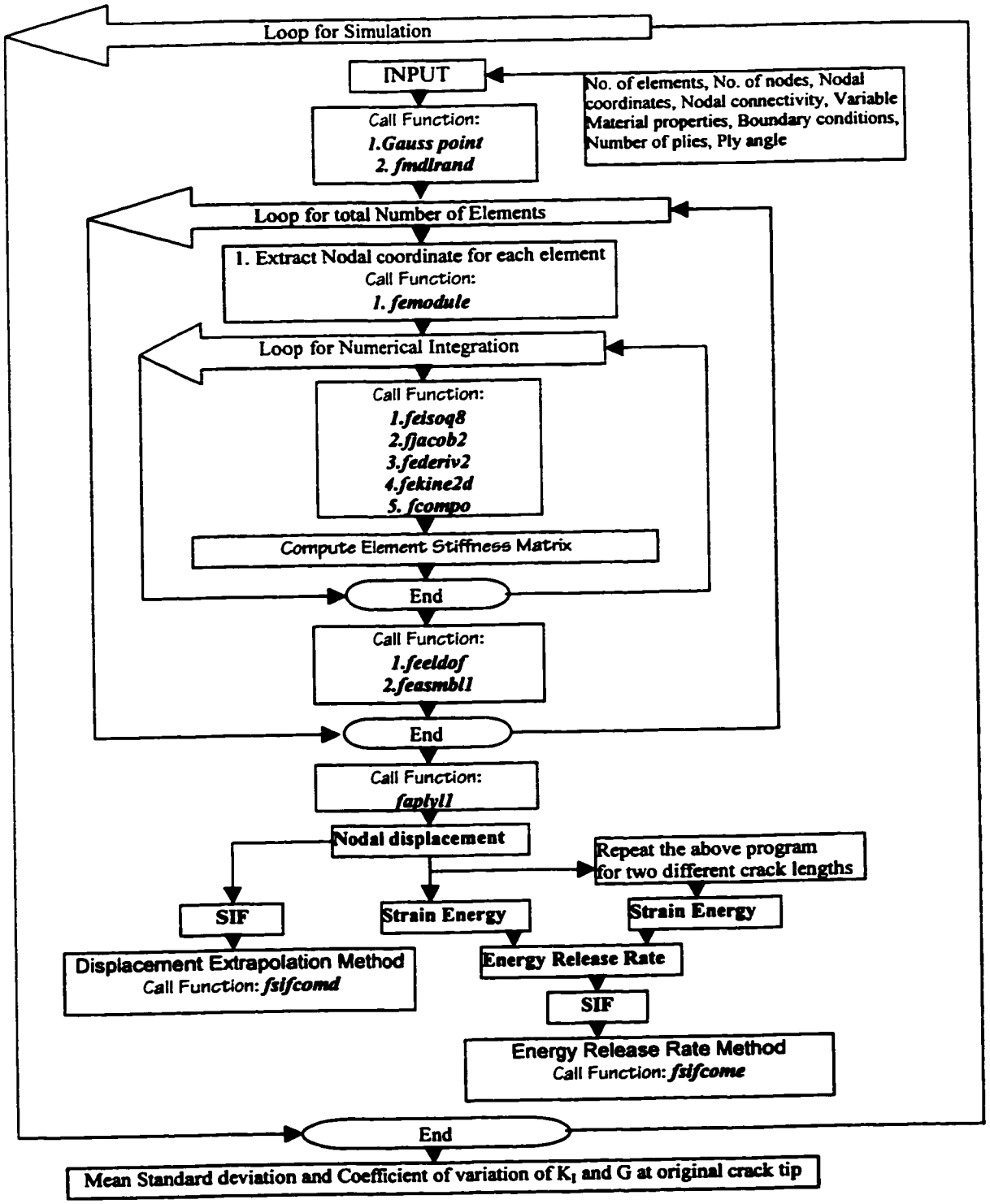

Figure 4.17 Program flow chart for calculation of SIF considering stochastic fields for elastic constants

4.5.2 Subroutine *femodule*

The purpose of this subroutine is to extract the variable material properties at each Gauss point within a element and to store them in the arrays Ee1, Ee2, Mu12, Mu21 and Ge12.

4.5.3 Subroutine *fsifcomd*

The main purpose of this subroutine is to calculate the SIF by Displacement Extrapolation Method. First it calculates the SIF at two different radial distances and hence calculates the slope and constant of the straight line which passes through these two values of SIF. Finally it evaluates the SIF at radial distance zero and stores the value in the array KI5 for 250 simulations.

4.5.4 Subroutine *fsifcome*

The purpose of this subroutine is to evaluate the SIF by the Strain Energy Release Rate Method. The SIF is calculated according to the procedure which is described in Chapter 3 and the value is stored in the array K5 for 250 simulations.

4.6 Example Applications

The MATLAB® program, developed in this chapter, is now demonstrated through the application to a composite laminate of configuration $[0/90]_{12S}$ made from NCT301

composite material. The example considered is the same example problem, which is described in Chapter 3 in Section 3.6. Also the finite element mesh employed in the solution is shown in Chapter 3 in Figure 3.8.

The values of mean, standard deviation and coefficient of variation of the elastic constants for NCT301 composite material that are determined from test data are listed in Table 4.2.

It is noted that, the standard deviation and coefficient of variation of ply angle and ply thickness are assumed to be equal to the maximum value of the standard deviation and coefficient of variation of material properties, which are found out by testing. The maximum separation distance is set to be equal to 25.99 mm because for any value more than this value the Choleski decomposition is not positive definite.

❑ **Simulated sample values of Young's modulus**

The fiber direction Young's modulus are computed at each Gauss point using the developed program for one simulation, and the simulated sample variations of Young's modulus are shown in Figure 4.16. Here only the variations of material properties are considered.

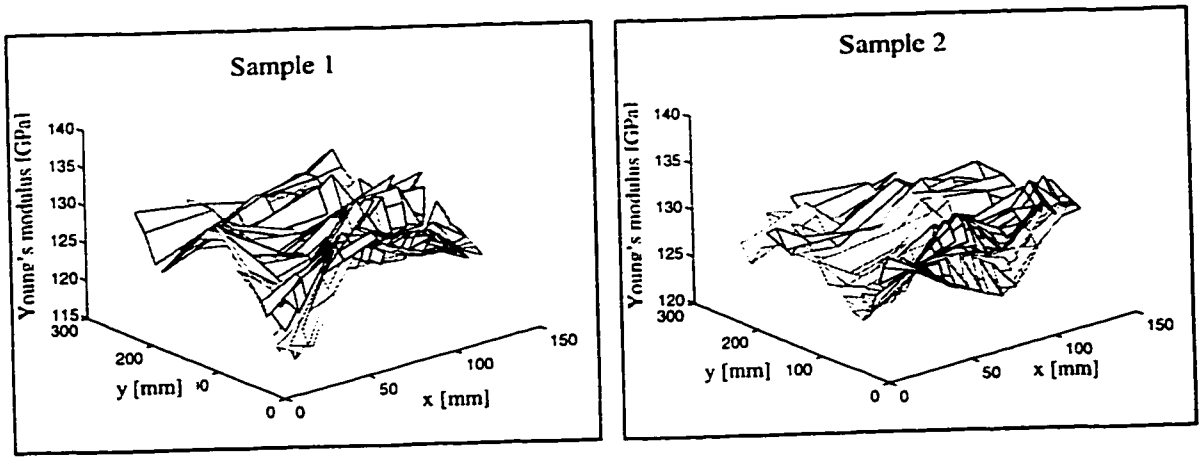

Figure 4.18 Simulated sample variations of fiber direction Young's modulus

❑ Stress Intensity Factor

The mean value, standard deviation and coefficient of variation of SIF are evaluated for 250 simulations of Gaussian Correlation Model using the following two methods.

(a) *Displacement Extrapolation Method*

By this method the SIF for the node 4 and node 3 along $\theta = 180°$ are calculated and then the slope m and constant C of the straight line, which passes through these two points of SIF, are calculated using Eqs.(4.25-4.26). The SIF at crack tip i.e. at node 5 is evaluated by using Eq.(4.24). Finally the mean, standard deviation and coefficient of variation of SIF at crack tip are computed for 250 simulations, which are listed in Table 4.4.

Table 4.4 The SIF of a cracked laminate $[0/90]_{6S}$ made of NCT301 composite material determined using the Gaussian correlation model based on the Displacement Extrapolation Method

Mode of variation	Mean value of K_I (MPa$\sqrt{m}$)	Standard deviation of K_I (MPa$\sqrt{m}$)	Coefficient of Variation of K_I
Material properties are variable	64.51	2.22	0.0344
Material properties and Ply angle are variable	59.41	4.35	0.0732
Material properties, Ply angle and Ply thickness are variable	58.44	3.09	0.0746

From Table 4.4 it is can be concluded that, when the ply angles are variable along with material elastic constants, the standard deviation and coefficient of variation of SIF are two times that of the case when only the elastic constants are variable as shown in Figure 4.19.

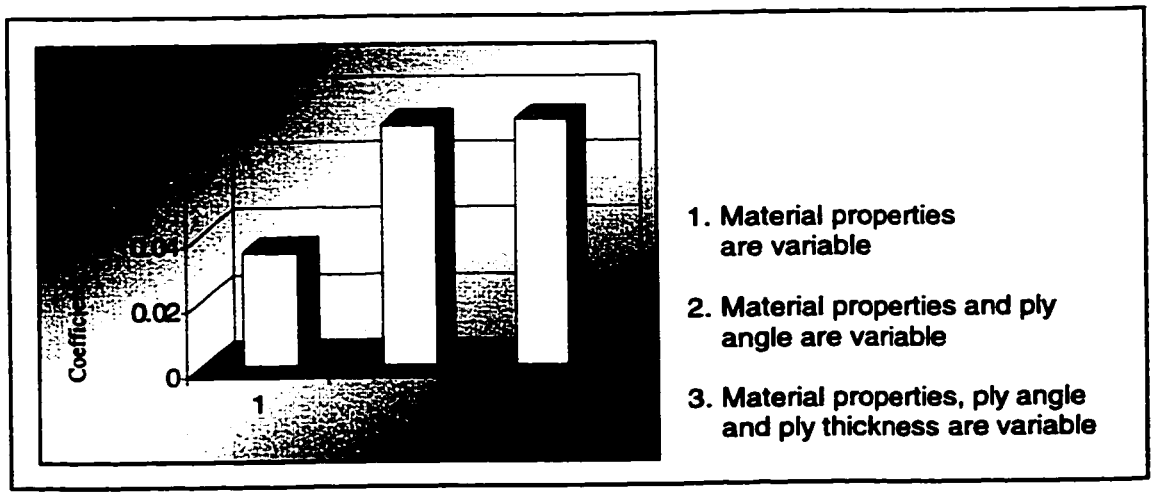

Figure 4.19 Coefficients of variation of SIF for a cracked laminate determined by Displacement Extrapolation Method

(b) ***Strain Energy Release Rate Method***

According to this method, the crack length is advanced by releasing nodes 5 and 6 one at a time and this procedure gives the final crack lengths equal to 50 mm and 60 mm respectively. Now the energy release rates are calculated for each of the final crack lengths and hence the SIF at original crack length is determined by extrapolations using Eqs.(4.24-4.26). After performing the 250 simulations of the above process, the mean, standard deviation and coefficient of variation of SIF are evaluated for Gaussian Correlation Model and they are presented in Table 4.5.

Table 4.5 The SIF of a laminate $[0/90]_{6S}$ made of NCT301 composite material for Gaussian correlation model determined by Energy Release Rate Method

Mode of variation	Mean value of K_I (MPa$\sqrt{m}$)	Standard deviation of K_I (MPa$\sqrt{m}$)	Coefficient of variation of K_I
Material properties are variable	59.14	1.14	0.0194
Material properties and Ply angle are variable	56.32	5.62	0.0998
Material properties, Ply angle and Ply thickness are variable	56.64	5.64	0.0996

From Table 4.5 it is observed that when the ply angles are variable, the coefficient of variation of SIF is increased by five times when compared to the case in which only the material properties are variable as shown in Figure 4.20.

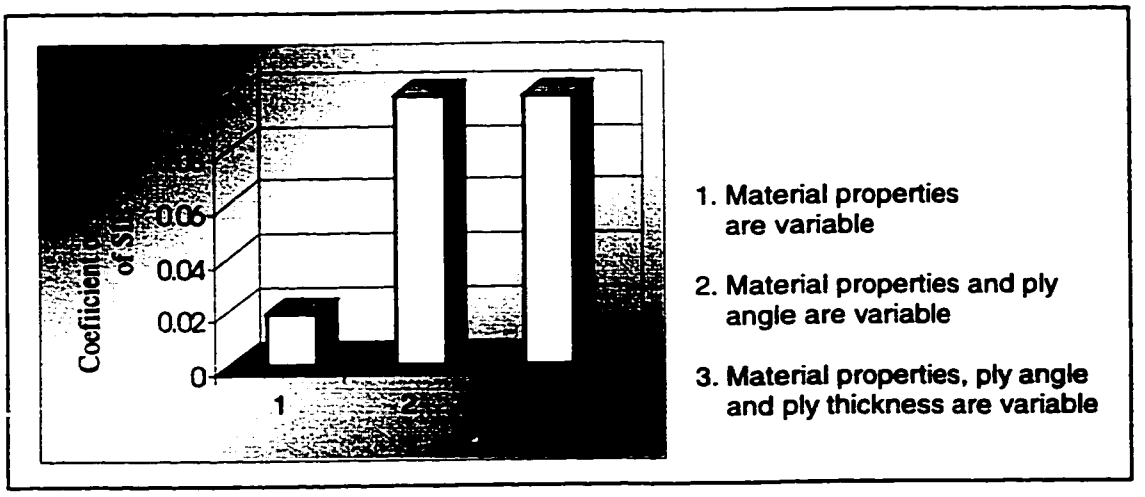

Figure 4.20 Coefficients of variation of SIF for a cracked laminate determined by Energy Release Rate Method

❑ Strain Energy Release Rate (G)

In the present thesis, the Strain Energy Release Rate is also evaluated for composite laminates. The calculation procedure for Strain Energy Release Rate is the same as described in Section 4.6 (b).

The mean value, standard deviation and coefficient of variation of Strain Energy Release Rate are listed in Table 4.6.

Table 4.6 Strain energy release rate of a laminate $[0/90]_{6S}$ made of NCT301 composite material for Gaussian correlation model

Mode of variation	Mean value of G_I (KJ/m)	Standard deviation of G_I (KJ/m)	Coefficient of variation of G_I
Material properties are variable	3.31	0.06	0.0195
Material properties and Ply angle are variable	3.04	0.58	0.1899
Material properties, Ply angle and Ply thickness are variable	2.95	0.52	0.1752

From Table 4.6 it is observed that the coefficient of variation of G_I is approximately ten times that of the case in which the ply angles are variable which is shown in Figure 4.21. So it can be concluded that the fracture parameter is more sensitive to the variation of ply angles and hence this variation is more important in the design of composite laminates.

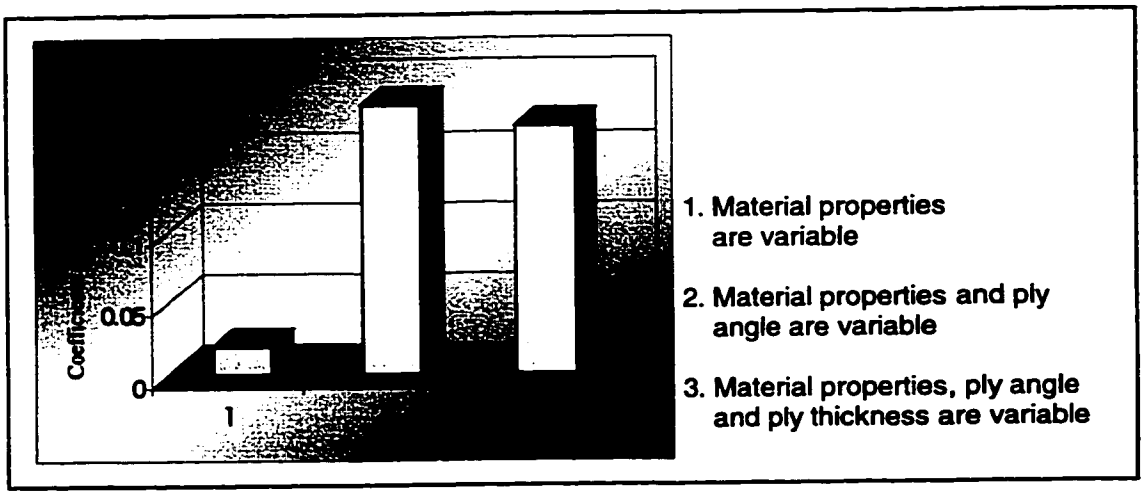

Figure 4.21 Coefficients of variation of energy release rate

4.7 Conclusion and Discussion

In this chapter, the Stress Intensity Factor and Energy Release Rate for anisotropic materials that have stochastic variation of material properties, ply angles and ply thicknesses are determined using the Stochastic FEA. The formulation for the stochastic field modeling of material properties in the finite element analysis of composite laminates is developed and described. Also the effects of these variabilities on the fracture parameters of composite laminates are brought out in this chapter. The computer program, which is developed in Chapter 3, is modified so as to incorporate the fluctuating components of material properties, ply angles and ply thicknesses.

An example problem is used to demonstrate the variation of elastic constant at each Gauss point. The mean, standard deviation and coefficient of variation of stress intensity factor are determined considering the variation of material properties, ply angle and ply thickness, and it is observed that the variation of ply angle has more pronounced effect in the fracture behavior of laminates.

As to the computational time, it is noted here that it takes about 3.5 hrs. to perform 250 simulations for one laminate configuration, when DEM is used. When ERRM is used, it takes about 4 hrs. The computer system is which the computations are performed is a Pentium II 333 MHz system.

Chapter 5

Parametric Study of Fracture in Composite Laminates

5.1 Introduction

When the fracture of composite laminates is considered from the point of view of linear elastic fracture mechanics, the engineer is concerned with two distinct aspects in design: (i) the prediction of the Stress Intensity Factor and (ii) the prediction of the Energy Release Rate. Composite laminates have inherent scatter in elastic and strength properties. A stochastic finite element analysis that can incorporate random material characteristics, ply angles and ply thickness in order to determine the probabilistic characteristics of fracture parameters in laminated composites has been developed in the previous chapter. Application of this analysis to the parametric study of the fracture behavior of orthotropic laminates is presented in this chapter. The stochastic finite element analysis, which is developed in Chapter 4, is now applied to different composite laminates made of the NCT-301 graphite/epoxy composite material, with the objective of analyzing their probabilistic fracture behavior.

In the parametric study, (i) the mean values, standard deviations and coefficients of variation of the stress intensity factor K_I and the energy release rate G_I for different laminates are determined and summarized, (ii) the Displacement Extrapolation Method (DEM) and the Energy Release Rate Method (ERRM) are used for fracture analysis, (iii) the effects of different Correlation Models and variabilities of material properties, ply angles and ply thickness on the fracture parameters of different laminates are determined and summarized, and (iv) efficient and reliable laminate configurations are determined based on the stochastic fracture behavior. When considering the effect of different correlation models, the correlation length of each of the stochastic fields, that represent the material properties, is set to be equal to a constant value. This constant value in turn is dictated by the positive definiteness of the Choleski decomposition.

In Section 5.2, the mean values, standard deviations, and coefficients of variation of the SIF and G_I for $[0/90]_{6S}$ laminate are determined and summarized. In Section 5.3, the mean values, standard deviations, and coefficients of variation of the SIF and G_I for $[90]_{12S}$ laminate are determined and summarized. In Section 5.4, a $[\pm 60/\pm 30]_{3S}$ laminate is considered and its probabilistic parameters are determined. In Section 5.5, a quasi-isotropic $[0/\pm 45/90]_{3S}$ laminate is considered and a similar analysis is performed. The stochastic fracture behavior of the above laminates are evaluated and summarized in Section 5.6. The concept of the reliability calculation for a laminate is summarized in Section 5.7.

A center-cracked laminate of 2W width, 2L length and 2a crack length with a tensile distributed loading of 1.5 KN/mm that is applied in a direction perpendicular to the crack length is considered, where a = 0.334W, W = 120 mm and L = 240 mm. For finite element modeling, one fourth of the cracked laminate is considered due to symmetry and this portion is analyzed for determining the fracture parameters. The finite element mesh employed in the analysis is shown in Figure 3.8 that is presented in Chapter 3, in Section 3.8.

5.2 Fracture Analysis of $[0/90]_{6S}$ NCT-301 Composite Laminate

Sample stochastic elasticity matrix [E] of this laminate is determined at two Gauss point locations and for one simulation they are given below:

At Gauss point 7 in Element 2 near crack edge (refer to Figure 4.15 in Chapter 4)

$$[E] = \begin{bmatrix} 67.44 & 2.33 & 0 \\ 2.33 & 67.44 & 0 \\ 0 & 0 & 4.12 \end{bmatrix} \text{GPa}$$

A Gauss point 9 in Element 31 near loaded edge (refer to Figure 4.15 in Chapter 4)

$$[E] = \begin{bmatrix} 70.8 & 2.69 & 0 \\ 2.69 & 70.8 & 0 \\ 0 & 0 & 4.07 \end{bmatrix} \text{GPa}$$

The mean value, standard deviation, and coefficient of variation of Stress intensity factors (SIF) and Energy release rates (G) obtained from 250 simulations are calculated for

different correlation models and for different modes of variations. These results are presented below in tabulated form, wherein the case of random values of material properties, random values of ply angles, and random values ply thickness are denoted by M, A and T, respectively.

First the case of Gaussian Correlation Model is considered and the results are summarized in Table 5.1.

Table 5.1 The SIF of a $[0/90]_{6S}$ laminate made of NCT-301 composite material in the case of Gaussian correlation model

Mode of variation	Displacement Extrapolation Method (DEM)			Energy Release Rate Method (ERRM)		
	Mean value (MPa√m)	Standard deviation (MPa√m)	Coefficient of Variation	Mean value (MPa√m)	Standard deviation (MPa√m)	Coefficient of Variation
M*	64.51	2.22	3.44	59.14	1.15	1.94
M+A*	59.41	4.35	7.32	56.32	5.62	9.98
M+A+T*	58.45	5.37	9.19	56.64	5.64	9.96

**M=Material properties are random, A = Ply Angles are random, T = Ply Thickness is random*

From Table 5.1, it can be observed that the Displacement Extrapolation Method (DEM) provides a higher mean value of SIF than the Energy Release Rate Method (ERRM) in all the three modes of property variation. The coefficient of variation of SIF is increasing (approximately 2.5 times in the case of DEM and 5 times in the case of ERRM) when the ply angle and ply thickness are variable along with material properties when compared to the case in which only the material properties are variable. However, the mean values of SIF display a decreasing trend. It is also observed that the respective mean values, respective standard deviations and respective coefficients of variation of SIF in the case of M+A and M+A+T differ by a relatively smaller value in case of ERRM. However, the

difference is slightly larger in case of DEM. Therefore, the DEM predicts that the effect of variation in ply thickness on the SIF is small and further, the ERRM predicts that this effect is negligible.

Now, the Markov Correlation Model is considered and the results are summarized in Table 5.2.

Table 5.2 The SIF of a $[0/90]_{6S}$ laminate made of NCT-301 composite material in the case of Markov correlation model

Mode of variation	Displacement Extrapolation Method (DEM)			Energy Release Rate Method (ERRM)		
	Mean value (MPa√m)	Standard Deviation (MPa√m)	Coefficient of Variation	Mean value (MPa√m)	Standard deviation (MPa√m)	Coefficient of Variation
M*	64.56	2.73	4.24	59.28	1.14	1.92
M+A*	58.49	4.47	7.65	55.93	5.55	9.91
M+A+T*	59.20	5.52	9.33	56.39	5.86	10.39

**M= Material properties are random, A =Ply Angles are random, T =Ply Thickness is random*

From Table 5.2, it can be observed that the DEM predicts a higher value of SIF than that of ERRM in all the three modes of property variation. In the case of DEM when the ply angles are variable along with material properties, the mean value of SIF is decreasing but the coefficient of variation of SIF is nearly 2 times more than that of the case of M. A similar trend is observed in the case of ERRM except that the coefficient of variation of SIF in the case of M+A is 5 times more than that of the case of M. Here also it is observed that the effect of variation of ply thickness on the SIF is small in the case of DEM and negligible in the case of ERRM.

The Second Order correlation model is considered next and the corresponding results are summarized in Table 5.3.

Table 5.3 The SIF of a $[0/90]_{6S}$ laminate made of NCT-301 composite material in the case of Second Order correlation model

Mode of variation	Displacement Extrapolation Method (DEM)			Energy Release Rate Method (ERRM)		
	Mean value (MPa√m)	Standard Deviation (MPa√m)	Coefficient of Variation	Mean value (MPa√m)	Standard deviation (MPa√m)	Coefficient of Variation
M*	64.66	3.85	5.95	59.24	1.18	2.00
M+A*	59.15	4.65	7.85	56.32	5.67	10.06
M+A+T*	58.89	4.89	8.29	56.59	5.66	10.00

**M =Material properties are random, A =Ply Angles are random, T =Ply Thickness is random*

From Table 5.3, it can be observed that this correlation model also gives higher values of SIF in the case of DEM than that of ERRM. The coefficient of variation of SIF is increasing when modes A and T are included in the case of DEM. The same is true in the case of ERRM and further, the coefficient of variation is 5 times more in the mode of M+A than the mode of M. The mean values of SIF are reduced when the variations of ply angles and ply thickness are considered in sequence. Also the effect of ply thickness variation on SIF is smaller when compared to the effect of the variation of ply angles.

Finally, the Triangular Correlation Model is considered and the results obtained for this case are summarized in Table 5.4.

Table 5.4 The SIF of a $[0/90]_{6S}$ laminate made of NCT-301 composite material in the case of Triangular correlation model

Mode of variation	Displacement Extrapolation Method (DEM)			Energy Release Rate Method (ERRM)		
	Mean value (MPa√m)	Standard Deviation (MPa√m)	Coefficient of Variation	Mean value (MPa√m)	Standard deviation (MPa√m)	Coefficient Of Variation
M*	64.66	3.85	5.95	59.18	1.10	1.86
M+A*	59.42	5.05	8.50	55.91	5.52	9.88
M+A+T*	59.51	5.49	9.23	56.35	5.78	10.25

**M =Material properties are random, A =Ply Angles are random, T =Ply Thickness is random*

From Table 5.4, observations that are the same as in the case of Table 5.3 can be written. Now, the SIF and its probabilistic characteristics corresponding to the four correlation models are compared in Table 5.5.

Table 5.5 The SIF of a $[0/90]_{6S}$ laminate made of NCT-301 composite material evaluated for four correlation models using the Displacement Extrapolation Method

Correlation Model	Mean value (MPa√m)			Coefficient of variation		
	Mode of Variation			Mode of Variation		
	M *	M+A*	M+A+T *	M *	M+A*	M+A+T *
Gaussian	64.51	59.41	58.45	3.44	7.32	9.19
Markov	64.56	58.50	59.20	4.24	7.65	9.33
Second order	64.83	59.15	58.89	4.10	7.85	8.29
Triangular	64.66	59.42	59.51	5.95	8.50	9.23

**M =Material properties are random, A =Ply Angles are random, T =Ply Thickness is random*

From Table 5.5, it is observed that the mean values of SIF obtained using DEM for the mode of variation of M are almost the same for four different correlation models and this observation is highlighted in Figure 5.1. So one can say that as long as the correlation length is the same, the effect of correlation models on the mean value of SIF is negligible

in the mode of variation of M. However, this effect is relatively more pronounced in the modes of variation of M+A as well as M+A+T. When the coefficient of variation of SIF is considered, the Triangular correlation model gives the maximum value in all the three modes of variation and the Gaussian correlation model gives the minimum value in all the three modes of variation as shown in Figure 5.2.

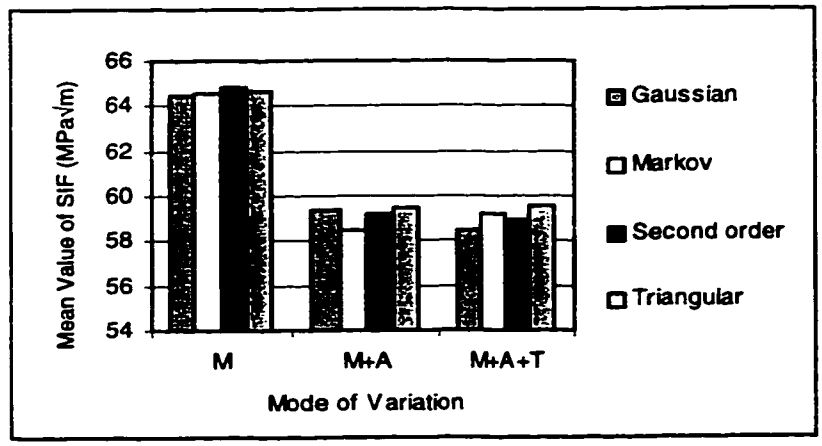

Figure 5.1 **Mean value of SIF obtained using DEM of a $[0/90]_{6S}$ laminate made of NCT-301 composite material**

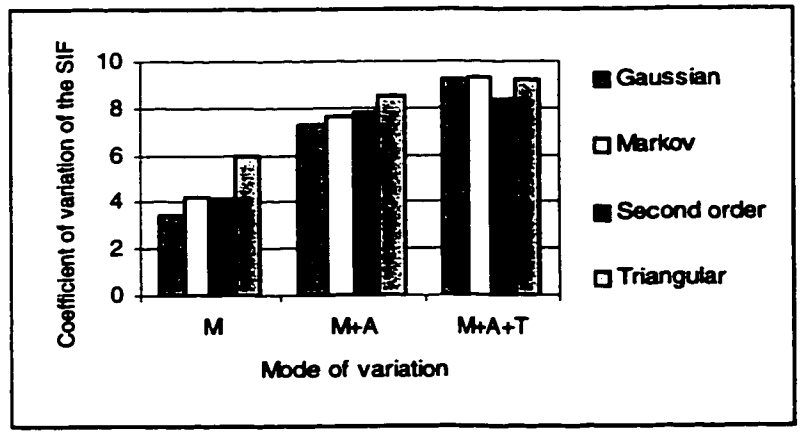

Figure 5.2 **Coefficient of variation of SIF obtained using DEM of a $[0/90]_{6S}$ laminate made of NCT-301 composite material**

Now the results obtained using the ERRM are summarized in a similar manner in Table 5.6.

Table 5.6 The SIF of a $[0/90]_{6S}$ laminate made of NCT-301 composite material evaluated for four correlation models using the Energy Release Rate Method

Correlation Model	Mean value (MPa√m)			Coefficient of variation		
	Mode of Variation			Mode of Variation		
	M*	M+A*	M+A+T*	M*	M+A*	M+A+T*
Gaussian	59.14	56.32	56.64	1.94	9.98	9.96
Markov	59.28	55.93	56.39	1.92	9.91	10.39
Second order	59.24	56.32	56.59	2.00	10.06	10.00
Triangular	59.18	55.91	56.35	1.86	9.88	10.25

**M =Material properties are random, A =Ply Angles are random, T =Ply Thickness is random*

When the ERRM is used, the mean value and the coefficient of variation of SIF are the same in each case for four different correlation models, as shown in Table 5.6, and in Figures 5.3 and 5.4. Hence, no considerable effects of different correlation models are observed in the case of ERRM.

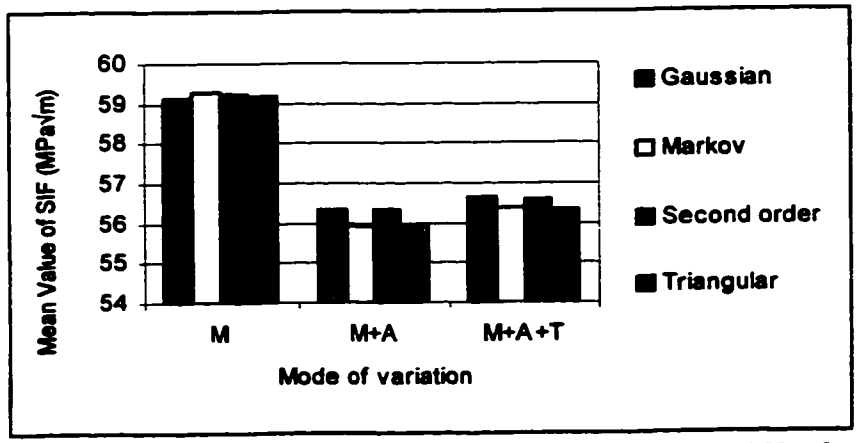

Figure 5.3 Mean value of SIF obtained using ERRM of a $[0/90]_{6S}$ laminate made of NCT-301 composite material

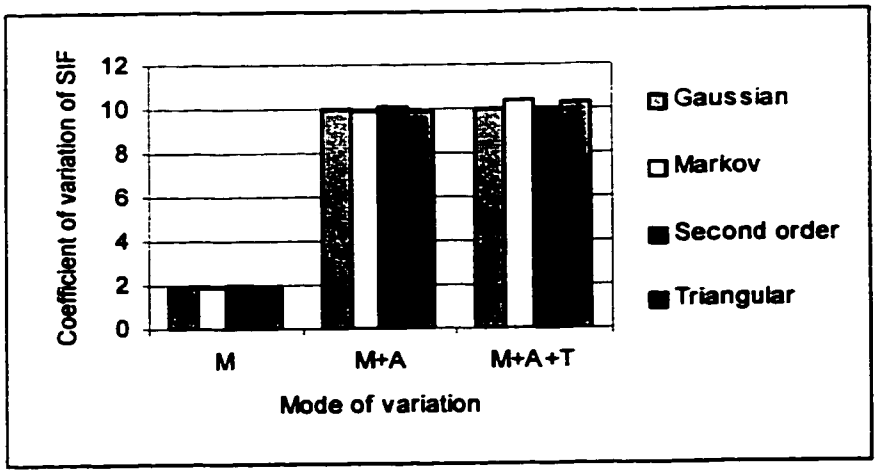

Figure 5.4 Coefficient of variation of SIF obtained using ERRM of a $[0/90]_{6S}$ laminate made of NCT-301 composite material

The Energy Release Rate (G_I) corresponding to the three modes of variation are now determined for Gaussian Correlation Model since as shown in the above analysis it was observed that the different correlation models do not affect the probabilistic characteristics of SIF (as long as the correlation length is the same) when the SIF is determined based on the Energy Release Rate Method. The mean value, standard deviation and coefficient of variation of G_I of a $[0/90]_{6S}$ laminate are presented in the following.

Table 5.7 The G_I of a $[0/90]_{6S}$ laminate made of NCT-301 composite material in the case of Gaussian correlation model

Mode of variation	Mean value of G_I (KJ/m)	Standard deviation (KJ/m)	Coefficient of variation
M*	1.3815	0.0276	2.00
M+A*	1.2454	0.2077	16.68
M+A+T*	1.2535	0.2109	16.83

**M =Material properties are random, A =Ply Angles are random, T =Ply Thickness is random*

It is observed from Table 5.7 that the value of G_I is maximum when only the material properties are variable. However, the coefficient of variation is maximum when random values of ply angles and ply thickness are incorporated along with random values of material properties. It is also observed that the coefficient of variation in the mode of variation of M+A+T is 8 times more than that of the case of M. This underscores the effects of variabilities in ply angles and ply thickness on the probabilistic characteristics of G_I.

5.3 Fracture Analysis of $[90]_{12S}$ NCT-301 Composite Laminate

Sample stochastic elasticity matrix [E] for this laminate is determined at two Gauss point locations and for one simulation they are given below:

(1) At Gauss point 7 in Element 2 near crack edge (refer to Figure 4.15 in Chapter 4)

$$[E]=\begin{bmatrix} 7.79 & 2.21 & 0 \\ 2.21 & 130.61 & 0 \\ 0 & 0 & 4.49 \end{bmatrix} \text{GPa}$$

(2) At Gauss point 9 in Element 31 near load edge (refer to Figure 4.15 in Chapter 4)

$$[E]=\begin{bmatrix} 7.62 & 2.69 & 0 \\ 2.69 & 131.63 & 0 \\ 0 & 0 & 4.39 \end{bmatrix} \text{GPa}$$

The mean value, standard deviation, and coefficient of variation of Stress intensity factors (SIF) are calculated from 250 simulations for different correlation models. The two

methods, Displacement Extrapolation Method (DEM) and Energy Release Rate Method (ERRM) are used to determine these values. These results are presented below in tabulated form.

First the case of Gaussian Correlation Model is considered and the results are summarized in Table 5.8.

Table 5.8 The SIF of a $[90]_{12S}$ laminate made of NCT-301 composite material in the case of Gaussian correlation model

Mode of variation	Displacement Extrapolation Method (DEM)			Energy Release Rate Method (ERRM)		
	Mean value (MPa√m)	Standard Deviation (MPa√m)	Coefficient Of Variation	Mean value (MPa√m)	Standard Deviation (MPa√m)	Coefficient Of Variation
M*	51.23	1.95	3.80	56.32	1.00	1.78
M+A*	43.68	2.71	6.21	51.20	3.63	7.10
M+A+T*	44.07	3.25	7.37	51.22	4.05	7.90

**M =Material properties are random, A =Ply Angles are random, T =Ply Thickness is random*

From Table 5.8, it is observed that in the case of M the mean values of SIF are high in both the methods (DEM and ERRM). The ERRM provided higher mean values of SIF than that provided by DEM for this laminate. The coefficients of variation of SIF are nearly 2 times more (by DEM) and 4 times more (by ERRM) in the case of M+A and M+A+T than that of the case of M. It is also observed that the DEM predicts that the effect of variation in ply thickness on the SIF is small and further, the ERRM predicts that this effect is negligible.

Now, the Markov Correlation Model is considered and the results are summarized in Table 5.9.

Table 5.9 The SIF of a $[90]_{12S}$ laminate made of NCT-301 composite material in the case of Markov correlation model

Mode of variation	Displacement Extrapolation Method (DEM)			Energy Release Rate Method (ERRM)		
	Mean value (MPa√m)	Standard Deviation (MPa√m)	Coefficient of variation	Mean value (MPa√m)	Standard deviation (MPa√m)	Coefficient of variation
M*	51.07	2.35	4.61	56.42	1.00	1.77
M+A*	43.88	2.74	6.23	51.14	3.58	7.00
M+A+T*	43.79	3.01	6.88	51.23	3.72	7.26

**M =Material properties are random, A =Ply Angles are random, T =Ply Thickness is random*

From Table 5.9, it can be observed that the ERRM predicts a higher value of SIF than that of DEM in all the three modes of property variation. In the case of DEM when the mode of variation is M+A, the mean value of SIF is decreasing but the coefficient of variation of SIF is nearly 1.5 times more than that of the case of M. A similar trend is observed in the case of ERRM except that the coefficient of variation of SIF in the case of M+A is 4 times more than that of the case of M. Here also it is observed that the effect of variation in ply thickness on the SIF is small in the case of DEM and negligible in the case of ERRM.

The Second order Correlation Model is considered and the results are summarized in Table 5.10.

Table 5.10 The SIF of a $[90]_{12S}$ laminate made of NCT-301 composite material in the case of Second Order correlation model

Mode of variation	Displacement Extrapolation Method (DEM)			Energy Release Rate Method (ERRM)		
	Mean value (MPa√m)	Standard Deviation (MPa√m)	Coefficient of Variation	Mean value (MPa√m)	Standard Deviation (MPa√m)	Coefficient of Variation
M *	51.20	2.23	4.35	56.36	1.03	1.83
M+A*	43.67	2.88	6.60	51.16	3.66	7.15
M+A+T*	43.84	2.94	6.72	51.21	4.04	7.90

**M =Material properties are random, A =Ply Angles are random, T =Ply Thickness is random*

From Table 5.10, it can be observed that this correlation model also gives higher values of SIF in the case of ERRM than that of DEM. The coefficient of variation of SIF is increasing when modes A and T are included in the case of DEM. The same is true in the case of ERRM and further, the coefficient of variation is 4 times more in the mode of M+A than the mode of M. The mean values of SIF are reduced when the variations of ply angles and ply thickness are considered in sequence. Also the effect of ply thickness variation on SIF is smaller when compared to the effect of the variation of ply angles. Finally, the Triangular Correlation Model is considered and the results obtained for this case are summarized in Table 5.11.

Table 5.11 The SIF of a $[90]_{12S}$ laminate made of NCT-301 composite material in the case of Triangular correlation model

Mode of variation	Displacement Extrapolation Method (DEM)			Energy Release Rate Method (ERRM)		
	Mean value (MPa√m)	Standard Deviation (MPa√m)	Coefficient of Variation	Mean value (MPa√m)	Standard Deviation (MPa√m)	Coefficient Of Variation
M *	50.85	3.26	6.41	56.26	0.86	1.53
M+A*	43.63	3.31	7.60	51.16	3.51	6.87
M+A+T*	43.79	3.62	8.26	51.16	3.58	7.01

**M =Material properties are random, A =Ply Angles are random, T =Ply Thickness is random*

From Table 5.11, observations that are the same as in the case of Table 5.10 can be written.

Now, the SIF and its probabilistic characteristics corresponding to the four correlation models are compared in Table 5.12.

Table 5.12 The SIF of a $[90]_{12S}$ laminate made of NCT-301 composite material evaluated for four correlation models using the Displacement Extrapolation Method

Correlation Model	Mean value (MPa√m)			Coefficient of variation		
	Mode of Variation			Mode of Variation		
	M *	M+A*	M+A+T *	M *	M+A*	M+A+T *
Gaussian	51.24	43.68	44.07	3.80	6.21	7.37
Markov	51.07	43.88	43.79	4.61	6.23	6.88
Second order	51.20	43.67	43.84	4.35	6.60	6.72
Triangular	50.85	43.63	43.79	6.41	7.60	8.26

**M =Material properties are random, A =Ply Angles are random, T =Ply Thickness is random*

From Table 5.12, it is observed that the mean values of SIF obtained using DEM for the mode of variation of M are almost the same for four different correlation models and this observation is highlighted in Figure 5.5. This is true also for the cases of M+A and M+A+T. So one can say that the effect of correlation models on the mean value of SIF is negligible (as long as the correlation length is the same) in the mode of variation of M. However, this effect is relatively more pronounced in the modes of variation of M+A as well as M+A+T. When the coefficient of variation of SIF is considered, the Triangular correlation model gives the maximum value and the Gaussian correlation model gives the minimum value in the case of M and M+A as shown in Figure 5.6.

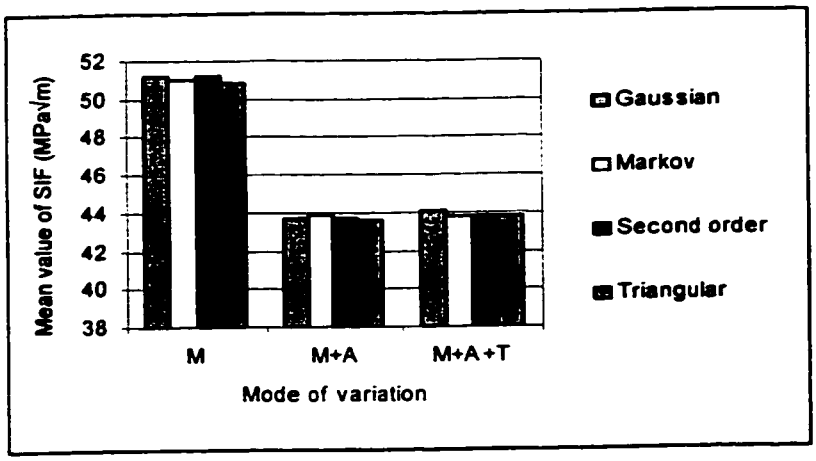

Figure 5.5 Mean value of SIF obtained using DEM for four correlation models

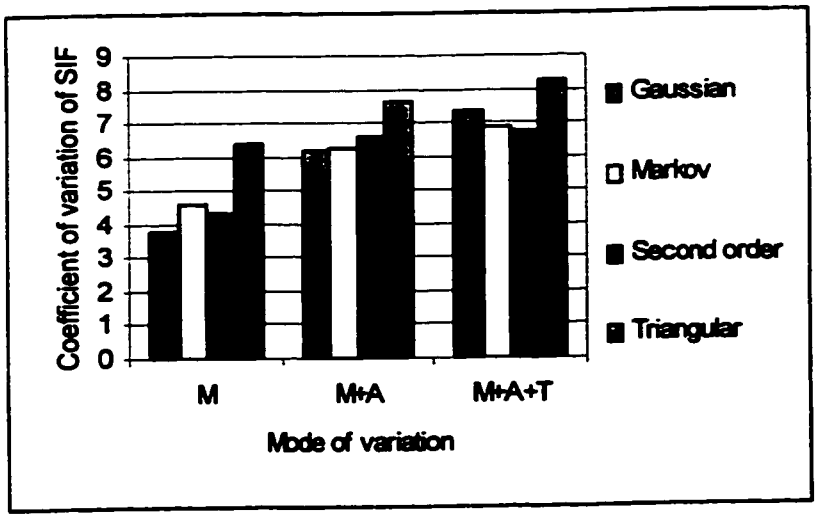

Figure 5.6 Coefficient of variation of SIF obtained using DEM of a $[90]_{12S}$ laminate made of NCT-301 composite material

Now the results obtained using the ERRM are summarized in a similar manner in Table 5.13.

Table 5.13 The SIF of a $[90]_{12S}$ laminate made of NCT-301 composite material evaluated for Four Correlation Models using the Energy Release Rate Method

Correlation Model	Mean value (MPa√m)			Coefficient of variation		
	Mode of Variation			Mode of Variation		
	M *	M+A*	M+A+T *	M *	M+A*	M+A+T *
Gaussian	56.32	51.20	51.22	1.78	7.10	7.90
Markov	56.42	51.14	51.23	1.77	7.00	7.26
Second order	56.36	51.16	51.21	1.83	7.15	7.90
Triangular	56.26	51.16	51.16	1.53	6.87	7.01

**M =Material properties are random, A =Ply Angles are random, T =Ply Thickness is random*

From Table 5.13 it can be observed that the mean value and the coefficient of variation of SIF have the same values in each case for four different correlation models, as shown in Figures 5.7 and 5.8. Hence, no considerable effects of different correlation models are observed in the case of ERRM.

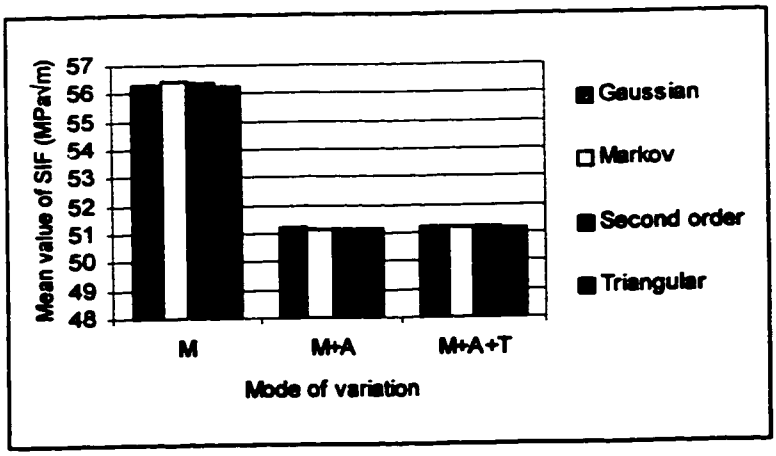

Figure 5.7 Mean value of SIF obtained using ERRM of a $[90]_{12S}$ laminate made of NCT-301 composite material

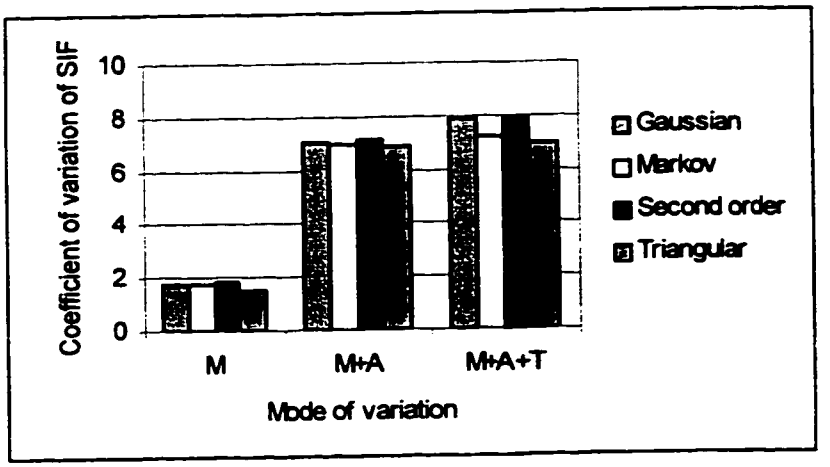

Figure 5.8 Coefficient of variation of SIF obtained using ERRM of a $[90]_{12S}$ laminate made of NCT-301 composite material

Since there is no effect of the different correlation models on the probabilistic characteristics of the SIF of a $[90]_{12S}$ laminate as long as the correlation length is the same, only the Gaussian correlation model is considered to evaluate the G_I and the results are summarized in Table 5.14.

Table 5.14 The G_I of a $[90]_{12S}$ laminate made of NCT-301 composite material in the case of Gaussian Correlation Model

Mode of variation	Mean value of G_I (KJ/m)	Standard deviation (KJ/m)	Coefficient of variation
M*	1.3110	0.0227	1.73
M+A*	1.0628	0.1149	10.81
M+A+T*	1.0691	0.1240	11.60

**M =Material properties are random, A =Ply Angles are random, T =Ply Thickness is random*

It is observed from Table 5.14 that the value of G_I is maximum in the case of M. However, the coefficient of variation is maximum when the mode of variation is M+A or

M+A+T. It is also observed that the coefficient of variation in the case of M+A+T is 6 times more than that of the case of M. This underscores the effects of variabilities in ply angles and ply thickness on the probabilistic characteristics of G_I.

5.4 Fracture Analysis of a $[\pm 60/\pm 30]_{3S}$ NCT-301 Composite Laminate

Sample stochastic elasticity matrix [E] for this laminate is determined at two Gauss point locations and for one simulation they are given below:

(1) At Gauss point 7 in Element 2 near crack edge (refer to Figure 4.15 in Chapter 4)

$$[E] = \begin{bmatrix} 47.27 & 24.38 & 0 \\ 24.38 & 47.27 & 0 \\ 0 & 0 & 26.4 \end{bmatrix} \text{GPa}$$

(2) At Gauss point 9 in Element 31 near loaded edge (refer to Figure 4.15 in Chapter 4)

$$[E] = \begin{bmatrix} 47.99 & 24.21 & 0 \\ 24.21 & 47.99 & 0 \\ 0 & 0 & 26.47 \end{bmatrix} \text{GPa}$$

The mean value, standard deviation and coefficient of variation of SIF are determined for a $[\pm 60/\pm 30]_{3S}$ center cracked composite laminate using the Gaussian Correlation Model and are summarized in Table 5.15.

Table 5.15 The SIF of a $[\pm 60/\pm 30]_{3S}$ laminate made of NCT-301 composite material in the case of Gaussian correlation model

Mode of variation	Displacement Extrapolation Method (DEM)			Energy Release Rate Method (ERRM)		
	Mean value (MPa√m)	Standard Deviation (MPa√m)	Coefficient Of Variation	Mean value (MPa√m)	Standard Deviation (MPa√m)	Coefficient of Variation
M *	41.29	1.88	4.56	54.65	1.01	1.84
M+A*	41.39	1.91	4.62	54.26	1.81	3.33
M+A+T*	41.38	3.09	7.46	54.24	1.81	3.34

**M =Material properties are random, A =Ply Angles are random, T =Ply Thickness is random*

From Table 5.15 it is observed that the ERRM provides a higher mean value of SIF than the DEM. The mean value of SIF is the same in all the three modes of property variation, when both the DEM as well as ERRM are used. So it can be concluded that the effects of variation of ply angles and ply thickness are negligible in the calculation of mean value of the SIF. However, the coefficient of variation of SIF is 1.5 times more when DEM is used and 2 times more when ERRM is used, in the case of M+A+T than in the case of M.

Now, the Markov correlation model is considered and the results are summarized in Table 5.16.

Table 5.16 The SIF of a $[\pm 60/\pm 30]_{3S}$ laminate made of NCT-301 composite material in the case of Markov correlation model

Mode of variation	Displacement Extrapolation Method (DEM)			Energy Release Rate Method (ERRM)		
	Mean value (MPa√m)	Standard Deviation (MPa√m)	Coefficient Of Variation	Mean value (MPa√m)	Standard Deviation (MPa√m)	Coefficient Of Variation
M *	41.12	2.19	5.33	54.67	0.97	1.78
M+A*	41.16	2.28	5.53	54.46	1.73	3.17
M+A+T*	41.78	2.48	5.93	54.48	2.13	3.90

**M =Material properties are random, A =Ply Angles are random, T =Ply Thickness is random*

From Table 5.16, observations that are the same as in the case of Table 5.15 can be made. The Second Order correlation model is considered and the results are summarized in Table 5.17.

Table 5.17 The SIF of a $[\pm 60/\pm 30]_{3S}$ laminate made of NCT-301 composite material in the case of Second Order correlation model

Mode of variation	Displacement Extrapolation Method (DEM)			Energy Release Rate Method (ERRM)		
	Mean value (MPa√m)	Standard Deviation (MPa√m)	Coefficient Of Variation	Mean value (MPa√m)	Standard Deviation (MPa√m)	Coefficient of Variation
M *	41.38	1.82	4.41	54.68	1.02	1.86
M+A*	41.20	2.04	4.69	54.22	1.88	3.46
M+A+T*	41.41	2.30	5.55	54.24	1.81	3.34

**M =Material properties are random, A =Ply Angles are random, T =Ply Thickness is random*

From Table 5.17, observations that are the same as in the case of Tables 5.15 and 5.16 can be made. Finally, the Triangular Correlation Model is considered and the results are summarized in Table 5.18.

Table 5.18 The SIF of a $[\pm 60/\pm 30]_{3S}$ laminate made of NCT-301 composite material in the case of Triangular correlation model

Mode of variation	Displacement Extrapolation Method (DEM)			Energy Release Rate Method (ERRM)		
	Mean value (MPa√m)	Standard Deviation (MPa√m)	Coefficient of Variation	Mean value (MPa√m)	Standard Deviation (MPa√m)	Coefficient of Variation
M *	41.18	2.93	7.11	54.56	0.81	1.49
M+A*	41.39	2.62	6.33	54.43	1.62	2.98
M+A+T*	41.43	2.87	6.63	54.49	1.99	3.66

**M =Material properties are random, A =Ply Angles are random, T =Ply Thickness is random*

From Table 5.18, observations that are the same as in the case of Tables 5.15, 5.16 and 5.17 can be made. Now the SIF and its probabilistic characteristics corresponding to the four correlation models are compared in Table 5.19.

Table 5.19 The SIF of a $[\pm 60/\pm 30]_{3S}$ laminate made of NCT-301 composite material evaluated for four correlation models using Displacement Extrapolation Method

Correlation Model	Mean value (MPa√m)			Coefficient of variation		
	Mode of Variation			Mode of Variation		
	M *	M+A*	M+A+T *	M *	M+A*	M+A+T *
Gaussian	41.29	41.39	41.38	4.56	4.62	7.46
Markov	41.12	41.16	41.78	5.33	5.53	5.93
Second order	41.38	41.20	41.41	4.41	4.96	5.55
Triangular	41.18	41.39	41.43	7.11	6.33	6.93

**M =Material properties are random, A =Ply Angles are random, T =Ply Thickness is random*

From Table 5.19, it is observed that the mean values of SIF obtained using DEM for all the three modes of property variation are the same for four different correlation models and this observation is highlighted in Figure 5.9. So one can say that the effect of correlation models on the mean value of SIF is negligible in this case too. However, the coefficients of variation of SIF are not the same. The Gaussian correlation model gives maximum value of coefficient of variation in the case of M+A+T, whereas the Triangular correlation model gives maximum value in the case of M which is shown in Figure 5.10.

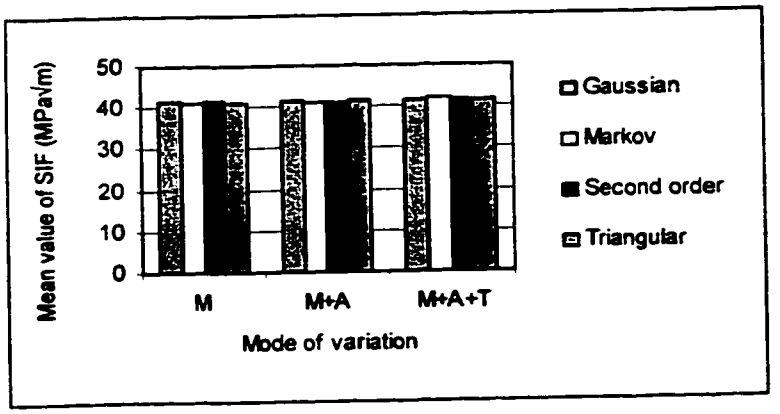

Figure 5.9 **Mean value of SIF obtained using DEM of a $[\pm 60/\pm 30]_{3S}$ laminate made of NCT-301 composite material**

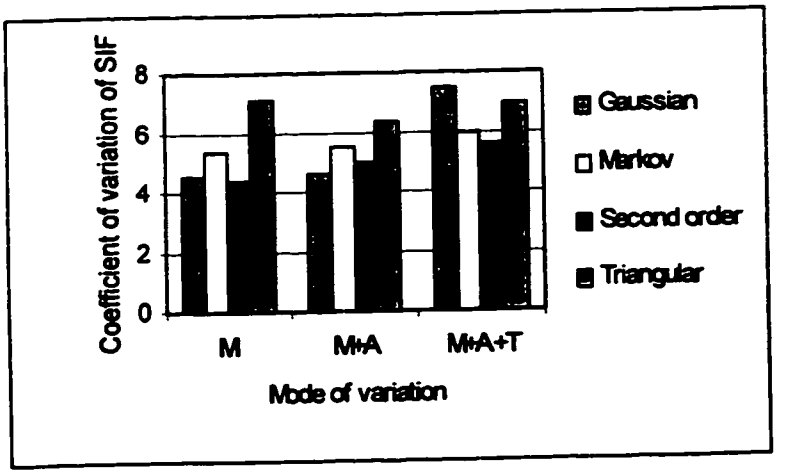

Figure 5.10 **Coefficient of variation of SIF obtained using DEM of a $[\pm 60/\pm 30]_{3S}$ laminate made of NCT-301 composite material**

Now the results obtained using ERRM are summarized in a similar manner in Table 5.20.

Table 5.20 The SIF of a $[\pm 60/\pm 30]_{3S}$ laminate made of NCT-301 composite material evaluated for four correlation models using Energy Release Rate Method

Correlation Model	Mean value (MPa√m)			Coefficient of variation		
	Mode of Variation			Mode of Variation		
	M*	M+A*	M+A+T*	M*	M+A*	M+A+T*
Gaussian	54.65	54.26	54.24	1.84	3.33	3.34
Markov	54.67	54.46	54.48	1.78	3.17	3.90
Second order	54.68	54.22	54.24	1.86	3.46	3.34
Triangular	54.58	54.43	54.49	1.49	2.98	3.66

**M =Material properties are random, A =Ply Angles are random, T =Ply Thickness is random*

From Table 5.20, observations that are the same as in the case of Table 5.19 can be written and these observations are graphically presented in Figures 5.11 and 5.12.

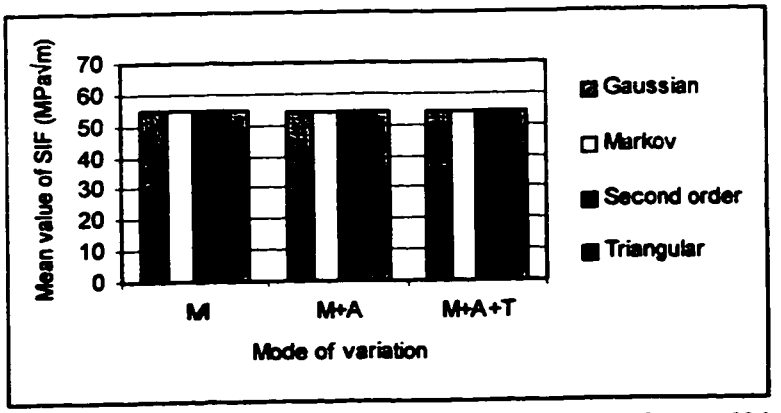

Figure 5.11 Mean value of SIF obtained using ERRM of a $[\pm 60/\pm 30]_{3S}$ laminate made of NCT-301 composite material

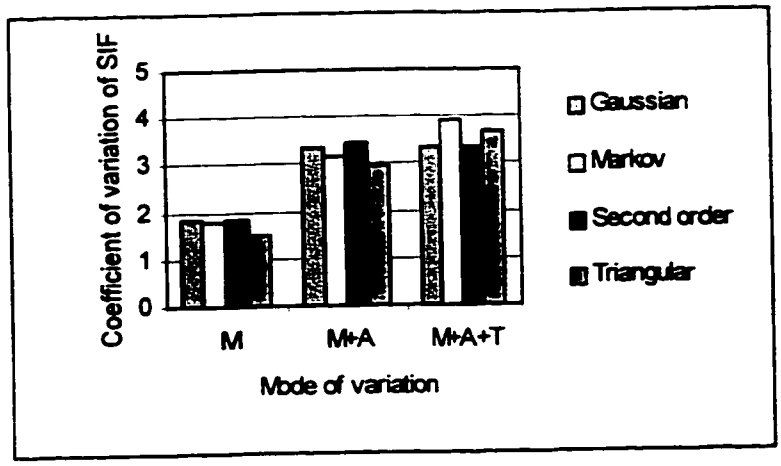

Figure 5.12 Coefficient of variation of SIF obtained using ERRM of a $[\pm 60/\pm 30]_{3s}$ laminate made of NCT-301 composite material

The Energy Release Rate of this laminate corresponding to the three modes of variation are now determined for Gaussian Correlation Model and summarized in Table 5.21.

Table 5.21 The G_I of a $[\pm 60/\pm 30]_{3s}$ laminate made of NCT-301 composite material in the case of Gaussian correlation model

Mode of variation	Mean value of G_I (KJ/m)	Standard deviation (KJ/m)	Coefficient of variation
M*	1.0174	0.0196	1.93
M+A*	1.0079	0.0524	5.20
M+A+T*	1.0103	0.0543	5.38

**M =Material properties are random, A =Ply Angles are random, T =Ply Thickness is random*

From Table 5.21, it can be observed that the G_I has almost the same values in the case of M, M+A and M+A+T. However, the coefficient of variation of G_I is 2.5 times more in the cases of M+A and M+A+T than in the case of M.

5.5 Fracture Analysis of a $[0/\pm45/90]_{3S}$ NCT-301 Composite Laminate

Sample stochastic elasticity matrix [E] for this laminate is determined at two Gauss point locations and for one simulation they are given below:

(1) At Gauss point 7 in Element 2 near crack edge (refer to Figure 4.15 in Chapter 4)

$$[E] = \begin{bmatrix} 53.96 & 16.99 & 0 \\ 16.99 & 53.96 & 0 \\ 0 & 0 & 18.48 \end{bmatrix} \text{GPa}$$

(2) At Gauss point 9 in Element 31 near loaded edge (refer to Figure 4.15 in Chapter 4)

$$[E] = \begin{bmatrix} 55.20 & 17.52 & 0 \\ 17.52 & 55.20 & 0 \\ 0 & 0 & 18.84 \end{bmatrix} \text{GPa}$$

A quasi-isotropic $[0/\pm45/90]_{3S}$ laminate is considered to determine the mean value, standard deviation and coefficient of variation of SIF. These values are calculated using DEM and ERRM for different correlation models and are presented below in tabulated form.

First the case of Gaussian correlation model is considered and the results are summarized in Table 5.22.

Table 5.22 The SIF of a $[0/\pm45/90]_{3S}$ laminate made of NCT-301 composite material in the case of Gaussian correlation model

Mode of variation	Displacement Extrapolation Method (DEM)			Energy Release Rate Method (ERRM)		
	Mean value (MPa√m)	Standard Deviation (MPa√m)	Coefficient of Variation	Mean value (MPa√m)	Standard Deviation (MPa√m)	Coefficient of Variation
M *	40.70	1.73	4.25	49.51	0.90	1.83
M+A*	41.04	2.00	4.88	50.02	2.25	4.49
M+A+T*	40.93	2.81	6.85	49.91	2.48	4.98

**M =Material properties are random, A =Ply Angles are random, T =Ply Thickness is random*

From Table 5.22 it is observed that the ERRM provides a higher mean value of SIF than the DEM in all three modes of property variation. It is also observed that the mean values of SIF obtained using DEM are almost the same for all the three modes of property variation. This is true for the case of ERRM. However, the coefficient of variation of SIF in the case of M+A+T is 1.5 times more than that of the case of M, based on DEM. But in the case of ERRM it is 2.5 times more.

Now, the Markov correlation model is considered and the results are summarized in Table 5.23.

Table 5.23 The SIF of a $[0/\pm45/90]_{3S}$ laminate made of NCT-301 composite material in the case of Markov correlation model

Mode of variation	Displacement Extrapolation Method (DEM)			Energy Release Rate Method (ERRM)		
	Mean value (MPa√m)	Standard Deviation (MPa√m)	Coefficient of Variation	Mean value (MPa√m)	Standard Deviation (MPa√m)	Coefficient of Variation
M *	40.56	1.91	4.72	49.48	0.93	1.89
M+A*	40.90	2.36	5.78	49.91	2.38	4.76
M+A+T*	40.84	2.64	6.47	50.21	2.20	4.39

**M =Material properties are random, A =Ply Angles are random, T =Ply Thickness is random*

From Table 5.23, observations that are the same as in the case of Table 5.22 can be written.

The Second order correlation model is considered and the results are summarized in Table 5.24.

Table 5.24 The SIF of a $[0/\pm45/90]_{3S}$ laminate made of NCT-301 composite material in the case of Second Order correlation model

Mode of variation	Displacement Extrapolation Method (DEM)			Energy Release Rate Method (ERRM)		
	Mean value (MPa√m)	Standard Deviation (MPa√m)	Coefficient of Variation	Mean value (MPa√m)	Standard Deviation (MPa√m)	Coefficient of Variation
M *	40.75	1.94	4.77	49.61	0.94	1.89
M+A*	41.14	2.22	5.39	50.02	2.27	4.53
M+A+T*	41.00	2.26	5.51	49.97	2.44	4.89

**M =Material properties are random, A =Ply Angles are random, T =Ply Thickness is random*

From Table 5.24, observations that are the same as in the case of Table 5.22 can be written. Finally, the Triangular correlation model is considered and the results are summarized in Table 5.25.

Table 5.25 The SIF of a $[0/\pm45/90]_{3S}$ laminate made of NCT-301 composite material in the case of Triangular correlation model

Mode of variation	Displacement Extrapolation Method (DEM)			Energy Release Rate Method (ERRM)		
	Mean value (MPa√m)	Standard Deviation (MPa√m)	Coefficient of Variation	Mean value (MPa√m)	Standard Deviation (MPa√m)	Coefficient of Variation
M *	40.47	2.35	5.81	49.59	0.74	1.49
M+A*	41.27	2.64	6.39	49.95	2.26	4.53
M+A+T*	41.32	2.96	7.16	50.21	2.08	4.15

**M =Material properties are random, A =Ply Angles are random, T =Ply Thickness is random*

From Table 5.25, observations that are the same as in the case of Table 5.22 can be written. Now, the SIF and its probabilistic characteristics corresponding to the four correlation models are compared in Table 5.26.

Table 5.26 The SIF of a $[0/\pm45/90]_{3S}$ laminate made of NCT-301 composite material evaluated for four correlation models using the Displacement Extrapolation Method

Correlation Model	Mean value (MPa√m)			Coefficient of variation		
	Mode of Variation			Mode of Variation		
	M*	M+A*	M+A+T*	M*	M+A*	M+A+T*
Gaussian	40.70	41.04	40.93	4.25	4.88	6.85
Markov	40.56	40.90	40.84	4.72	5.78	6.47
Second order	40.75	41.14	41.00	4.77	5.39	5.51
Triangular	40.47	41.27	41.32	5.81	6.39	7.16

**M =Material properties are random, A =Ply Angles are random, T =Ply Thickness is random*

From Table 5.26 it is observed that the mean values of SIF obtained using DEM for all the three modes of property variation are almost the same for four different correlation models and this observation is highlighted in Figure 5.13. So the effect of correlation models on the mean value of SIF is negligible. The difference between the coefficients of

variation of SIF for all the three modes of variation (M, M+A, and M+A+T) is relatively small. Only the Triangular Model provided a slightly higher value of coefficient of variation of SIF, which is highlighted in Figure 5.14.

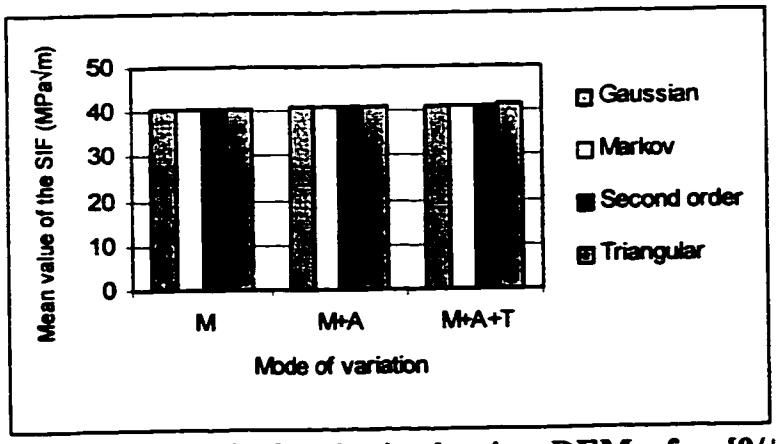

Figure 5.13 Mean value of SIF obtained using DEM of a $[0/\pm45/90]_{3S}$ laminate made of NCT-301 composite material

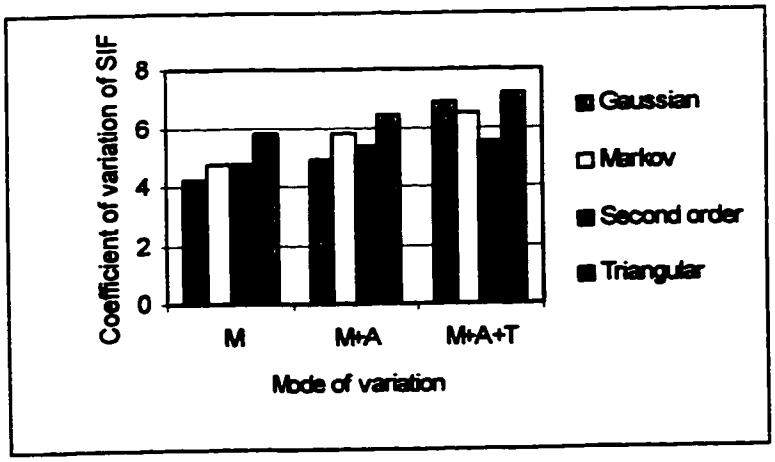

Figure 5.14 Coefficient of variation of SIF obtained using DEM of a $[0/\pm45/90]_{3S}$ laminate made of NCT-301 composite material

Now the results obtained using the ERRM are summarized in a similar manner in Table 5.27.

Table 5.27 The SIF of a $[0/\pm45/90]_{3S}$ laminate made of NCT-301 composite material evaluated for four correlation models using the Energy Release Rate Method

Correlation Model	Mean value (MPa√m)			Coefficient of variation		
	Mode of Variation			Mode of Variation		
	M*	M+A*	M+A+T*	M*	M+A*	M+A+T*
Gaussian	49.51	50.02	49.91	1.83	4.49	4.98
Markov	49.48	49.91	50.21	1.89	4.76	4.39
Second order	49.61	50.02	49.97	1.89	4.53	4.89
Triangular	49.59	49.95	50.21	1.49	4.53	4.15

**M =Material properties are random, A =Ply Angles are random, T =Ply Thickness is random*

When the ERRM is used, the mean value and the coefficient of variation of SIF have the same values in each case for four different correlation models, as shown in Table 5.27 and in Figures 5.15 and 5.16. Hence, no considerable effects of different correlation models are observed in the case of ERRM as long as the correlation length is the same.

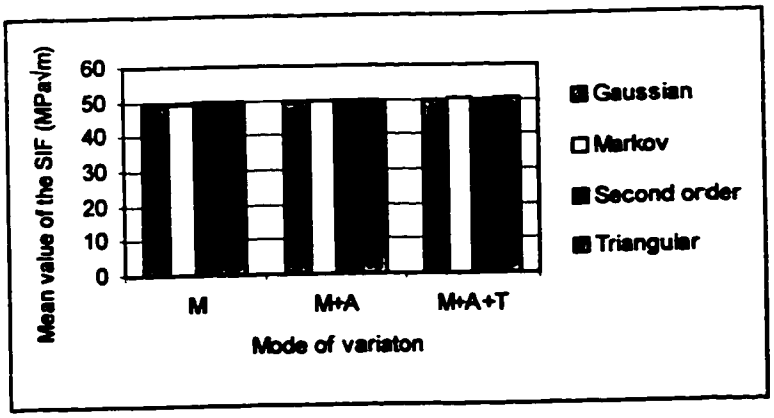

Figure 5.15 Mean value of SIF obtained using ERRM of a $[0/\pm45/90]_{3S}$ laminate made of NCT-301 composite material

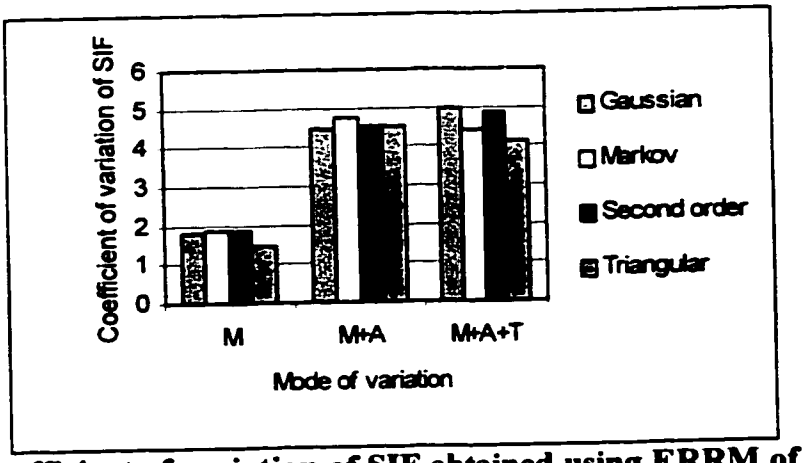

Figure 5.16 Coefficient of variation of SIF obtained using ERRM of a $[0/\pm45/90]_{3S}$ laminate made of NCT-301 composite material

The Energy Release Rate (G_I) corresponding to the three modes of variation are now determined for Gaussian correlation model since there is no considerable effect of different correlation models on the probabilistic characteristics of SIF are observed in the above analysis for the case of ERRM. The mean value, standard deviation and coefficient of variation of G_I of a $[0/\pm45/90]_{3S}$ laminate are presented in the following.

Table 5.28 The G_I of a $[0/\pm45/90]_{3S}$ laminate made of NCT-301 composite material in the case of Gaussian correlation model

Mode of variation	Mean value of G_I (KJ/m)	Standard deviation (KJ/m)	Coefficient of variation
M*	0.8888	0.0163	1.84
M+A*	0.9000	0.0575	6.39
M+A+T*	0.8980	0.0659	7.34

**M =Material properties are random, A =Ply Angles are random, T =Ply Thickness is random*

It is observed from Table 5.28, that the values of G_I are almost the same in all the three modes of property variation (M, M+A, and M+A+T). However, the coefficient of variation of G_I is 4 times more in the case of M+A+T than in the case of M.

5.6 Evaluation of the Fracture Behavior of Laminates

Composite laminates with four different ply orientations have been analyzed for their stochastic fracture behavior. For evaluation of laminates in terms of the stress intensity factor and the energy release rate, only the Gaussian Correlation Model is considered, since as shown in the previous section, different correlation models give values of fracture parameters that are nearly the same. This is true as long as the correlation length is the same. The mean value and the coefficient of variation of K_I and that of G_I for different laminates are presented below.

Table 5.29 The SIF for different NCT-301 composite laminates obtained using Gaussian correlation model based on Displacement Extrapolation Method

Laminate configuration	Mean value of K_I (MPa$\sqrt{m}$)			Coefficient of variation of K_I		
	Mode of Variation			Mode of Variation		
	M*	M+A*	M+A+T*	M*	M+A*	M+A+T*
$[0/90]_{6S}$	64.51	59.41	58.45	3.44	7.32	9.19
$[90]_{12S}$	51.24	43.68	44.07	3.80	6.21	7.37
$[\pm60/\pm30]_{3S}$	41.29	41.39	41.38	4.56	4.62	7.46
$[0/\pm45/90]_{3S}$	40.70	41.04	40.93	4.25	4.88	6.85

**M =Material properties are random, A =Ply Angles are random, T =Ply Thickness is random*

From Table 5.29, it is observed that the value of the SIF obtained using the DEM, is maximum in the case of the $[0/90]_{6S}$ laminate. On the other hand, the value of the SIF is minimum for the $[0/\pm45/90]_{3S}$ laminate as can also be seen from Figure 5.17. The coefficient of variation of SIF in the case of M+A+T, is also minimum for the $[0/\pm45/90]_{3S}$ laminate. It is also seen for the $[0/\pm45/90]_{3S}$ laminate, that the values of

coefficient of variation are not varying too much with different modes of variation, that are M, M+A, and M+A+T, when compared to other types of laminates. Again in the case of the $[0/90]_{6S}$ laminate, these variations are very high and this is shown in Figure 5.18.

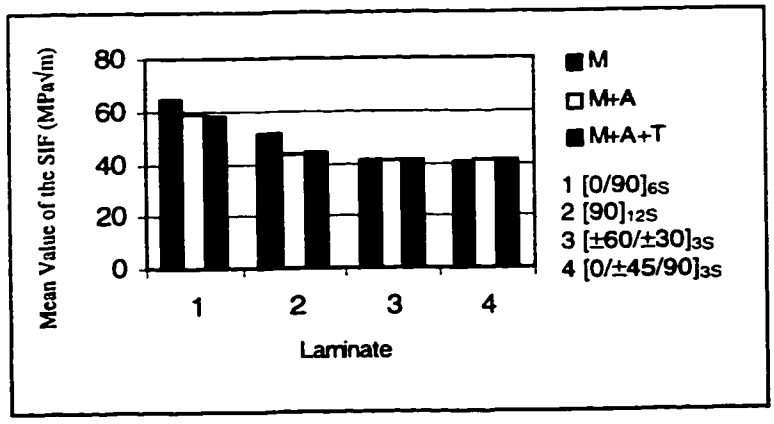

Figure 5.17 The SIF for different NCT-301 laminates obtained using Gaussian correlation model based on Displacement Extrapolation Method

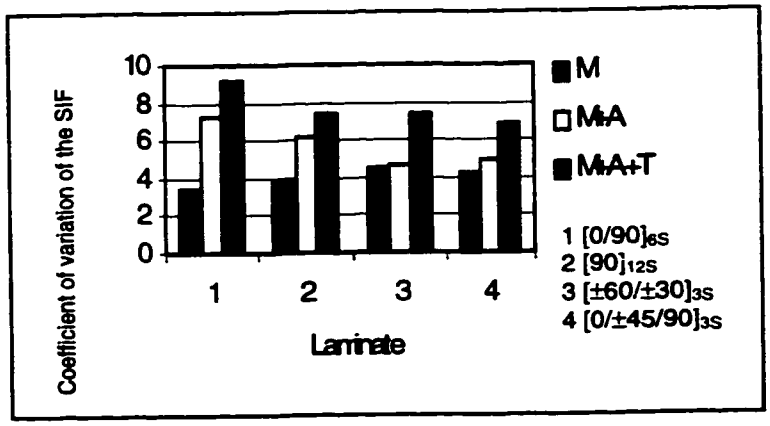

Figure 5.18 Coefficient of variation of the SIF for different NCT-301 laminates obtained using Gaussian correlation model based on Displacement Extrapolation Method

From the above observations, it can be concluded that the stochastic fracture behavior of $[0/\pm45/90]_{3S}$ laminate is such that the laminate will have a higher value of reliability when the SIF is determined based on Displacement Extrapolation Method.

Now the stochastic fracture behavior of the laminates is considered based on the values of SIF that are determined using the Energy Release Rate Method. The relevant results are presented below in Table 5.30.

Table 5.30 The SIF for different NCT-301 composite laminates obtained using Gaussian correlation model based on Energy Release Rate Method

Laminate configuration	Mean value K_I (MPa$\sqrt{m}$)			Coefficient of variation of K_I		
	Mode of Variation			Mode of Variation		
	M*	M+A*	M+A+T*	M*	M+A*	M+A+T*
$[0/90]_{6S}$	59.14	56.32	56.64	1.94	9.98	9.96
$[90]_{12S}$	56.32	51.20	51.22	1.78	7.10	7.90
$[\pm60/\pm30]_{3S}$	54.65	54.26	54.24	1.84	3.33	3.34
$[0/\pm45/90]_{3S}$	49.51	50.02	49.91	1.83	4.49	4.98

**M =Material properties are random, A =Ply Angles are random, T =Ply Thickness is random*

It can be observed from Table 5.30 that in any mode of variation, the mean value of the SIF is maximum for the $[0/90]_{6S}$ laminate when the Energy Release Rate Method is used, and for the $[0/\pm45/90]_{3S}$ laminate, the mean value is minimum. These facts are also shown in Figure 5.19. Considering the coefficient of variation of the SIF, it can be seen that the $[\pm60/\pm30]_{3S}$ laminate gives the minimum value and the $[0/90]_{6S}$ laminate gives the maximum value in any mode of variation, as shown in Figure 5.20. It is also shown in Figure 5.20 that the value of the coefficient of variation for $[0/\pm45/90]_{3S}$ laminate in any mode of variation is close to the corresponding value for the $[\pm60/\pm30]_{3S}$ laminate.

However, minor variations between the corresponding values in different modes of M, M+A, and M+A+T are noted.

This way, it can be concluded, based on the Energy Release Rate Method, that the $[0/\pm45/90]_{3S}$ laminate displays a better stochastic fracture behavior.

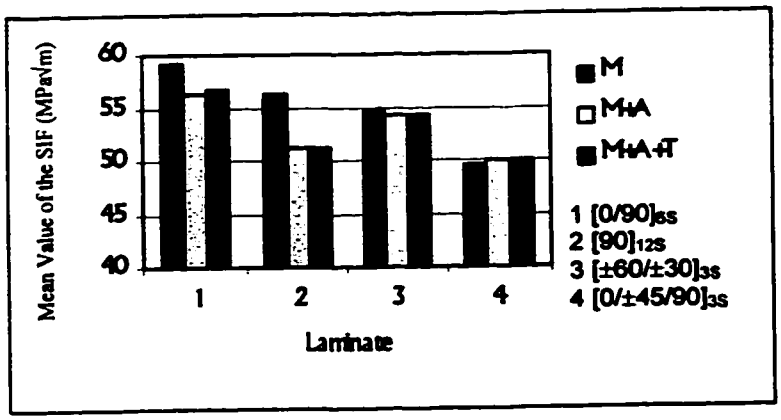

Figure 5.19 The SIF for different NCT-301 laminates obtained using Gaussian correlation model based on Energy Release Rate Method

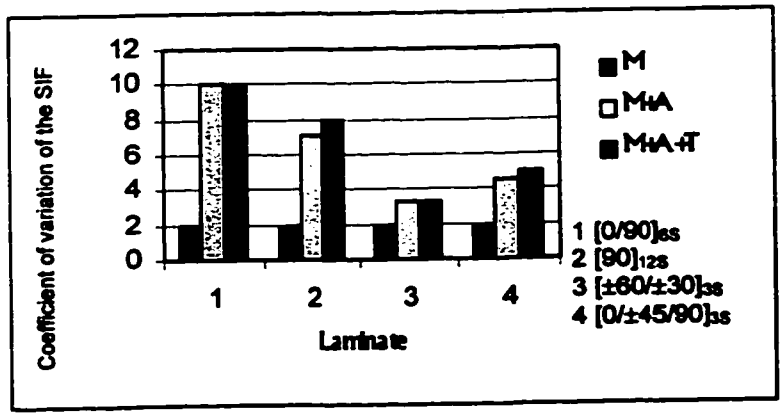

Figure 5.20 Coefficient of variation of the SIF for different NCT-301 laminates obtained using Gaussian correlation model based on Energy Release Rate Method

The Energy Release Rate G_I is an important fracture parameter. A laminate with a low value of G_I with minimum fluctuations is desirable in terms of fracture behavior. The mean values and coefficients of variation of G_I for different modes of variation are determined for different laminates and are presented in Table 5.31.

Table 5.31 The energy release rate for different NCT-301 composite laminates obtained using Gaussian correlation model

Laminate configuration	Mean value of G_I (KJ/m)			Coefficient of variation of G_I		
	Mode of Variation			Mode of Variation		
	M*	M+A*	M+A+T*	M*	M+A*	M+A+T*
$[0/90]_{6S}$	1.382	1.245	1.254	2.00	16.68	16.83
$[90]_{12S}$	1.311	1.063	1.069	1.73	10.81	11.60
$[\pm60/\pm30]_{3S}$	1.017	1.008	1.010	1.93	5.20	5.38
$[0/\pm45/90]_{3S}$	0.889	0.900	0.898	1.84	6.39	7.34

**M =Material properties are random, A =Ply Angles are random, T =Ply Thickness is random*

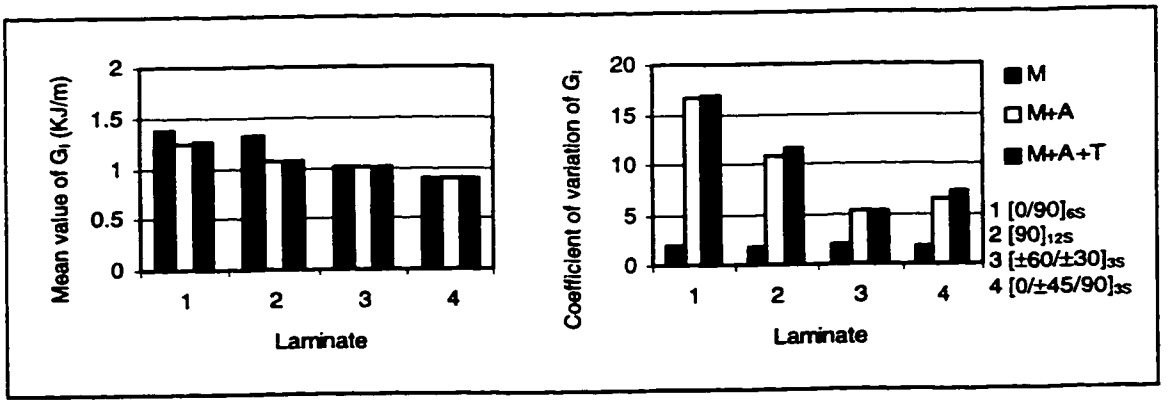

Figure 5.21 Mean value and coefficient of variation of energy release rate for different NCT-301 composite laminate

From Table 5.31 and Figure 5.21, it can be observed that the mean value of G_I in any mode of variation for $[0/90]_{6S}$ laminate is maximum in comparison with other laminates. However, the coefficient of variation is also high. On the other hand, the mean value of

G_I is minimum for $[0/\pm45/90]_{3S}$ laminate, but the fluctuations of G_I are minimum for $[\pm60/\pm30]_{3S}$ laminate. Therefore, in the design for fracture, one can select the $[\pm60/\pm30]_{3S}$ laminate or the $[0/\pm45/90]_{3S}$ laminate that have lesser variability in their fracture behavior with minimum mean value of G_I.

5.7 Reliability of Laminates in Fracture

The purpose of stochastic fracture analysis, when the stress intensity factor K_I and the critical stress intensity factor K_C (fracture toughness) are involved, is to determine the reliability with both stress intensity factor and fracture toughness distributions known at the critical location in a component. It is assumed that both the stress intensity factor and the fracture toughness are Gaussian or lognormal random variables, and hence that [119]

$$K_I \sim N(\mu_{KI}, \sigma_{KI}); \qquad K_C \sim N(\mu_{KC}, \sigma_{KC}) \tag{5.1}$$

or

$$K_I \sim LN(\mu_{KI}, \sigma_{KI}); \qquad K_C \sim LN(\mu_{KC}, \sigma_{KC}) \tag{5.2}$$

where μ and σ are the mean value and the standard deviation, respectively.

It is convenient to define the term stress intensity factor margin m, which is the difference between the fracture toughness and stress intensity factor. Thus, for specific values of K_C and K_I,

$$m = K_C - K_I \tag{5.3}$$

Reliability is the probability that the fracture toughness exceeds the stress intensity factor, or, alternatively, the probability that the stress intensity factor margin is greater than zero. This can be expressed in the form

$$R = p(K_C > K_I) = p[(K_C - K_I) > 0] = p(m > 0) \tag{5.4}$$

First the case of Gaussian distribution is considered. The central limit theorem of statistics says, in part, that the difference between variables that each have a normal distribution is likewise normally distributed. Therefore

$$m \sim N(\mu_m, \sigma_m) \tag{5.5}$$

The distribution of m is shown in Figure 5.22.

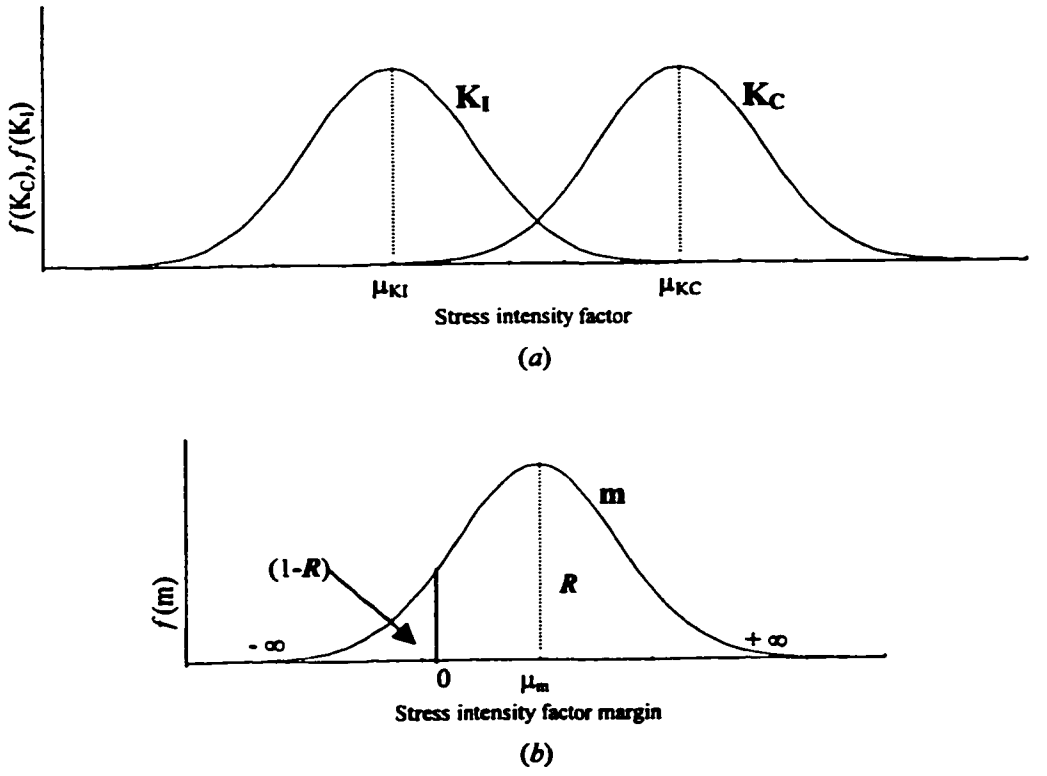

Figure 5.22 **Plot of density function showing how the interference of K_C and K_I is used to obtain the stress intensity factor margin m. (a) Stress intensity factor and fracture toughness distributions. (b) Distribution of interference; the reliability R is the area of the density function for all m's greater than zero; the interference is the area (1-R).**

Since m is the difference between two independent random variables, one can write that

$$\mu_m = \mu_{KC} - \mu_{KI}; \qquad \sigma_m = \left(\sigma_{KC}^2 + \sigma_{KI}^2\right)^{\frac{1}{2}} \tag{5.6}$$

To find the probability that m>0, one has to find the z variable corresponding to m=0 in Figure 5.22 and this gives

$$z = \frac{m-\mu_m}{\sigma_m} = \frac{0-\mu_m}{\sigma_m} = -\frac{\mu_m}{\sigma_m} \tag{5.7}$$

Substituting Eq. (5.6) in Eq. (5.7) yields

$$z = -\frac{\mu_{KC} - \mu_{KI}}{\left(\sigma_{KC}^2 + \sigma_{KI}^2\right)^{\frac{1}{2}}} \tag{5.8}$$

The above equation is called the coupling equation, because it relates the reliability, through z, to the statistical parameters of the normally distributed fracture toughness and stress intensity factor. The reliability is then given by

$$R = \int_z^{\infty} \frac{1}{\sqrt{2\pi}} \exp\left(-\frac{u^2}{2}\right) du \tag{5.9}$$

or by using the normal distribution table as (1- tabulation), when z is negative (that is, when high reliability exists).

The mean value and standard deviation of fracture toughness K_C can be determined experimentally from 35 specimens. In the present work, this experiment has not been performed. However, the concept of the reliability of a laminate is introduced in this section. An example application to determine the reliability of a laminate is presented below.

Let us consider a $[0/90]_{6s}$ laminate, which provided $K_I \sim N(59.41,4.35)$ MPa$\sqrt{m}$ in the case of M+A based on DEM from Table 5.1. And let us assume that the fracture toughness of this laminate is $K_C \sim N(80,5)$ MPa$\sqrt{m}$. Now substitute these values in Eq.(5.8) which then yields

$$z = -\frac{\mu_{KC} - \mu_{KI}}{\left(\sigma_{KC}^2 + \sigma_{KI}^2\right)^{\frac{1}{2}}} = -\frac{80 - 59.41}{\left(5^2 + 4.35^2\right)^{\frac{1}{2}}} = -3.10$$

From the Normal distribution table, the tabulation value of 0.000968 is obtained at z=3.10, Therefore the reliability is

$R = R(z) = R(-3.10) = 1\text{-tabulation} = 1 - 0.000968 = 0.999$

Suppose that there is an interference between a fracture toughness and a stress intensity factor which are both lognormal and are given by $K_C \sim LN(\mu_{KC}, \sigma_{KC})$ and $K_I \sim LN(\mu_{KI}, \sigma_{KI})$. Since both are lognormal, it can be written that

$$K_{C\ln} = \ln K_C \qquad K_{I\ln} = \ln K_I \tag{5.10}$$

Also, it can be written that

$$\sigma_{\ln KC} = \frac{\sigma_{KC}}{\mu_{KC}} \quad \text{and} \quad \sigma_{\ln KI} = \frac{\sigma_{KI}}{\mu_{KI}} \tag{5.11}$$

and

$$\begin{aligned} \mu_{\ln KC} &= \ln \mu_{KC} - \frac{1}{2}\sigma_{KC}^2 \\ \mu_{\ln KI} &= \ln \mu_{KI} - \frac{1}{2}\sigma_{KI}^2 \end{aligned} \tag{5.12}$$

With these transformations, the coupling equation [Eq.(5.8)] can be written as

$$z = -\frac{\mu_{\ln KC} - \mu_{\ln KI}}{\left(\sigma^2_{\ln KC} + \sigma^2_{\ln KI}\right)^{\frac{1}{2}}} \tag{5.13}$$

With the help of the above equation the reliability can be determined using Eq.(5.9).

5.8 Conclusion and Discussion

In this chapter, the application of the stochastic finite element method to the fracture analysis of different orthotropic composite laminates is presented. The mean value, standard deviation, and coefficient of variation of two important parameters, K_I and G_I, for $[0/90]_{6S}$, $[90]_{12S}$, $[\pm 60/\pm 30]_{3S}$, and $[0/\pm 45/90]_{3S}$ NCT-301 composite laminates are determined using 250 simulations. The values of K_I are determined in two different ways, (1) Displacement Extrapolation Method, and (2) Strain Energy Release Rate Method. Three different modes of variations, (1) material properties are random at each Gauss point, (2) material properties and ply angles are random, and (3) material properties, ply angles, and ply thickness are random, are considered to analyze their effect on the variabilities in K_I and G_I for the above laminates. Also the effect of the correlation characteristics of property variations are studied through employing four correlation models, that are (1) Gaussian, (2) Markov, (3) Second order, and (4) Triangular Correlation Model.

From the simulated results, it is observed that the effect of these four correlation models on the stress intensity factor and energy release rate, is negligible as long as the

correlation length is the same. So one of these correlation models is sufficient for stochastic fracture analysis. Also it is seen that the variation of ply thickness does not greatly affect the fracture parameters. Comparing the results for various composite laminates, it is also seen that the values of stress intensity factor obtained using both the methods (DEM and ERRM) for the $[0/\pm45/90]_{3S}$ laminate are minimum, and at the same time, the coefficient of variation is also minimum for this laminate with minimum fluctuations between various modes of property variations. Also the value of energy release rate for this laminate is low. In the case of the $[0/90]_{6S}$ laminate, these values are high.

The concept and the formulation of the reliability of a composite laminate in fracture are described. The use of stochastic finite element analysis in the reliability evaluation is demonstrated.

In the probabilistic design for fracture, one can separately consider two criteria based on the mean value, one that desires a low stress intensity factor or another one that desires a low energy release rate. In addition, less fluctuations in these parameters, that is less degree of variability is also desired. On the basis of these considerations, one can see that the $[0/\pm45/90]_{3S}$ laminate displays a desirable fracture behavior compared to other laminates.

Chapter 6

Conclusion and Recommendation

In the present thesis, a combined experimental and stochastic finite element formulation that can incorporate the variabilities in material properties, fiber orientation in each ply and ply thickness, and based on these variabilities predict the stochastic characteristics of the stress intensity factor and the strain energy release rate of composite laminates is developed.

The formulation employing the finite element modeling and analysis for evaluating the stress intensity factor and the energy release rate for laminated anisotropic plates subjected to any type of loading in Mode I and Mode II is developed and described. The 8-Node quadratic isoparametric element is employed in the finite element analysis. The corresponding computer program is developed in MATLAB® software environment and the program development is explained in sufficient details.

Composite laminates display significant randomness due to stochastic spatial variation of properties in fibers, in matrices, and at interfaces. A series of experiments is performed so as to determine the mean value, standard deviation and coefficient of variation of

Young's moduli, Poison's ratios and shear modulus of composite laminates made of NCT-301 graphite/epoxy composite material. These results are then used to determine the stochastic elasticity matrix of the composite laminate at each Gauss point of a finite element mesh. The fracture parameters are then determined based on the stochastic elasticity matrices of the finite element mesh.

In the present thesis composite laminates with four different configurations are considered in order to evaluate their stochastic fracture behavior. The mean value, standard deviation and coefficient of variation of the stress intensity factor and the energy release rate are calculated from 250 simulations using four correlation models based on two methods, viz., (1) Displacement Extrapolation Method and (2) Strain Energy Release Rate Method. The following three modes of property variations, that are, (1) material properties are random, (2) material properties and ply angles are random, and (3) material properties, ply angles and ply thickness are random, are considered separately in order to analyze their influence on the fracture parameters.

The fracture behavior of laminates and the variability in the fracture behavior are both quantified. The methodology of predicting the reliability of laminates based on the stochastic finite element fracture analysis is described and demonstrated. A detailed parametric study of the fracture behavior of laminates made of NCT-301 graphite/epoxy composite material, is performed. Several aspects related to the design of composite laminates are obtained based on the parametric study. The parametric study also yields the following conclusions.

1) As long as the correlation length of the material property stochastic fields remains the same, different correlation models do not affect the mean values of the SIF and the energy release rate of an orthotropic composite laminate.

2) Variations in ply thickness do not greatly affect the fracture parameters when compared to the effects of the variations in the ply angles.

3) The quasi-isotropic $[0/\pm45/90]_{3S}$ laminates display desirable fracture behavior compared to other laminate configurations in terms of the stress intensity factor and the energy release rate.

It may be noted here that the formulation and stochastic FEA methodology are more general in nature. They can be applied to any composite material such as the NCT-301 graphite/epoxy composite material considered here in the parametric study. They can be employed in the reliability based design of composite laminates for fracture. However, the material properties for a specific material have to be determined experimentally. The probabilistic characteristics of material properties have to be obtained from the test data.

The following recommendations may be considered in the future studies.

1) A three-dimensional stochastic finite element analysis can be developed based on the formulation developed in the present thesis.

2) The stochastic finite element formulation may be applied to other general composite laminate configurations.

3) A stochastic description of weighting factors can be developed and this description will be more compatible to the stochastic description of elasticity matrices for composite laminates.

4) A series of experiments can be conducted to determine the fracture toughness of composite laminates. Based on the test data, the evaluation of the reliability of the laminate can be completed for a particular composite material.

References

[1] Richard, W.H., "*Deformation and Fracture Mechanics of Engineering Materials*", 4th Ed., John Wiley, NewYork, 1996.

[2] Owen, D.R.J., and Fawkes, A.J., "*Engineering Fracture Mechanics: Numerical Methods and Applications*", Pineridge Press, Swansea, 1983.

[3] Hull, D., "*Introduction to Composite Materials*", Cambridge University Press, Cambridge, 1981.

[4] Roulin-Moloney, A.C., "*Fractography and Failure Mechanisms of Polymers and Composites*", Elsevier Applied Science Publishers, Barking, 1989.

[5] Hoa, S.V., Ed., "*Computer-Aided Design of Polymer-Matrix Structures*", Marcel Dekker, 1995.

[6] Lakshminarayana, H.V., "Stress Distribution around a Semi-circular Edge-notch in a Finite Laminated Composite Plate under Uniaxial Tension", *Journal of Composite Materials*, Vol. 17, 1983, pp. 357-367.

[7] Wang, C.M.S. and Matthews, F.L., "A Finite Element Analysis of Single and Two-hole Bolted Joints in Fiber Reinforced Plastic", *Journal of Composite Materials*, Vol. 15, 1981, pp. 484-491.

[8] Hori, M., "Statistical Theory of Effective Electrical, Thermal and Magnetic Properties of Random Heterogeneous Materials-II", *J. of Math. Phys.*, Vol. 14, 1973, pp. 1942-1948.

[9] Borri, A., "Stochastic Behavior of Special Materials: The Composite Material", In "*Dynamic Motion: Chaotic and Stochastic Behavior*", Ed.:F. Casciati, Springer-Verlag, 1993, pp. 171-202.

[10] Hearmon, R.F.S., "*An Introduction to Applied Anisotropic Elasticity*", Oxford University Press, Oxford, 1969.

[11] Lekhnitskii, S.G., "*Theory of Elasticity of an Anisotropic Elastic Body*", Trans. P. Fern, Holden Day, San Francisco, 1963.

[12] Muskhelishvili, N.I., "*Some Basic Problems of the Mathematical Theory of Elasticity*", Noordhoff, Groningen, The Netherlands, 1953.

[13] Barrell, J.D., "Effect of Crack-Front Width on Fracture Toughness of Douglas-Fir", *Engineering Fracture Mechanics*, Vol. 9, 1976, pp. 711-717.

[14] Chen, P.E., "Stress Fields Around Parallel Edge Cracks", *Journal of Composite Materials*, Vol. 1, 1967, pp. 82-90.

[15] Davies, P. and Benzeggagh, M.L., "Interlaminar Mode-I Fracture Testing", *Application of Fracture Mechanics to Composite Materials*, Ed.: K. Friedrich, Composite Materials Series, Vol. 6, Elsevier Science Publishers B.V., 1989, pp. 81-157.

[16] Charalambides, M., Kinlock, A.J., Wang, Y. and Williams, J.G., "On the Analysis of Mixed-Mode Fracture", *International Journal of Fracture*, Vol. 54, 1992, pp. 269-291.

[17] Williams, J.G., "Fracture Mechanics of Anisotropic Material", *Application of Fracture Mechanics to Composite Materials*, Edited by K. Friedrich, 1989, pp. 3-38.

[18] Choi, N.S., Kinloch, A.J. and Williams, J.G., "Delamination Fracture of Multidirectional Carbon-Fiber/Epoxy Composites under Mode-I, Mode-II and Mixed-Mode-I/II Loading", *Journal of Composite Materials*, Vol. 33, 1999, pp. 73-100.

[19] Whitcomb, J.D., "Finite Element Analysis of Instability Related Delamination Growth", *Journal of Composite Materials*, Vol. 15, 1981, pp. 403-426.

[20] Waszczak, J.P. and Cruse, T.A., "Failure Mode and Strength Predictions of Anisotropic Bolt Bearing Specimens", *Journal of Composite Materials*, Vol. 5, 1971, pp. 421-425.

[21] Tang, S., "Failure of Composite Joints under Combined Tension and Bolt Loads", *Journal of Composite Materials*, Vol. 15, 1981, pp. 329-335.

[22] York, J.L., Wilson, D.W. and Pipes, R.B., "Analysis of Tension Failure Mode in Composite Bolted Joints", *Journal of Reinforced Plastics and Composites*, Vol. 1, 1982, pp. 141-153.

[23] Tsujimoto, Y. and Wilson, D., "Elasto-Plastic Fracture Analysis of Composite Bolted Joints", *Journal of Composite Materials*, Vol. 20, 1985, pp. 236-251.

[24] Eisenmann, J.R., "Bolted Joint Static Strength Model for Composite Materials", *NASA TM-X-3377*, pp. 563-602.

[25] Wong, C.M.S. and Matthews, F.L., "A Finite Element Analysis of Single and Two-Hole Bolted Joints in Fiber Reinforced Plastic", *Journal of Composite Materials*, Vol. 15, 1981, pp. 481-490.

[26] Kurt, C.S. and Paul, F.P., "A Tension-Mode Fracture Model for Bolted Joint in Laminated Composites", *Journal of Composite Materials*, Vol. 29, 1995, pp. 37-58

[27] Whitney, J.M. and Nuismer, R.J., "Stress Fracture Criteria for Laminated Composites Containing Stress Concentrations", *Journal of Composite Materials*, Vol. 8, 1974, pp. 253-265.

[28] Waddoups, M.E., Eisenmann, J.R. and Kaminski, B.E., "Microscopic Fracture Mechanics of Advanced Composite Material", *Journal of Composite Materials*, Vol. 5, 1971, pp. 446-454.

[29] Pipes, R.B., Wetherhold, R.C. and Gillespie, J.W., Jr., "Notched Strength of Composite Materials", *Journal of Composite Materials*, Vol. 12, 1979, pp. 1151-1155.

[30] Karlak, R.F., "Hole effects in a Related Series of Symmetrical Laminates", *Proceedings of Fracture Modes in Composites*, IV, Metallurgical Society of American Inst. of Mining Metallurgical and Petroleum Engineers, Chicago, IL, 1977, pp. 105-117.

[31] Awerbuch, J. and Madhukar, M.S., "Notched Strength of Composite Laminates: Prediction and Experiments-A Review", *Journal of Reinforced Plastics and Composites*, Vol. 4, 1985, pp. 3-15.

[32] Rajesh, S.V. and Sun, C.T., "Fracture Criterion for Notched Thin Composite Laminates", *AIAA Journal*, Vol. 35, 1997, pp. 311-316.

[33] Guofang, S., "Fracture of Fiber glass Reinforced Composites", *Journal of Composite Materials*, Vol. 15, 1981, pp. 521-530.

[34] Aronsson, C., and Backluwd, J., "Tensile Fracture of Laminates with Cracks", *Journal of Composite Materials*, Vol. 20, 1986, pp. 287-307.

[35] Wang, J.Z. and Darrell, F.S., "Failure Strength and Damage Mechanisms of E-Glass/Epoxy Laminates under In-plane Biaxial Compressive Deformation", *Journal of Composite Materials*, Vol. 27, 1993, pp. 40-58.

[36] Rice, J.R., "Some Remarks on Elastic Crack-tip Stress Fields", *Int. J. Solid Structures*, Vol. 8, 1972, pp. 751-758.

[37] Lee, L.J. and Wang, C.H., "Stress Intensity Factor by Weight Function Method for Cracked Composite Laminates", *Engineering Fracture Mechanics*, Vol. 48, No. 2, 1994, pp. 267-279.

[38] Ruijia, M. and Reddy, D.V., "Stress Intensity Factor and Weight Function for Semi-Elliptical Crack using Finite Element Alternating Method", *Engineering Fracture Mechanics*, Vol. 48, No. 3, 1994, pp. 305-323.

[39] Tan, P.W. and Bigelow, C.A., "Analysis of Cracked Laminates with Holes Using The Boundary Force Method", *AIAA Journal*, Vol. 26, No. 9, 1988, pp. 1094-1099.

[40] Nairn, J. A., "Fracture Mechanics of Unidirectional Composites Using the Shear-Lag Mode I: Theory", *Journal of Composite Materials*, Vol.22, 1988, pp. 561-588.

[41] Case, S.W., Carman, G.P., Lesko, J.J., Fajardo, A.B. and Peifsnider, K.L., "Fiber Fracture in Unidirection Composite", *Journal of Composite Materials*, Vol. 29, 1995, pp. 208- 228.

[42] Snyder, M.D. and Cruse, T.A., "Crack Tip Stress Intensity Factor in Finite Anisotropic Plates", *Air Force Material Laboratory*, AFML-TR-73-209, 1973.

[43] Yeh, J.R., "Fracture Analysis of A Stiffened Orthotropic Sheet", *Engineering Fracture Mechanics*, Vol. 46, No. 5, 1993, pp. 857-866.

[44] Mandell, J.F., McGarry, F.J., Wang, S.S. and Im, J., "Stress Intensity Factors for Anisotropic Fracture Test Specimens of Several Geometry", *Journal of Composite Materials*, Vol. 8, 1974, pp. 106-116.

[45] Phillips, D.C., "The Fracture Mechanics of Carbon Fiber Laminates, *Journal of Composite Materials*, Vol. 8, 1974, pp. 130-141.

[46] Victor, E.S. and Efthimios, S.S., "Stress Intensity Factor in Anisotropic Bodies Using Singular Isoparametric Elements", *Engineering Fracture Mechanics*, Vol. 25, No. 1. 1986, pp. 115-121.

[47] Tian, Z. and Swanson, S.R., "The Fracture Behavior of Carbon/Epoxy Laminates Containing Internal Cut Fibers", *Journal of Composite Materials*, Vol. 25, 1991, pp. 1427-1444.

[48] Ko, W.L., "Finite Element Microscopic Stress Analysis of Cracked Composite Systems", *Journal of Composite Materials*, Vol. 12, 1978, pp. 97-109.

[49] Heppler, G.R., Frisken, S. and Hansen, J.S., "Stress Intensity Factor Calculation for Designing with Fiber-Reinforced Composite Materials", *AIAA Journal*, Vol. 23, No. 6, 1985, pp. 893-901.

[50] Heppler, G. and Hansen, J.S., "Mixed Mode Fracture Analysis of Rectilinear Anisotropic Plates by High Order Finite Elements", *International Journal for Numerical Methods in Engineering*, Vol. 17, 1981, pp. 445-464.

[51] Zhu, H. and Sankar, B.V., "Evaluation of Failure Criteria for Fiber Composites Using Finite Element Micromechanics", *Journal of Composite Materials*, Vol. 32, 1998, pp. 766-782.

[52] Yeh, J.H., "Stress Singularity in Composite Laminates by Finite Element Method", *Journal of Composite Materials*, Vol. 20, 1986, pp. 347-364.

[53] Chen, A.T. and Yang, T.Y., "Static Dynamic and Buckling Formulation of a Symmetrically Laminated Plate Finite Element for a Microcomputer", *Journal of Composite Materials*, Vol. 21, 1987, pp. 441-453.

[54] Nassehi, V., Kinsella, M. and Mascia, L., "Finite Element Modeling of the Stress Distribution in Polymer Composites with Coated Fiber Interlayers", *Journal of Composite Materials*, Vol. 27, 1993, pp. 195-214.

[55] Thomas, J.B., Paul, A.W. and Anthony, R.I., "Finite Element Modelling of Fracture Propagation in Orthotropic Materials", *Engineering Fracture Mechanics*, Vol. 26, No. 2, 1987, pp. 185-201.

[56] Tasu, L.R. and Plunkett, R., "Finite Element Analysis of Progressive Failure for Laminated FRP Plates with Inplane Loading", *Engineering Fracture Mechanics*, Vol. 45, No. 4, 1993, pp. 529-546.

[57] Tsai, S.W. and Wu, E.M., "A General Theory of Strength for Anisotropic Materials", *Journal of Composite Materials*, Vol. 5, 1971, pp. 58-80.

[58] Sih, G.C., Chen, E.P., Huang, S.L. and McQuillen, E.J., "Material Characterization on the Fracture of Filament-Reinforced Composites", *Journal of Composite Materials*, Vol. 9, 1975, pp. 167-186.

[59] Buczek, M.B. and Herakovich, C.T., "A Normal Stress Criterion for Crack Extension Direction in Orthotropic Composite Materials", *Journal of Composite Materials*, Vol. 19, 1985, pp. 544-553.

[60] Kadi, H.E., Ellyin, F., "Crack Extension in Unidirectional Composite Laminate", *Engineering Fracture Mechanics*, Vol. 51, No. 1, 1995, pp. 27-36.

[61] Ellyin, F. and Kadi, H.E., "Predicting Crack Growth Direction in Unidirectional Composite Laminate", *Engineering Fracture Mechanics*, Vol. 36, 1990, pp. 27-37.

[62] Krawczak, P. and Pabiot, J., "Fracture Mechanics Applied to Glass Fiber/Epoxy Matrix Interface Characterization", *Journal of Composite Materials*, Vol. 29. 1995, pp. 2230-2253.

[63] Sih, G.C. and Chen, E.P., "Fracture Analysis of Unidirectional Composites", *Journal of Composite Materials*, Vol. 7, 1973, pp. 230-244.

[64] Gu, Y.H., "Fracture Behavior of Continuous Alumina Fiber Reinforced Epoxy", *Journal of Composite Materials*, Vol. 28, 1994, pp. 1227-1236.

[65] William, W.F., "A Failure Criterion for Composite Materials", *Journal of Composite Materials*, Vol. 25, 1991, pp. 88-100.

[66] Ovchinskii, A.S., "*Fracture Process in Composite Materials: Computer Imitation of Micro and Macromechanisms*", Nauka, Moscow, 1988, (in Russian)

[67] Stock, T.A., Bellini, P.X., Murthy, L.N. and Chamis, C.C., "Probabilistic Composite Micromechanics", *Proceeding of the AIAA/ASME/ASCE/AHS/ASC 29th Structures,* Srtuctural Dynamics and Materials Conference (Williamsburg, VA), AIAA, Washington, DC, April 1988, Pt. 3, pp. 1289-1293.

[68] Fukuda, H., "Monte Carlo Simulation of the Strength of Hybrid Composite", *Journal of Composite Materials*, Vol. 16, 1982, pp. 371-385.

[69] Dzenis, Y.A., Joshi, S.P. and Bogdanovich, A.E., "Damage Evaluation Modeling in Orthotropic Laminated Composites", *AIAA Journal*, Vol. 32, No. 2, 1994, pp.357-364.

[70] Joshi, S.P. and Frantziskonis, G., "Damage Evaluation in Laminated Advanced Composites", *Composite Structures International Journal*, Vol. 17, No. 2, 1991, pp. 127-139.

[71] Larder, R.A., "The Stochastic Finite Element Simulation of Parallel Fiber Composites", *Journal of Composite Materials*, Vol. 10, 1976, pp. 21-31.

[72] Wang, A.S.D., Chou, P.C. and Lei, S.C., "A Stochastic Model for the Growth of Matrix Crack in Composite laminates", *Journal of Composite Materials*, Vol. 18, 1984, pp. 239-254.

[73] Cassenti, B.N., "Probabilistic Static Failure of Composite Material", *AIAA Journal*, Vol. 22, No. 1, 1984, pp. 103-110.

[74] Fukunaga, H. and Chou, T.W., "Probabilistic Failure Strength Analysis of Graphite/Epoxy Cross-Ply laminates", *Journal of Composite Materials*, Vol. 18, 1984, pp. 339-351.

[75] Rosen, B.W., "Tensile Failure of Fibrous Composite", *AIAA Journal*, Vol. 2, No. 11, 1964, pp. 1985-1991.

[76] Zweben, C., "Tensile failure of Fiber Composite", *AIAA Journal*, Vol. 6, No. 12, 1968, pp. 2325-2332.

[77] Harlow, D.G. and Phoenix, S.L., "The Chain of Bundles Probability Model for the Strength of Fibrous materials I: Analysis and Conjectures", *Journal of Composite Materials*, Vol. 12, 1978, pp. 195-214.

[78] Harlow, D.G. and Phoenix, S.L., "The Chain of Bundles Probability Model for the Strength of Fibrous materials II: A Numerical Study of Convergence", *Journal of Composite Materials*, Vol. 12, 1978, pp. 314-334.

[79] Batdorf, S.B., "Tensile Strength of Unidirectionally Reinforced Composites-I", *Journal of Reinforced Plastics and Composites*, Vol. 1, 1982, pp. 153-164.

[80] Tamuzs, V.P., "Some Peculiarities of Fracture in Heterogeneous Materials", *Fracture of Composite Materials*, Edited by G.C. Sih and V.P. Tamuzs, Martinus Hijhoff, Boston, MA, 1982, pp. 131-137.

[81] Yushanov, S.P. and Joshi, S.P., "Stochastic Modeling of Fracture Processes in Fiber Reinforced composites", *AIAA Journal*, Vol. 33, No. 9, 1995, pp. 1689-1697.

[82] Contreras, H., "The Stochastic Finite Element Method", *Int. J. for Computers and Structures*, Vol. 12, 1980, pp. 341-348.

[83] Vanmarcke, E., Shinozuka, M., Nakagiri, S., Schueller, G.I., and Grigoriu, M., "Random Fields and Stochastic Finite elements", *Structural Safety*, Vol. 3, 1986, pp. 143-166.

[84] Benaroya, H., and Rehak, M., "Finite Element Methods in Probabilistic Structural Analysis: A Selective Review", *Appl. Mech. Rev.*, Vol. 41, No. 5, May 1988, pp. 201-213.

[85] Yamazaki, F., Shinozuka, M., and Desgupta, G., "Neumann Expansion for Stochastic Finite Element Analysis", *Journal of Engineering Mechanics*, Vol. 114, No. 8, 1986, pp. 1335-1354.

[86] Ostoja-Starzewski, M., "Micromechanics as a basis of Stochastic Finite Elements and Differences: An Overview", *Appl. Mech. Rev.*, Vol. 46, No. 2, November 1993, pp. S136-S147.

[87] Vanmarcke, E.H., "Stochastic Finite Elements and Experimental Measurements", *Probabilistic Engineering Mechanics*, Vol. 9, 1994, pp. 103-114.

[88] Bucher, C.G., and Brenner, C.F., "Stochastic Response of Uncertain Systems", *Archives of Applied mechanics*, Vol. 62, 1992, pp. 507-516.

[89] Iwan, W.D., and Jensen, H., "On the Dynamic Response of Continuous Systems Including Model Uncertainty", *Journal of Applied Mechanics*, Vol. 60, 1993, pp. 484-490.

[90] Koyluoglu, H.U., Nielsen, S.R.K., and Cakmak, A.S., "Stochastic Dynamics of Geometrically Non-Linear Structures with Random Properties Subject to Stationary Random Excitation", *Journal of Sound and Vibration*, Vol. 190, 1996, pp. 821-841.

[91] Ramu, S.A., and Ganesan, R., "A Galerkin Finite Element Technique for Stochastic Field Problems", *Computer Methods in Applied Mechanics and Engineering*, Vol. 105, 1993, pp. 315-331.

[92] Zhu, W.Q., Ren, Y.J., and Wu, W.Q., "Stochastic FEM Based on Local Averages of Random vector Fields", *Journal of Engineering Mechanics*, Vol. 118, No. 3, 1992, pp. 496-511.

[93] Jensen, H., and Iwan, W.D., "Response of Systems with Uncertain Parameters to Stochastic Excitation", *Journal of Engineering Mechanics*, Vol. 118, No. 5, 1992, pp. 1012-1025.

[94] Liu, W.K., Belytschko, T., and Mani, A., "Applications of Probabilistic Finite Element Methods in Elastic/Plastic Dynamics", *Journal of Engineering for Industry*, Vol. 109, 1987, pp. 2-8.

[95] Ghanem, R., and Spanos, P.D., "Polynomial Chaos in Stochastic Finite Elements", *Journal of Applied Mechanics*, Vol. 57, 1990, pp. 197-202.

[96] Ganesan, R., Sankar, T.S., and Ramu, S.A., "Non-Conservatively Loaded Stochastic Columns", *Int. J. Solids Structures*, Vol. 30, No. 17, 1993, pp. 2407-2424.

[97] Shinozuka, M., Kako, T., and Tsurui, A., "Random Vibration Analysis in Finite Element Formulation", *Random vibration – status and recent development*, Ed. I. Elishakoff and R.H. Lyon, Elsevier, NewYork, 1986.

[98] Ramu, S.A., and Ganesan, R., "Free Vibration of a Stochastic Beam-Column using Stochastic FEM", *Int. J. for Computers and Structures*, Vol. 41, No. 5, 1991, pp. 987-994.

[99] Ren, Y.J., Elishakoff, I., and Shinozuka, M., "Finite Element Method for Stochastic Beams based on Variational Principles", *Journal of Applied Mechanics*, Vol. 64, 1997, pp. 664-669.

[100] Sankar, T.S., Ramu, S.A., and Ganesan, R., "Variability of SIF and COD of Stochastic Structural Systems", *Int. J. for Computers and Structures*, Vol. 43, No. 6, 1992, pp. 1135-1145.

[101] Sankar, T.S., Ramu, S.A., and Ganesan, R., "Stochastic Finite Element Analysis for High Speed Rotors", *Journal of Vibration and Acoustics*, Vol. 115, 1993, pp. 59-64.

[102] Liaw, D.G., and Yang, H.T.Y., "Reliability of Initially Compressed uncertain Laminated Plates in Supersonic Flow", *AIAA Journal*, Vol. 29, No. 6, 1991, pp. 952-945.

[103] Ganesan, R., and Hoa, S.V., "Stochastic Finite Element Analysis of Composite Structures", *CANCAM 95*, 15th Canadian Congress of Applied Mechanics, May 95, Victoria, Canada.

[104] Nakagiri, S., Takabatake, H., and Tani, S., "Uncertain Eigenvalue Analysis of Composite Laminated Plates by the Stochastic Finite Element Method", *Journal of Engineering for Industry*, Vol. 109, 1987, pp. 9-12.

[105] Engelstad, S.P., and Reddy, J.N., "Probabilistic Nonlinear Finite Element Analysis of Composite Structures", *AIAA Journal*, Vol. 31, No. 2, 1993, pp. 362-369.

[106] Chang, C., and Yang, H.T.Y., "Reliability of Uncertain Flexible Laminated Skewed Plates under Random Compressions", *AIAA Journal*, Vol. 30, No. 2, 1992, pp. 464-472.

[107] Slattery, K., "A Random-damage Finite Element for Modeling Failure in Advanced Composite Materials", *Composite Materials: Fatigue and Fracture*, Vol. 5, Ed. R.H. Martin, ASTM, Philadelphia, 1995, pp. 231-245.

[108] Ewalds, H.L., and Wanhill, R.J.H., "*Fracture Mechanics*", Edward Arnold Publishers, Maryland, 1986.

[109] Reddy, J.N., "*An Introduction to the Finite Element Method*", 2nd edition, McGraw-Hill, New York, 1993.

[110] Barsoum, R.S., "On the use of Isoparametric Finite Elements in Linear Fracture Mechanics", *Int. J. Num. Meth. Engng.*, Vol. 10, 1976, pp. 537-545.

[111] Henshell, R.D., and Shaw, K.G., "Crack Tip Elements are Unnecessary", *Int. J. Num. Meth. Engng.*, Vol. 9, 1975, pp. 495-509.

[112] Hellen, T.K., "On the Method of Virtual Crack Extensions", *Int. J. Num. Meth. Engng.*, Vol. 9, 1975, pp. 187-208.

[113] Kageyama, K., "Fracture Mechanics of Notched Carbon/Epoxy Laminates", *Application of Fracture Mechanics to Composite Materials*, Edited by K. Friedrich, 1989, pp. 327-396.

[114] Hyer, M.W., "*Stress Analysis of Fiber-Reinforced Composite Materials*", McGraw-Hill, New York, 1998.

[115] Daniel, I.M., and Ishai, O., "*Engineering Mechanics of Composite Materials*", Oxford University Press, Oxford, 1994.

[116] D3039, "*Standard Test Method for Tensile Properties of Fiber-Resin Composites*", Annual Book of ASTM Standard, 1989, pp. 118-122.

[117] D3518, "*Standard Practice for In-Plane Shear Stress-Strain Response of Unidirectional Polymer matrix Composite*", Annual Book of ASTM Standard, 1991, pp. 114-148.

[118] Vanmarcke, E., "*Random Fields: Analysis and Synthesis*", MIT Press, Cambridge, 1983.

[119] Shigley, J.E., and Mischke, C.R., "*Mechanical Engineering Design*", 5th edition, McGraw-Hill, NewYork, 1989.

Appendix I

Program for the Finite Element Fracture Analysis of Isotropic Plates

```
clc; clear all;
% PROGRAM FOR STRESS ANALYSIS USING 8-NODE ISOPARAMETRIC ELEMENT
%-------------------------------------------------------------------------------
% Variable descriptions

%  k = element stiffness matrix
%  f = element force vector
%  kk = system force matrix
%  ff = system stiffness vector
%  U = system nodal displacement vector
%  gcoord = coordinate values of each node
%  nodes = nodal connectivity of each element
%  index = a vector containing system dofs associated with each element
%  point2 = matrix containing sampling points
%  weight2 = matrix containing weighting coefficients
%  bcdof = a vector containing dofs associated with boundary conditions
%  bcval = a vector containing boundary condition values associated with
%  the dofs in 'bcdof'
%  cdof = total constrain dof
%  fdof = total force dof
%  forcedof = force dof
%-------------------------------------------------------------------------------
% Input data for control parameters

disp('Do you want input DATA to be read from a file');
disp('if YES press 1, if NO press 0');

indata=input('PRESS 1 OR 0 >');
            if indata==0,
            elseif indata==1,
%Open the input data file 'fdataf.txt' to get data of the problem

            fid=fopen('Nfig51.txt');% Input DATA File NAME
else; break; end

%Input data for total No# of Element

if indata ==0,
nel=input('Enter the Number of Elements >');
            elseif indata==1,
            if feof(fid)==1, disp('Unexpected end of data file');break;end
            nel=str2num(fgetl(fid))
end
pause; clc;

%Data for Tatal No# of node

if indata ==0,
nnode=input('Enter the Total Number of NODES in the System >');
            elseif indata==1,
            if feof(fid)==1, disp('Unexpected end of data file');break;end
            nnode=str2num(fgetl(fid))
end
```

```
pause; clc;

%Input data for Nodal connectivity

if indata ==0,
disp('Enter the Element Nodal Connectivity');
        for i=1:nel;
                for j=1:8,
                sprintf('for Element %d Node %d',i,j),
                nodes(i,j)=input('');
                end
        end
        elseif indata==1,
        if feof(fid)==1, disp('Unexpected end of data file');break;end
        nodes=str2num(fgetl(fid))
end
pause; clc;

%Input data for Global nodal coordinate

if indata ==0,
disp('Enter the Global Nodal Coordinate values');
        for i=1:nnode,
                for j=1:2,
                        if j==1
                                coord='X';
                                else
                                coord='Y';
                        end
                        sprintf('of Global node %d, %c Coordinate ',i,coord),
                        gcoord(i,j)=input('');
                end
        end
                elseif indata==1,
                if feof(fid)==1, disp('Unexpected end of data file');break;end
                gcoord=str2num(fgetl(fid))
end
pause; clc;

% Input Data for displacement-boundary-condition

if indata ==0,

disp('Input Data for CONSTRAIN NODE');
disp('odd dof is X-direction and even dof is Y-direction');
pause;

cdof=input('Enter Total Number of CONSTRAIN dof >');

elseif indata ==1
        if feof(fid)==1, disp('Unexpected end of data file');break;end
        cdof=str2num(fgetl(fid))
end

if indata==0,
        for i=1:cdof;
                sprintf('Constrain dof %d',i),
                bcdof(i)=input('');
                bcval=zeros(size(bcdof));
        end
        elseif indata==1,
        if feof(fid)==1, disp('Unexpected end of data file');break;end
        bcdof=str2num(fgetl(fid))
        bcval=zeros(size(bcdof))
end
pause; clc;

%Data-for-Young Modulus

if indata ==0,
```

```
emodule=input('Enter the value of Young modulus of material >');

elseif indata==1,
        if feof(fid)==1, disp('Unexpected end of data file');break;end
        emodule=str2num(fgetl(fid))
end

%Data-for-Poisson's ratio

if indata ==0,
poisson=input('Enter Poisson's ratio >');

elseif indata==1,
        if feof(fid)==1, disp('Unexpected end of data file');break;end
        poisson=str2num(fgetl(fid))
end

%Data-for-Thickness

if indata ==0,
thk=input('Enter the thickness >');

elseif indata==1,
        if feof(fid)==1, disp('Unexpected end of data file');break;end
        thk=str2num(fgetl(fid))
end

%Data-for-Guess-Integration-Point

if indata ==0,
ngl=input('Entre number of integration points >');

elseif indata==1,
        if feof(fid)==1, disp('Unexpected end of data file');break;end
        ngl=str2num(fgetl(fid))
end
pause; clc;

%Define Constant

nnel=8;                 % Number of Node per element
ndof=2;                 % dof per Node
sdof=nnode*ndof;        % System dof
edof=nnel*ndof;         % Element dof
nglxy=ngl*ngl;          % No. of sampling points per element

%initialization of matrices and vectors

kk=zeros(sdof,sdof);            % system matrix
ff=zeros(sdof,1);               % Initialization of load vector
U=zeros(sdof,1);                % system displacement vector
eldisp=zeros(edof,1);           % element displacement vector
stress=zeros(nglxy,3);          % matrix containing stress components
strain=zeros(nglxy,3);          % matrix containing strain components
index=zeros(edof,1);            % index vector
kinmtx2=zeros(3,edof);          % kinematic matrix
matmtx=zeros(3,3);              % constitutive matrix

%Force Boundary Condition
%-------------------------------
%Input data for Nodal Point Load

if indata==0,

disp('Input Menu for POINT load at Node')
disp('Press any KEY to continue...    ')
pause;

fdof=input('Total Number of Force dof >')
        for i=1:fdof
```

```
                forcedof=input('Enter force dof >')
                ff(forcedof)=input('Enter corresponding applied force >')
        end
elseif indata==1,

        if feof(fid)==1,disp('Unexpected end of data file'),break,end
        fdof=str2num(fgetl(fid))
        for i=1:fdof
                forcedof=str2num(fgetl(fid))
                ff(forcedof)=str2num(fgetl(fid))
        end
end     % end for indata==0
%-------------------------------------------------------------------------
%Computation of element matrices and vectors and their assembly
%-------------------------------------------------------------------------
[pointx,pointy,weightx,weighty]=fgauss(ngl); );% sampling points & weights

matmtx=fematiso(1,emodule,poisson);% compute constitutive matrix

for iel=1:nel% loop for the total number of elements

        for i=1:nnel
                nd(i)=nodes(iel,i);             % extract connected node
                xcoord(i)=gcoord(nd(i),1);      %extract x value of the node
                ycoord(i)=gcoord(nd(i),2);      % extract y value of the node
        end
                k=zeros(edof,edof);% initialization of element matrix to zero
        for int=1:nglxy; % Loop for numerical integration

                x=pointx(int);
                wtx=weightx(int);
                y=pointy(int);
                wty=weighty(int) ;

                [shape,dhdr,dhds]=feisoq8(x,y); % compute shape functions and derivatives at sampling point
                jacob2=fejacob2(nnel,dhdr,dhds,xcoord,ycoord); % compute Jacobian
                detjacob=det(jacob2); % determinant of Jacobian
                invjacob=inv(jacob2); % inverse of Jacobian matrix
                [dhdx,dhdy]=federiv2(nnel,dhdr,dhds,invjacob); % derivatives w.r.t. physical coordinate
                kinmtx2=fekine2d(nnel,dhdx,dhdy); % compute kinematics matrix
                k=k+kinmtx2'*matmtx*kinmtx2*thk*wtx*wty*detjacob; % element matrix
        end % end of numerical integration loop

        index=feeldof(nd,nnel,ndof); % extract system dofs associated with element
        kk=feasmbl1(kk,k,index); % assemble element matrices

end % end of total number of element

[kk]=feaplyc2(kk,bcdof,bcval); %apply boundary conditions

U=kk\ff;% System displacement vector

ix=1:2:2*nnode;% extract odd number
UX=U(ix,1);% extraction of X-dir. displacement

iy=2:2:2*nnode;% extract even number
UY=U(iy,1);% extraction of Y-dir. displacement

disp('Nodal Displacement');
disp('---------------------- ');
disp('   NODE     UX       UY');
num=1:1:nnode;    % counting node number
Uxy=[num' UX UY]  % print nodal displacements

ENERGY1=U'*ff;
clc;

% Stress Intensity Factor by Displacement Extrapolation Method

[KIH,RNdis]= fsifisod(emodule,poisson,)
```

```
% Stress Intensity factor by Energy Release Rate

%NOTE: Repeat the main program for different crack length and calculate ENERGY2

[KEI]=fsifisoe(emodule,poisson,ENERGY1,ENERGY2);
```

Subroutines (Functions) of the Program

```
function [pointx,pointy,weightx,weighty]=fgauss(ngl)
%-------------------------------------------------------------------------------
%The integration points and weighting coefficients of Gauss-Legendre quadrature for two-dimensional integration
%-------------------------------------------------------------------------------

if ngl==2  % 2-point quadrature rule
           pointx=[-0.5774;-0.5774;0.5774;0.5774]; pointy=[-0.5774;0.5774;-0.5774;0.5774];
           weightx=[1;1;1;1]; weighty=[1;1;1;1];

elseif ngl==3      % 3-point quadrature rule

           pointx=[-0.7746;-0.7746;-0.7746;0.0;0.0;0.0;0.7746;0.7746;0.7746];
           pointy=[-0.7746;0.0;0.7746;-0.7746;0.0;0.7746;-0.7746;0.0;0.7746];
           weightx=[0.5556;0.5556;0.5556;0.8889;0.8889;0.8889;0.5556;0.5556;0.5556];
           weighty=[0.5556;0.8889;0.5556;0.5556;0.8889;0.5556;0.5556;0.8889;0.5556];

elseif ngl==4      % 4-point quadrature rule

           pointx=[-0.861136311594053;-0.861136311594053;-0.861136311594053;-0.861136311594053;
                   -0.339981043584856;-0.339981043584856;-0.339981043584856;-0.339981043584856;
                    0.339981043584856;0.339981043584856;0.339981043584856;0.339981043584856;
                    0.861136311594053;0.861136311594053;0.861136311594053;0.861136311594053];

           pointy=[-0.861136311594053;-0.339981043584856;0.339981043584856;0.861136311594053;
                    0.861136311594053;0.339981043584856;-0.339981043584856;-0.861136311594053;
                   -0.861136311594053;-0.339981043584856;0.339981043584856;0.861136311594053;
                    0.861136311594053;0.339981043584856;-0.339981043584856;-0.861136311594053];

           weighty=[0.347854845137454;0.652145154862546;0.652145154862546;0.347854845137454;
                    0.347854845137454;0.652145154862546;0.652145154862546;0.347854845137454;
                    0.347854845137454;0.652145154862546;0.652145154862546;0.347854845137454;
                    0.347854845137454;0.652145154862546;0.652145154862546;0.347854845137454];

           weightx=[0.347854845137454;0.347854845137454;0.347854845137454;0.347854845137454;
                    0.652145154862546;0.652145154862546;0.652145154862546;0.652145154862546;
                    0.652145154862546;0.652145154862546;0.652145154862546;0.652145154862546;
                    0.347854845137454;0.347854845137454;0.347854845137454;0.347854845137454];

end


function [matrntrx]=fematiso(iopt,elastic,poisson)
%-------------------------------------------------------
% The constitutive equation for isotropic material
%-------------------------------------------------------
if iopt==1      % plane stress
          matrntrx= elastic/(1-poisson*poisson)*[1  poisson 0;poisson  1  0;0  0  (1-poisson)/2];
```

```
        elseif iopt==2    % plane strain
        matmtrx= elastic/((1+poisson)*(1-2*poisson))* [(1-poisson)  poisson 0;poisson  (1-poisson)  0;0  0  (1-
                2*poisson)/2];
end


function [shapeq8,dhdrq8,dhdsq8]=feisoq(r,s)
%-------------------------------------------------------------------------------------------------------------
% Isoparametric eight-node quadilateral shape functions  and their derivatves at the selected (integration) point
% in terms of the natural coordinate
%-------------------------------------------------------------------------------------------------------------

% shape functions

 shapeq8(1)=0.25*(1-r)*(1-s)*(-1-r-s);
 shapeq8(2)=0.25*(1+r)*(1-s)*(-1+r-s);
 shapeq8(3)=0.25*(1+r)*(1+s)*(-1+r+s);
 shapeq8(4)=0.25*(1-r)*(1+s)*(-1-r+s);
 shapeq8(5)=0.5*(1-r*r)*(1-s);
 shapeq8(6)=0.5*(1+r)*(1-s*s);
 shapeq8(7)=0.5*(1-r*r)*(1+s);
 shapeq8(8)=0.5*(1-r)*(1-s*s);

% Derivatives w.r.t r

 dhdrq8(1)=0.25*(s+2*r-2*r*s-s*s);
 dhdrq8(2)=0.25*(-s+2*r-2*r*s+s*s);
 dhdrq8(3)=0.25*(2*r+s+2*r*s+s*s);
 dhdrq8(4)=0.25*(-s+2*r+2*r*s-s*s);
 dhdrq8(5)=-r*(1-s);
 dhdrq8(6)=0.5*(1-s*s);
 dhdrq8(7)=-r*(1+s);
 dhdrq8(8)=0.5*(-1+s*s);

% Derivatives w.r.t s

 dhdsq8(1)=0.25*(r+2*s*(1-r)-r*r);
 dhdsq8(2)=0.25*(-r+2*s-r*r+2*r*s);
 dhdsq8(3)=0.25*(2*s+r+r*r+2*r*s);
 dhdsq8(4)=0.25*(-r+r*r+2*s*(1-r));
 dhdsq8(5)=0.5*(-1+r*r);
 dhdsq8(6)=-s*(1+r);
 dhdsq8(7)=0.5*(1-r*r);
 dhdsq8(8)=-s*(1-r);


function [jacob2]=fejacob2(nnel,dhdr,dhds,xcoord,ycoord)
%-------------------------------------------------------
%The Jacobian for two-dimensional mapping
%-------------------------------------------------------

jacob2=zeros(2,2);

for i=1:nnel
            jacob2(1,1)=jacob2(1,1)+dhdr(i)*xcoord(i);
            jacob2(1,2)=jacob2(1,2)+dhdr(i)*ycoord(i);
            jacob2(2,1)=jacob2(2,1)+dhds(i)*xcoord(i);
            jacob2(2,2)=jacob2(2,2)+dhds(i)*ycoord(i);
end


function [kinmtx2]=fekine2d(nnel,dhdx,dhdy)
%-------------------------------------------------------------------------------------------------------------
% The kinematic equation between strains and displacements for two-dimensional solids
%-------------------------------------------------------------------------------------------------------------

for i=1:nnel
```

```
        i1=(i-1)*2+1;
        i2=i1+1;
        kinmtx2(1,i1)=dhdx(i);
        kinmtx2(2,i2)=dhdy(i);
        kinmtx2(3,i1)=dhdy(i);
        kinmtx2(3,i2)=dhdx(i);
end


function [dhdx,dhdy]=federiv2(nnel,dhdr,dhds,invjacob)
%-------------------------------------------------------------------------
% Derivatives of 2-D isoparametric shape functions with respect to physical coordinate system
%-------------------------------------------------------------------------

for i=1:nnel
        dhdx(i)=invjacob(1,1)*dhdr(i)+invjacob(1,2)*dhds(i);
        dhdy(i)=invjacob(2,1)*dhdr(i)+invjacob(2,2)*dhds(i);
end


function [index]=feeldof(nd,nnel,ndof)
%-------------------------------------------------
% System dofs associated with each element
%-------------------------------------------------

edof = nnel*ndof;
k=0;
for i=1:nnel
        start = (nd(i)-1)*ndof;
        for j=1:ndof
                k=k+1;
                index(k)=start+j;
        end
end


function [kk]=feasmbl1(kk,k,index)
%-------------------------------------------------------------
% Assembly of element matrices into the system matrix
%-------------------------------------------------------------

edof = length(index);
for i=1:edof
        ii=index(i);
        for j=1:edof
                jj=index(j);
                kk(ii,jj)=kk(ii,jj)+k(i,j);
        end
end


function [kk]=feaplyc2(kk,bcdof)
%-------------------------------------------------
% Apply constraints to matrix equation [kk]{x}={ff}
%-------------------------------------------------

n=length(bcdof);
sdof=size(kk);

for i=1:n
        c=bcdof(i);
        for j=1:sdof
                kk(c,j)=0;
        end
        kk(c,c)=1;
end
```

```
function [KIH,RNdis]= fsifisod(emodule,poisson,)
%-------------------------------------------------------------------------
% Stress Intensity Factor based on Displacement Extrapolation Method
%-------------------------------------------------------------------------

dig=180; %radial angle in dig.
theta=dig*pi/180;
Mu=emodule/(2*(1+poisson))
p=(3-poisson)/(1+poisson)
CN=4*Mu*sqrt(2*pi)/((2*p+1)*sin(theta/2)-sin(3*theta/2))
ENode=6; %Number of extrapolation nodes

for i=1:ENode
        ENodeN(i)=input('Ex Node number >')
        RNdis(i)=input('Radial distance >')
        x=ENodeN(i);
        KIH(i)=CN*sqrt(1/RNdis(i))*U(2*x)
end

plot(RNdis,KIH)
xlabel('Radial distance,(r)')
ylabel('Stress Intensity Factor,(KI)')
title('DISPLACEMENT EXTRAPOLATION METHOD')
grid


function[KEI]=fsifisoe(emodule,poisson,Energy1,Energy2);
%-------------------------------------------------------------------------
% Stress Intensity Factor based on Energy Release Rate Method
%-------------------------------------------------------------------------

dU=ENERGY2-ENERGY1

Mu=emodule/(2*(1+poisson))
p=(3-poisson)/(1+poisson)
da=0.25 % Increase in Crack length
GI=dU/da

CON=sqrt(8*Mu/(1+p))

KEI=CON*sqrt(GI)
```

Appendix II

Program for the Stochastic Finite Element Fracture Analysis of Composite laminates

```
clc; clear all;
%-------------------------------------
% Input data for control parameters
%-------------------------------------
for T=1:250; % Loop for simulation

% Open the input data file 'fdataf.txt' to get data of the problem

        fid=fopen('or090q.txt');    % Input DATA File NAME

        nel=str2num(fgetl(fid));        % Input data for total No# of Element
        nnode=str2num(fgetl(fid));      % Data for Tatal No# of node
        nodes=str2num(fgetl(fid));      % Input data for Nodal connectivity
        gcoord=str2num(fgetl(fid));     % Input data for Global nodal coordinate

% Input Data for displacement-boundary-condition
        cdof=str2num(fgetl(fid));
        bcdof=str2num(fgetl(fid));
        bcval=zeros(size(bcdof));

% data for composite
        E1=str2num(fgetl(fid));         % 1-dir. Young's modulus
        E2=str2num(fgetl(fid));         % 2-dir. Young's modulus
        M12=str2num(fgetl(fid));        % Major Poisson's ratio
        G12=str2num(fgetl(fid));        % Shear  modulus
        tply=str2num(fgetl(fid));       % Number of ply
        t=str2num(fgetl(fid));          % ply thickness
        theta=str2num(fgetl(fid));      % ply orientation angle
        ngl=str2num(fgetl(fid))          % Guess-Integration-Point
% Define Constant
        nnel=8;                         % Number of Node per element
        ndof=2;                         % dof per Node
        sdof=nnode*ndof;                % System dof
        edof=nnel*ndof;                 % Element dof
        nglxy=ngl*ngl;                  % No. of sampling points per element
% Initialization of matrices and vectors
        kk=zeros(sdof,sdof);   % system matrix
        ff=zeros(sdof,1);      % Initialization of load vector
        U=zeros(sdof,1);       % system displacement vector
        index=zeros(edof,1);   % index vector
        kinmtx2=zeros(3,edof); % kinematic matrix
        matmtx=zeros(3,3);     % constitutive matrix
% Force Boundary Condition
        fdof=str2num(fgetl(fid));
        for i=1:fdof
                forcedof=str2num(fgetl(fid));
                ff(forcedof)=str2num(fgetl(fid));
        end

        % Computation of element matrices and vectors and their assembly

        gn=[1 2 3 4 5 6 7 8 9]; % Gauss point numbering
        [pointx,pointy,weightx,weighty]=fgauss(ngl);
        % For stochastic field
        [E11,E22,P12,G,theta,tp]=fmdlrand(nel,ngl,nodes,gcoord,E1,E2,G12,M12.pointx,pointy,theta,t);
```

```
        for iel=1:nel           % loop for the total number of elements
                for i=1:nnel
                        nd(i)=nodes(iel,i);
                        xcoord(i)=gcoord(nd(i),1);
                        ycoord(i)=gcoord(nd(i),2);
                end
                k=zeros(edof,edof);
                [Ee1,Ee2,Mu12,Mu21,Ge12,gn]=femodule(iel,nglxy,gn,E11,E22,P12,G);
                % Numerical integration
                        for int=1:nglxy         % Loop for numerical integration
                        x=pointx(int);
                        wtx=weightx(int);
                        y=pointy(int);
                        wty=weighty(int) ;

                        [shape,dhdr,dhds]=feisoq8(x,y);
                        jacob2=fejacob2(nnel,dhdr,dhds,xcoord,ycoord);
                        detjacob=det(jacob2);
                        invjacob=inv(jacob2);
                        [dhdx,dhdy]=federiv2(nnel,dhdr,dhds,invjacob);
                        kinmtx2=fekine2d(nnel,dhdx,dhdy);
                        [matrntx]=fcompo(int,Ee1,Ee2,Mu12,Mu21,Ge12,theta,tp,Ply);
                        k=k+kinmtx2'*matmtx*kinmtx2*(tp*tply)*wtx*wty*detjacob;
                end     % end of numerical integration loop
                index=feeldof(nd,nnel,ndof);
                kk=feasmbl1(kk,k,index);
        end     % end of total number of element
        [kk]=feaplyc2(kk,bcdof);
        U=kk\ff;                % Nodal displacement
        SE5=U'*ff;              %Energy release rate

        % Stress Intensity Factor based on Displacement Extrapolation Method
                [m,C]=fsifcomd(E11,E22,G,P12,U);
                KI5(T)=C;

        % Stress Intensity Factor based on Energy Release Rate Method
        %NOTE: Run the main program for different crack length to calculate SE6 and SE7
                [m,C]=fsifcome(SE5,SE6,SE7,E11,E22,P12,G);
                K5(T)=m*40+C
end % end for simulation

fid=fopen('Result.m','w');
fprintf(fid,'Laminate:\n');
fprintf(fid,'%1.0f\t',theta);
fprintf(fid,'Stress Intensity factor:\n');
fprintf(fid,'----------Node:4\n');
MKI4=mean(KI4);
fprintf(fid,'Mean_K4:%10.4f\n',MKI4);
SKI4=std(KI4);
fprintf(fid,'STD_K4 :%10.4f\n',SKI4);
CKI4=SKI4/MKI4;
fprintf(fid,'COV_K4 :%10.4f\n',CKI4);
fprintf(fid,'----------Node:3\n');
MKI3=mean(KI3);
fprintf(fid,'Mean_K3:%10.4f\n',MKI3);
SKI3=std(KI3);
fprintf(fid,'STD_K3 :%10.4f\n',SKI3);
CKI3=SKI3/MKI3;
fprintf(fid,'COV_K3 :%10.4f\n',CKI3);
fprintf(fid,'----------At Crack tip:\n');
MKI5=mean(KI5);
fprintf(fid,'Mean_K5:%10.4f\n',MKI5);
SKI5=std(KI5);
fprintf(fid,'STD_K5 :%10.4f\n',SKI5);
CKI5=SKI5/MKI5;
fprintf(fid,'COV_K5 :%10.4f\n',CKI5);
fprintf(fid,'----------\n');

fclose(fid);
```

Additional Subroutines (Functions) of the Program

```
function[matmtx]=fcompo(int,Ee1,Ee2,Mu12,Mu21,Ge12,theta,tp,tply)
%-------------------------------------------------------------------------
% The constitutive equation for orthotropic material
%-------------------------------------------------------------------------
% 1-2 dir. stiffness component
q11=Ee1(int)/(1-Mu12(int)*Mu21(int));
q12=Mu21(int)*Ee1(int)/(1-Mu12(int)*Mu21(int));
q22=Ee2(int)/(1-Mu12(int)*Mu21(int));
q33=Ge12(int);

% Initialization
A11=0;A22=0;A33=0;A12=0;A23=0;A13=0;

for j=1:tply
        m=cos(theta(1,j)*pi/180);
        n=sin(theta(1,j)*pi/180);

        % Calculation of [Q bar] matrix
        Q11(1,j)=(m)^4*q11+(n)^4*q22+2*(m*n)^2*q12+4*(m*n)^2*q33;
        Q12(1,j)=(m*n)^2*q11+(m*n)^2*q22+((m)^4+(n)^4)*q12...
                -4*(m*n)^2*q33;
        Q13(1,j)=(m)^3*n*q11-m*(n)^3*q22+(m*(n)^3-(m)^3*n)*q12...
                +2*(m*(n)^3-(m)^3*n)*q33;
        Q23(1,j)=m*(n)^3*q11-(m)^3*n*q22+((m)^3*n-m*(n)^3)*q12...
                +2*((m)^3*n-m*(n)^3)*q33;
        Q22(1,j)=(n)^4*q11+(m)^4*q22+2*(m*n)^2*q12+4*(m*n)^2*q33;
        Q33(1,j)=(m*n)^2*q11+(m*n)^2*q22-2*(m*n)^2*q12...
                +((m)^2-(n)^2)^2*q33;

        % Calculation of [A] matrix
        A11=A11+Q11(1,j)*tp;
        A22=A22+Q22(1,j)*tp;
        A33=A33+Q33(1,j)*tp;
        A12=A12+Q12(1,j)*tp;
        A13=A13+Q13(1,j)*tp;
        A23=A23+Q23(1,j)*tp;
end
% Laminate [A] matrix
A=[A11 A12 A13;A12 A22 A23;A13 A23 A33];
% Equivalent [E] matrix for composite
a=inv(A); e=a*(tp*tply);
matmtx=inv(e);


function[E11,E22,P12,G]=fmdlrand(nel,ngl,nodes,gcoord,E1,E2,G12,M12,pointx,pointy)
%-------------------------------------------------------------------------
% Stochastic modules at each gauss point of the system
%-------------------------------------------------------------------------
SDe1=0.022188;SDe2=0.041248;SDp=0.095527 ;SDs=0.05523;%Standard daviation
d=25.99;%Seperation distance[max=2.1]

nglxy=ngl*ngl;
nnel=8;
for iel=1:nel % loop for the total number of elements
        % Extract element nodal coordinate
        for i=1:nnel
                nd(i)=nodes(iel,i);
                xcoord(i)=gcoord(nd(i),1); % nodal X-coord value
                ycoord(i)=gcoord(nd(i),2); % nodal Y-coord value
        end
        % Extract gauss point coordinatr
        for g=1:nglxy
```

```
                x=pointx(g);
                y=pointy(g);
                [shape]=feisoq8(x,y); % 8-node shape function
                X=0; % initialization
                Y=0; % initialization
                        for j=1:nnel
                                X=X+xcoord(j)*shape(j);
                                Y=Y+ycoord(j)*shape(j);
                        end
                XX(iel,g)=X; YY(iel,g)=Y;
                Xg=XX'; Yg=YY';
        end
end % for total element

% Calculation of randomness of material properties
for i=1:nglxy*nel
        for j=1:nglxy*nel
                % Gause point seperation distance
                GD(i,j)=sqrt((Xg(j)-Xg(i))^2+(Yg(j)-Yg(i))^2);
                % Gaussian Autocoleration function
                ACe1(i,j)=SDe1^2*exp(-(GD(i,j)/d)^2); ACe2(i,j)=SDe2^2*exp(-(GD(i,j)/d)^2);
                ACp(i,j)=SDp^2*exp(-(GD(i,j)/d)^2); ACs(i,j)=SDs^2*exp(-(GD(i,j)/d)^2);
                %Markov Model
                %ACe1(i,j)=SDe1^2*exp(-(GD(i,j)/d)); %ACe2(i,j)=SDe2^2*exp(-(GD(i,j)/d));
                %ACp(i,j)=SDp^2*exp(-(GD(i,j)/d)); %ACs(i,j)=SDs^2*exp(-(GD(i,j)/d));
        end
end

% cholesky decomposition & lower triangular matrix
CDe1=chol(ACe1); Le1=CDe1'; CDe2=chol(ACe2); Le2=CDe2';
CDp=chol(ACp); Lp=CDp'; CDs=chol(ACs); Ls=CDs';

% Creat randomness
ae1=Le1*randn(nglxy*nel,1); ae2=Le2*randn(nglxy*nel,1);
ap=Lp*randn(nglxy*nel,1); as=Ls*randn(nglxy*nel,1);

% Stochastic material properties
E11=E1*(1+ae1); E22=E2*(1+ae2); P12=M12*(1+ap); G=G12*(1+as);
%Stochastic ply angle and ply thickness

stdQ=0.1; %Standard daviation of ply angle
stdtp=0.1;%Standard daviation of ply thickness
tp=0;%Initialization of ply thickness

for c=1:tply
        RQ=stdQ*randn(1);
        Rtp=stdtp*randn(1);
        theta(c)=Mtheta(c)*(1+RQ);
        stp(c)=t*(1+Rtp);
        tp=Ltp+stp(c);
end


function[Ee1,Ee2,Mu12,Mu21,Ge12,gn]=femodule(iel,nglxy,gn,E11,E22,P12,G)
%-----------------------------------------------------------------------
%Stochastic material properties for each element (at each gauss point)
%-----------------------------------------------------------------------
for i=1:nglxy
        Ee1(i)=E11(gn(i)); Ee2(i)=E22(gn(i));
        Mu12(i)=P12(gn(i)); Mu21(i)=(Mu12(i)*Ee2(i))/Ee1(i);
        Ge12(i)=G(gn(i));
end
gn=gn+nglxy;


function[m,C]=fsifcomd(E11,E22,G,P12,U)
%-----------------------------------------------------------------------
% Stress Intensity Factor based on Displacement Extrapolation Method
%-----------------------------------------------------------------------
clear i;
```

```
%for nude 4
E1=E11(13);E2=E22(13);G12=G(13);M12=P12(13);
i=sqrt(-1);
a11=1/E1;a22=1/E2;a66=1/G12;a12=-M12/E1;
s1=sqrt(a22/a11);s2=(2*a12+a66)/(2*a11);
m1=i*0.707106*(sqrt(s2+s1)+sqrt(s2-s1)); m2=i*0.707106*(sqrt(s2+s1)-sqrt(s2-s1));
F1=-i;F2=-i;
p1=m1^2*a11+a12;p2=m2^2*a11+a12; q1=m1*a12+a22/m1;q2=m2*a12+a22/m2;
B=1/(m1-m2);C1=m1*p2/F2;D1=m2*p1/F1; C2=m1*q2/F2;D2=m2*q1/F1;
v=real(B*(C2-D2));

KI4=(1/v)*pi*(1/sqrt(2*pi*5))*U(2*4)*sqrt(1000);      %Mpa.sqrt(m)

%for node 3
E1=(E11(10)+E11(7))/2;E2=(E22(10)+E22(7))/2;G12=(G(10)+G(7))/2;M12=(P12(10)+P12(7))/2;
a11=1/E1;a22=1/E2;a66=1/G12;a12=-M12/E1;
s1=sqrt(a22/a11);s2=(2*a12+a66)/(2*a11);
m1=i*0.707106*(sqrt(s2+s1)+sqrt(s2-s1)); m2=i*0.707106*(sqrt(s2+s1)-sqrt(s2-s1));
F1=-i;F2=-i;
p1=m1^2*a11+a12;p2=m2^2*a11+a12; q1=m1*a12+a22/m1;q2=m2*a12+a22/m2;
B=1/(m1-m2);C1=m1*p2/F2;D1=m2*p1/F1; C2=m1*q2/F2;D2=m2*q1/F1;
v=real(B*(C2-D2));
KI3=(1/v)*pi*(1/sqrt(2*pi*20))*U(2*3)*sqrt(1000);
m=(KI3-KI4)/10;      %slope
C=KI4-(m*10);        %A constant



function[m,C]=fsifcome(SE5,SE6,SE7,E11,E22,P12,G)
%-------------------------------------------------------------------------
% Stress Intensity Factor based on Energy Release Rate Method
%-------------------------------------------------------------------------
dE56=SE6-SE5; GI56=dE56/10; dE57=SE7-SE5; GI57=dE57/20;

SUM=(1/6)+(4/6)+(2/6)+(4/6)+(2/6)+(4/6)+(1/6);

WA110=(1/6)*(1/E11(273)); WA111=(4/6)*(1/E11(276)); WA112=(2/6)*(2/(E11(279)+E11(264)));
WA113=(4/6)*(1/E11(267)); WA114=(2/6)*(2/(E11(270)+E11(263))); WA115=(4/6)*(1/E11(266));
WA116=(1/6)*(1/E11(269));
a11=(WA110+WA111+WA112+WA113+WA114+WA115+WA116)/SUM;

Wa110=(1/6)*(1/E22(273)); Wa111=(4/6)*(1/E22(276)); Wa112=(2/6)*(2/(E22(279)+E22(264)));
Wa113=(4/6)*(1/E22(267)); Wa114=(2/6)*(2/(E22(270)+E22(263))); Wa115=(4/6)*(1/E22(266));
Wa116=(1/6)*(1/E22(269));
a22=(Wa110+Wa111+Wa112+Wa113+Wa114+Wa115+Wa116)/SUM;

Wg110=(1/6)*(1/G(273)); Wg111=(4/6)*(1/G(276)); Wg112=(2/6)*(2/(G(279)+G(264)));
Wg113=(4/6)*(1/G(267)); Wg114=(2/6)*(2/(G(270)+G(263))); Wg115=(4/6)*(1/G(266));
Wg116=(1/6)*(1/G(269));
a66=(Wg110+Wg111+Wg112+Wg113+Wg114+Wg115+Wg116)/SUM;

Wm110=(1/6)*(P12(273)/E11(273)); Wm111=(4/6)*(P12(276)/E11(276));
Wm112=(2/6)*((P12(279)+P12(264))/(E11(279)+E11(264))); Wm113=(4/6)*(P12(267)/E11(267));
Wm114=(2/6)*((P12(270)+P12(263))/(E11(270)+E11(263))); Wm115=(4/6)*(P12(266)/E11(266));
Wm116=(1/6)*(P12(269)/E11(269));
a12=(Wm110+Wm111+Wm112+Wm113+Wm114+Wm115+Wm116)/SUM;

s1=sqrt(a22/a11); s2=(2*a12+a66)/(2*a11);
ORF=a22*(sqrt((s2+s1)/(2*s1)));
%When crack length=50mm
KI56=sqrt(GI56/ORF)*sqrt(1000);%Mpa.sqrt(m)
%When Crack length=60mm
KI57=sqrt(GI57/ORF)*sqrt(1000);%Mpa.sqrt(m)
m=(KI57-KI56)/10;
C=KI57-(m*60);
```